C266/X/68

Southampton Oceanography Centre

INTERNAL DOCUMENT No. 68

The 5m long recirculating flume at the School of Ocean and Earth Sciences (SOES), University of Southampton
Part II: Flow characteristics

D Paphitis & M B Collins

INDEXED

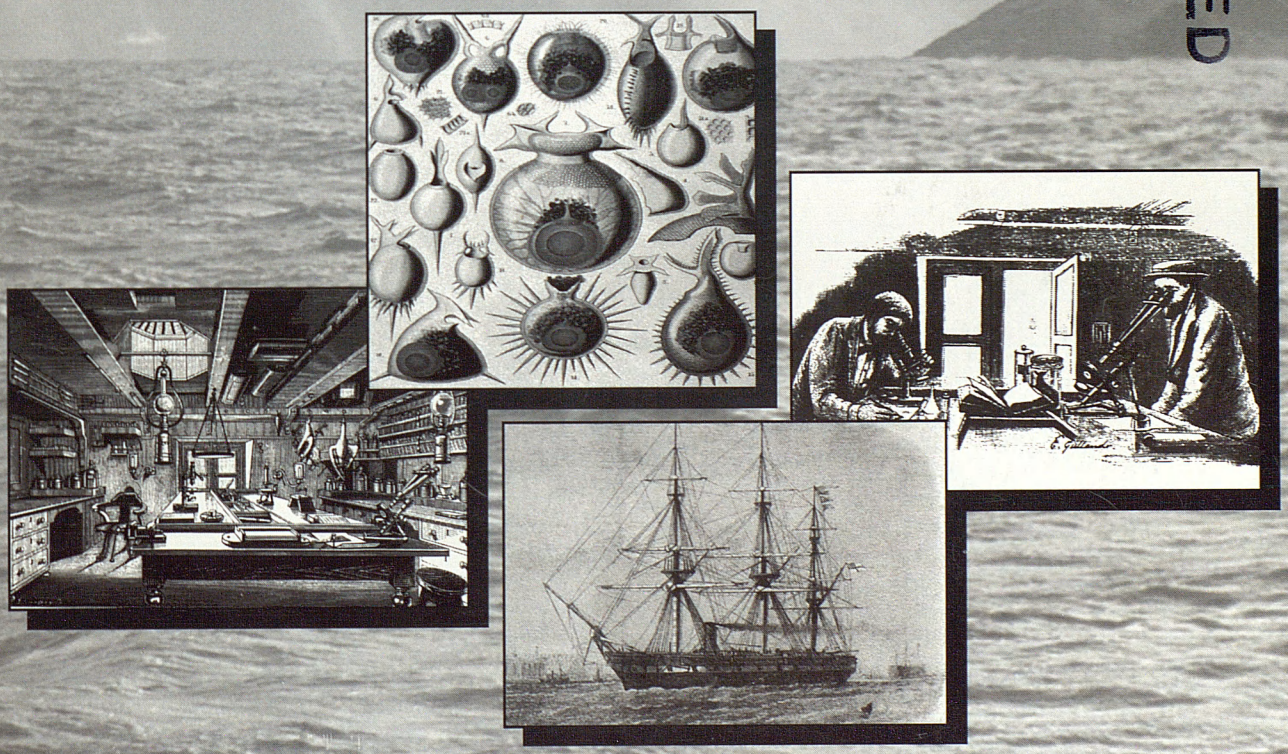

Natural Environment Research Council

University of Southampton

SOUTHAMPTON OCEANOGRAPHY CENTRE

INTERNAL DOCUMENT No. 68

The 5m long recirculating flume at the School of Ocean and Earth Sciences (SOES), University of Southampton Part II: Flow characteristics

D Paphitis & M B Collins

2001

NATIONAL OCEANOGRAPHIC LIBRARY
09 APR 2001
SOUTHAMPTON OCEANOGRAPHY CENTRE
Southampton SO14 3ZH

School of Ocean and Earth Sciences
Southampton Oceanography Centre
University of Southampton
Waterfront Campus
European Way
Southampton
Hants SO14 3ZH
UK

Tel: +44 (0)23 8059 6470
Fax: +44 (0)23 8059 3059
Email: D.Paphitis@soton.ac.uk

DOCUMENT DATA SHEET

AUTHOR	*PUBLICATION DATE*
PAPHITIS, D & COLLINS, M B	2001

TITLE

The 5m long recirculating flume at the School of Ocean and Earth Sciences (SOES), University of Southampton. Part I: Descriptive manual.

REFERENCE

Southampton Oceanography Centre Internal Document, No. 68, 72pp. (Unpublished manuscript)

ABSTRACT

This report reviews the relevant properties of an idealised one-dimensional turbulent open-channel flow, for which the 5m long recirculating flume was designed; it includes the concept of boundary layers and the various equations describing the mean flow conditions and shear stress at the bed, for various parts of the layer.

A measurement programme was designed to evaluate the performance of the flume and measure quantities such as, mean velocities, turbulence intensity and velocity spectra. Measured profiles of mean velocity, turbulence intensity and velocity spectra appear to be consistent with theoretical and empirical results obtained elsewhere. Measured spectra, although consistent with expectations over a wide range of frequencies, indicate a few unexpected features, these include oscillations in the velocity records (possibly, the result of small-amplitude standing surface waves within the flume) and the presence of some low-frequency fluctuations in the flume (possibly, due to fluctuations in the power supplied to the pump, or fluctuations due to the mechanical behaviour of the pump itself). These unexpected features were not found to have a significant effect on the mean quantities and low-order statistics, but they may be important in some applications. Shear velocity determinations (using several methods), for sandy beds, have indicated that the single point method of estimating u_* was more consistent than the log-profile method (velocity gradient).

KEYWORDS

LABORATORY FLUME, OPEN CHANNEL FLOWS, SHEAR VELOCITY DETERMINATIONS, UNIDIRECTIONAL FLOW

ISSUING ORGANISATION

Southampton Oceanography Centre
University of Southampton
Waterfront Campus
European Way
Southampton SO14 3ZH
UK

Not generally distributed - please refer to author

Abstract

This Report reviews the relevant properties of an idealised one-dimensional turbulent open-channel flow, for which the 5m long recirculating flume was designed; it includes the concept of boundary layers and the various equations describing the mean flow conditions and shear stress at the bed, for various parts of the layer.

A measurement programme was designed to evaluate the performance of the flume and measure quantities such as, mean velocities turbulence intensity and velocity spectra. Measured profiles of mean velocity, turbulence intensity and velocity spectra appear to be consistent with theoretical and empirical results obtained elsewhere. Measured spectra, although consistent with expectations over a wide range of frequencies, indicate a few unexpected features, these include oscillations in the velocity records (possibly, the result of small-amplitude standing surface waves within the flume) and the presence of some low-frequency fluctuations in the flume (possibly, due to fluctuations in the power supplied to the pump, or fluctuations due to the mechanical behaviour of the pump itself). These unexpected features were not found to have a significant effect on the mean quantities and low-order statistics, but they may be important in some applications. Shear velocity determinations (using several methods), for sandy beds, have indicated that the single point method of estimating u_* was more consistent than the log-profile method (velocity gradient).

Contents

Abstract i
Contents ii
List of Figures iv
List of Tables vi
List of Symbols vii

1. Introduction 1

2. Background 2
2.1 Conditions for One-dimensional Flows 2
2.2 Behaviour of Open-Channel Flows 3
2.2.1 Reynolds Number 3
2.2.2 Froude Number 4
2.2.3 Grain Reynolds Number 4
2.2.4 Flow Regimes 5
2.3 Statistical Description of Turbulent Motion 6
2.4 Distribution of Shear Stress 9
2.4.1 Shear Stress in Laminar Flows 9
2.4.2 Shear Stress in Turbulent Flows 10
2.5 Boundary Layer 12
2.5.1 Thickness and Development of the Boundary Layer 12
2.5.2 Boundary Layer Regions 14
Inner Region 15
Overlap Region 16
Outer Region 20
2.6 Velocity Distribution in Turbulent Flows 20
2.6.1 Hydrodynamically Smooth Surfaces 20
2.6.2 Hydrodynamically Rough Surfaces 24
2.7 Water Depth: A Note 25

3. Experimental Procedure 27
3.1 Flow Characterisation Experiments 27
3.2 Observations and Data Acquisition 27
3.3 Experimental Errors 28

4. Results and Discussion 29
4.1 Accuracy of the Mean Velocity Measurements 29
4.1.1 Sampling Errors 29
4.1.2 Synchronicity of Flow Measurements at Different Levels 29
4.1.3 Positional Error of the LDA and Streamflo 30
4.1.4 Non-uniformity of Flow in the Downstream Direction 31
4.2 Preliminary Experiments 32
4.2.1 Flow Development 32
4.2.2 Mean Velocity Estimations 34
4.2.3 Depth-Averaged Velocities 35
4.2.4 Maximum Velocities 35
4.2.5 Streamflo Positioning 36

4.3 Cross-sectional Character of the Flow **37**
4.4 Vertical Flow Velocity Profiles **43**
4.4.1 Standard Deviation **46**
4.4.2 Longitudinal Turbulence Intensity (LTI) **48**
4.5 Determination of Shear Velocity **51**
4.5.1 Problems with Shear Velocity Determinations **51**
4.5.2 The Log-Profile Method **52**
4.5.3 The Log-Profile Method: An Evaluation **55**
Smooth Boundary **56**
Rough Boundary **57**
4.5.4 Shear Velocity Estimates using the Single Point Method **60**
4.5.5 Detailed Analysis of Mean Velocity Profiles **63**

5. Summary and Conclusions **67**

References **69**

Appendix: Other Methods of Estimating Shear Stress **A-1**
Quadratic Stress Law **A-1**
Reynolds Stress or Eddy Correlation **A-1**
Inertial-Dissipation Method **A-1**
Water Surface and Energy Slope **A-2**
Seventh Power-Law **A-4**

List Of Figures

Figure 1: Depth-velocity relationships for four regimes of open-channel flow (adopted from Robertson and Rouse, 1941).

Figure 2: Typical (schematic) curve showing the correlation (R) between two velocity components at varying distance (r) in a turbulent flow; at large r, the velocity fluctuations become independent of one another and R asymptotes to 0 (R has a maximum value of 1, at r=0).

Figure 3: Definition diagram for the analysis of the mean stress distribution in turbulent one-dimensional open-channel flow (for details see text).

Figure 4: A schematic representation of the transport of momentum due to turbulent velocity fluctuation, in the generation of the Reynolds stress (turbulent shear stress).

Figure 5: Relative contributions of the viscous and turbulent shear stress components to the total shear stress at different heights, throughout the boundary layer (adopted from Tritton, 1988).

Figure 6: Growth of a boundary layer over a flat plate at zero incidence, suspended in a free-stream of velocity U_s; this illustrates the variation in bed shear stress with distance from the leading edge of the plate (adopted form Tritton, 1988).

Figure 7: Use of velocity measurements to illustrate the subdivision of smooth turbulent boundary layer (adopted from Middleton and Southard, 1977).

Figure 8: Schematic representation of the subdivision of smooth and rough turbulent boundary layers (not to scale).

Figure 9: Experimental relationship between B and $\log(u_* k_s/\nu)$, showing the empirical evaluation of C_S and C_R (adopted from Nikuradse, 1933).

Figure 10: Example of a velocity profile in turbulent one-dimensional open-channel flow, derived theoretically, for conditions similar to those encountered in the 5m flume (h=8cm, u_*=2cm/s and ν=0.01cm^2/s). Solid line: complete profile based upon Eqs 41, 43 and 44. Dashed line: logarithmic approximation based upon Eq. 45.

Figure 11: Example of a turbulent boundary layer mean velocity profile over a hydrodynamically smooth velocity profile, plotted on log-linear coordinates; the solid lines correspond to specific equations as indicated, whereas the dashed line shows the trend of data (adopted form Tritton, 1988).

Figure 12: Profiles of mean velocity at various distances along the channel, obtained in the preliminary measurement programme. All measurements were taken along the centreline. The distance from the entrance to the working section is given by x.

Figure 13: Running average $\hat{u}(t_+)$, as defined by Eq. 54, as a function of the averaging time t_+. The vertical axis is the departure of the running average from the mean of the total record, normalised by the mean of the total record.

Figure 14: Possible flow velocities, that can be generated in the flume, at different water depths.

Figure 15: Diagram illustrating Streamflo positional effect on the recorded LDA velocity measurements.

Figure 16: Cross-sectional diagram of the flume (looking downstream) showing the grid sampling system.

Figure 17: Lateral variations in the mean velocity (u, cm/s), with distance (y, cm) across the flume. z is the elevation above the bed, • RHS and o LHS (looking in a downstream direction).

Figure 18: Vertical variations in the mean velocity (u, cm/s), with elevation (z, cm). y is the distance across the flume, • RHS and o LHS (looking in a downstream direction).

Figure 19: The general pattern of velocity distribution within the flume; the contours represent equal velocities in the channel section.

Figure 20: Mean velocity (u, cm/s) variations with elevation (z, cm) for the various flow rates. The identification given to the profiles is such that S (slow), M (moderate) and F (fast) relate to the flow rate, whereas R (rough) and S (smooth) relate to the boundary state (i.e. MR1 is the first profile under moderate flow rate over a rough boundary).

Figure 21: Mean velocity (u, cm/s) variations with elevation (z, cm) for the various flow rates, plotted on a semi-logarithmic scale.

Figure 22: Standard deviation (σ, cm/s) variations, with elevation (z, cm), for the various flow rates (plotted on a semi-logarithmic scale).

Figure 23: LTI variations, with elevation (z, cm), for the various flow rates (plotted on a semi-logarithmic scale).

Figure 24: LTI variations, with elevation (z, cm), scaled to flow depth (h, cm) for the various flow rates (plotted on a linear scale).

Figure 25: Mean velocity (u, cm/s) variations with elevation (z, cm) for the various flow rates over the smooth boundary. The Figure shows the u_* isovels for the smooth-wall law and zu_*/ν contours (plotted on a semi-logarithmic scale); u_* isovels calculated from Eq. 45, with κ=0.4, C_S=5.5 and ν=0.0114cm^2/s.

Figure 26: Mean velocity (u, cm/s) variations with elevation (z, cm) for the various flow rates over the rough boundary, illustrating the u_* isovels for both the smooth-wall law (dashed lines, with italic labels) and the rough-wall law (solid lines, with normal labels), plotted on a semi-logarithmic scale. u_* isovels calculated from Eqs 45 and 49, respectively, with κ=0.4, C_S=5.5, k_s=0.0651cm, C_S=8.5 and ν=0.0114cm^2/s.

Figure 27: Shear velocity (u_*, cm/s), as a function of the grain effective roughness (k_s, cm). Re$_*$ (u_*k_s/ν) isovels (at 15°C) are also included, indicating the surface classification limits (Re$_*$=3.42 isovel, at 15°C is also included).

Figure 28: A comparison of u_* estimates derived from the smooth- (dashed line) and rough- (solid line) wall laws (Eqs 45 and 49, respectively), based upon $u_{0.5}$ and $u_{2.5}$ (κ=0.4, C_S=5.5, k_s=0.0651cm, C_S=8.5 and ν=0.0114cm^2/s).

Figure 29: u_* profiles derived from the single observation method according to various relationships ((+) Eq. 45; (×) Eq. A-9; and (-) Eq.49): (a) over the smooth boundary; and (b) over the rough boundary.

Figure 30: Mean velocity profiles for the various flow rates over the smooth boundary. Solid line: semi-empirical expression based upon Eqs 41, 43 and 44.

Figure 31: Mean velocity profiles for the various flow rates over the rough boundary. Solid line: semi-empirical expression based upon: (a) the hydrodynamically smooth boundary equations (Eqs 41, 43 and 44); and (b) the hydrodynamically rough boundary equations (Eqs. 47, 48 and 44).

Figure A-1: Definition sketch for the surface water slope associated with bed shear stress. Key to symbols: F_u is the upstream hydrostatic force, F_d is the downstream hydrostatic force, W is the resultant gravitational force, L is the selected unit length, γ_f is the specific gravity of water, γ_a is the specific gravity of air, A is the cross-sectional area, a is the angle of slope and τ_o is the bed shear stress.

Figure A-2: Definition sketch for the energy head associated with bed shear stress. Key to symbols: h_v kinetic head (=[$v_A^2/2g$] where v_A is the kinematic viscosity and g is the acceleration due to gravity), $D + Z$ add to give the potential head (where D is the density slope and Z the seabed slope).

List of Tables

Table 1: Comparative results between the different methods for estimating shear velocity.
Table 2: Shear velocity estimations, using the 'profile-fitting method'.

List Of Symbols

b	-	channel width
h	-	water depth
τ_o	-	bed shear stress
ρ	-	fluid density
ν	-	kinematic fluid viscosity
g	-	gravitational acceleration
k_s	-	grain effective roughness
u_*	-	critical shear velocity
U	-	depth-averaged mean flow velocity
Re	-	Reynolds number
F	-	Froude number
Re_*	-	grain Reynolds number
A	-	a constant (usually taken to be 11.6)
δ_v	-	viscous sublayer thickness
u, v, w	-	instantaneous local velocity components in the x, y and z directions
x, y, z	-	downstream, cross-stream and vertical orthogonal directions
$\overline{u}, \overline{v}, \overline{w}$	-	temporal mean values of velocity
u', v', w'	-	instantaneous fluctuating components of velocity
$\overline{p}$	-	temporal mean values of pressure
p'	-	instantaneous fluctuating component of pressure
σ	-	standard deviation (or root mean square RMS)
SE	-	standard error
LTI	-	longitudinal turbulent intensity
q	-	total turbulent intensity
$\overline{u'^2}, \overline{v'^2}, \overline{w'^2}$	-	mean square velocity fluctuations
Y	-	intermittency factor of a turbulent event
E	-	kinetic energy per unit volume
Sk	-	skewness
Kr	-	kurtosis
$\overline{u_1' u_2'}$	-	correlation between two velocity fluctuations u_1' and u_2'
R	-	correlation coefficient
u_1', u_2'	-	simultaneous values of the same velocity component
r	-	distance separating u_1' and u_2'
θ	-	boundary slope
τ_z	-	bed shear stress at elevation z
z	-	elevation above the bed
du/dz	-	velocity gradient
u_z	-	mean flow velocity at elevation z
C	-	constant of integration
δ	-	boundary layer thickness
X	-	distance from the leading edge of the boundary
U_s	-	free-stream velocity
l	-	Prandtl's mixing length
κ	-	von Karman's constant (dimensionless)
z_o	-	bed roughness length

C_z	-	Chézy coefficient
I	-	water surface slope
B	-	dimensionless property of the flow in the vicinity of the bed
C_S	-	empirical constant for hydrodynamically smooth flow regimes
C_R	-	empirical constant for hydrodynamically rough flow regimes
z_s	-	elevation defining the lower limit of the outer region
P	-	empirical constant related to the suspended sediment concentration
$f(zu_*/\nu)$	-	empirical wall function
$W(z/h)$	-	empirical expression for the wake correction
α, β	-	empirical constants (in this Report, 7.8 and 11, respectively)
Π	-	Coles empirical parameter
D	-	grain diameter
T	-	longest period of fluctuation
L	-	length scale
$\hat{u}(t_+)$	-	running average of the flow velocity
t_+	-	averaging time
u_y	-	lateral mean velocity variations
du_y/dy	-	velocity gradient of the lateral profiles
m	-	slope of the line
b	-	intercept value on $\log(z)$ axis
C_D	-	drag coefficient
θ_τ	-	direction of mean stress, with respect to the flow
ε	-	rate of energy dissipation
$\Delta\gamma$	-	difference in specific gravity between air and water
R	-	hydraulic radius

Acknowledgements

The authors would like to thank Mrs K. Davis for her help in the preparation of some of the Figures.

I. Introduction

Artificial channels are those constructed or developed by human effort; the flume facility of the School of Ocean and Earth Science, University of Southampton is considered an artificial open channel. The hydraulic properties of such channels can be controlled either to the extent desired, or designed to meet certain requirements. The application of hydraulic theories to artificial channels will produce, therefore, results representative of natural conditions; hence, they are reasonably accurate for simulating and characterising natural environmental conditions.

This report presents the results of a measurement programme designed to evaluate the performance of the 5m flume, located in the School of Ocean and Earth Science (SOES, University of Southampton), in the Southampton Oceanography Centre. A companion report (Paphitis and Collins, 2001) provides a comprehensive description of the flume facility, the associated hardware and instrumentation, the data acquisition and processing software and guidelines for operation.

The 5m flume is designed to produce steady uniform flows, the mean properties of which are approximately independent of time (steady), independent of along-channel position (uniform) and independent of cross-channel position (large depth to width ratio, suggesting that the side boundaries can have no effect on the area of flow under investigation i.e. the centerline of the channel). Such flows can be considered one-dimensional, in the sense that the mean quantities depend only upon a single spatial coordinate (away from the boundary, vertically upwards). The measurement programme described here was designed to determine whether the unidirectional flow characteristics within the 5m flume can, in fact, be approximated to an one-dimensional flow, with the expected properties. The report aims to set up a framework, in terms of flow characteristics, for sediment investigations. Hence, a mixture of both smooth and rough boundary conditions is examined under slow, moderate and fast flow rates. An evaluation of different ways in which the shear velocity can be calculated, depending on the flow conditions, is also presented. The measurements described in this report were obtained with a Laser Doppler Anemometer (LDA) and a Streamflo impeller current meter (for more details, see Paphitis and Collins, 2001).

2. Background

The prediction of sediment transport (initiation of movement, subsequent transport as bed-load or suspended-load and eventual sedimentation) by unidirectional flows requires an in-depth understanding of the interaction of fluid with the erodible material of its confining boundaries. For one-dimensional turbulent experimental flows in an open channel, such as those for which the 5m flume has been designed, where clear water flows over a (fixed) smooth or rough bottom boundary, the basic properties are well established on the basis of classical analysis (e.g. Clauser, 1956; Coles, 1956) and experimental studies (e.g. Nezu and Rodi, 1986). An extensive literature is available on the characteristics of such flows (e.g. Hinze, 1975; Townsend, 1976), with less rigorous accounts orientated towards sedimentological applications (e.g. Komar, 1976; Raudkivi, 1976). This report presents a brief outline of the features of such flows, considered to be most relevant to the subsequent designed measurement programme.

2.1 Conditions for One-dimensional Flows

Steady uniform flow is the fundamental characteristics of open channel hydraulics. Open-channel flows are said to be steady if the depth of the flow does not change, or if it can be assumed to be constant during the time interval under consideration; it is uniform if the depth of the flow is the same at every section of the channel. The mean properties of such flows are, therefore, approximately, independent of both time and space (along-channel). However, for the flow to be approximated to one-dimensional, the open channel must be both sufficiently long and wide; the former is to allow the vertical flow structure to fully develop from the poorly constrained conditions at the channel entrance, whereas the latter is to eliminate the effects of the side walls on the flow near the centreline. Turbulent boundary layer theory (e.g. Schlichting, 1979) suggest that the vertical structure of a turbulent open-channel flow is fully developed at distances greater than roughly 50 water depths downstream of the channel entrance. Based upon laboratory measurements, Nakagawa *et al.* (1983) have suggested that a turbulent open-channel flow is independent of cross-channel position, at distances away from the channel centreline of less than about $(h/2)[(b/h)-4]$, where b is the channel width and h is the water depth. It can be concluded that the 5m flume can, in fact, produce a section (about 4m from the channel entrance) in which the flow is approximately one-dimensional near the channel centreline, provided that the water depth is less than about 8cm.

2.2 Behaviour of Open-Channel Flows

The state or behaviour of steady one-dimensional turbulent flow in an open channel is governed primarily by the effects of viscosity and gravity, relative to the inertial forces of the flow. Water surface tension may also affect the behaviour of flow under certain circumstances, but it does not play a significant role in most open-channel applications that are anticipated in the 5m flume. Therefore, the statistical properties of such flows are determined 'in principle' completely by the bed shear stress (τ_o), the fluid density (ρ), the kinematic fluid viscosity (ν), the gravitational acceleration (g), the fluid depth (h) and the bottom characteristics (e.g. k_s, the grain effective roughness). Through the use of dimensional analysis and dynamic similarity, these variables can be combined to form dimensionless groups to characterise the flow; this approach is extremely important as it reduces the number of variables involved. Three-dimensional parameters are defined as follows:

Reynolds number: $$\mathrm{Re} = \frac{U\,h}{\nu} \tag{1}$$

Froude number: $$\mathrm{F} = \frac{U}{\sqrt{gh}} \tag{2}$$

Grain Reynolds number: $$\mathrm{Re}_* = \frac{u_*\,k_s}{\nu} \tag{3}$$

where $u_* = \sqrt{\tau_o/\rho}$ is the critical shear velocity at sediment threshold conditions and U is the depth-averaged mean flow velocity which is a function of τ_o, ρ, ν, g, h and k_s.

2.2.1 Reynolds Number

The Reynolds number (Re) represents the effect of viscous, relative to inertial, forces in the large-scale energy-containing eddies. If the Re is sufficiently small, the nature of the flow is stable where the water particles appear to move in definite smooth paths; this condition is termed laminar flow. When the Re exceeds a certain value, instability occurs and the fluid develops vorticity and the flow degenerates into a relatively disordered, chaotic condition termed turbulent flow; in this case, the water particles no longer follow straight trajectories but random fluctuating motions. The changeover from laminar to turbulent flow conditions occurs progressively, over a range of Re values, within which the flow is said to be in a mixed or transitional state. The transitional range in open-channel flows is not so well defined as it is for pipe flows (where the flow depth is taken as the characteristic length, the corresponding Re range is from 500 to 12500 whilst, in the cases where the diameter is used, the upper value may

be as high as 50000). In open-channel flow, the lower critical Re depends (to some extent) on channel shape, but the value varies between 500 to 600; it is generally larger than the value for pipe flows. For practical purposes, the transitional range of Re for open-channel flows may be assumed to be 500 to 2000. However, it should be noted that the upper value is arbitrary, since there is no definite upper limit for all flow conditions.

2.2.2 Froude Number

The Froude number (F) is the ratio of inertial to gravity forces; it represents the effect of gravity upon the state of flow. In the mechanics of water waves, the velocity $\sqrt{gh}$ is identified as the celerity of the small gravity waves that occur, in shallow water in channels, as a result of any momentary change in the local depth of the water. Such a change may be developed by disturbances (or obstacles) in the channel, that cause a displacement of water above and below the mean surface level; thus, creating a weight or gravity force. If F is equal to unity, the flow is said to be in a critical state. If F is less than unity, the flow is subcritical; in this state, the role played by gravity is pronounced, so the flow has a low velocity and is often described as tranquil and streaming. If F is greater than unity the flow is supercritical; in this state, the inertial forces become dominant, so the flow has a high velocity and is usually described as rapid, shooting and torrential. For the conditions assumed in this report, for the development of an one-dimensional turbulent open-channel flow, the Froude number does not have a significant effect on the vertical structure of the flow; however, it remains an important parameter for characterising the flow.

2.2.3 Grain Reynolds Number

The grain Reynolds number (Re_*) is proportional to the ratio of the grain diameter to the thickness of the viscous sublayer. It has been shown (Sleath, 1984) that the shear velocity is related to the thickness of the viscous sublayer, through $\delta_v = A\nu/u_*$, where A is a constant (usually taken to be 11.6). Substituting into Eq. 2, then

$$\mathrm{Re}_* = A\frac{k_s}{\delta_v} \tag{4}$$

This ratio between grain effective roughness height (k_s) and the thickness of the viscous sublayer (δ_v), illustrates the functional importance of the grain Reynolds number, to provide an indication of the degree of grain protrusion through the viscous sublayer; this is important in defining whether turbulent eddies are produced and the nature of the boundary layer flow (see below, Section 2.5). If the Re_* is less than about 5, the bottom roughness has no significant effect on the

flow, so that the bottom is effectively smooth. If the Re_* is greater than about 70, the viscous sublayer is completely disrupted; at such times, the viscosity has very little direct effect on the mean flow or the large-scale fluctuations. The progressive conversion from smooth to rough boundary conditions, within the range $5<Re_*<70$ is termed 'transitional'. These conditions were suggested by Colebrook and White (1937) (and, later, by Schlichting, 1979), in connection with flow in pipes, considered to be a good approximation for channels (see Section 2.5).

2.2.4 Flow Regimes

The combined effect of viscosity and gravity (Re and F, respectively) may produce any one of four regimes of flow in an open channel, namely: (a) Laminar-Subcritical (F<1, Re<500); (b) Laminar-Supercritical (F>1, Re<500); (c) Turbulent-Subcritical (F<1, Re>2000); and (d) Turbulent-Supercritical (F>1, Re>2000). The depth-velocity relationship for the four flow regimes in an open channel can be shown by a logarithmic plot (Figure 1). The heavy line for F=1 and the envelope for the laminar-turbulent transitional range (500<R<2000, shown by the two heavy lines) intersect on the graph and divide the whole area into four portions, each of which represents a flow regime.

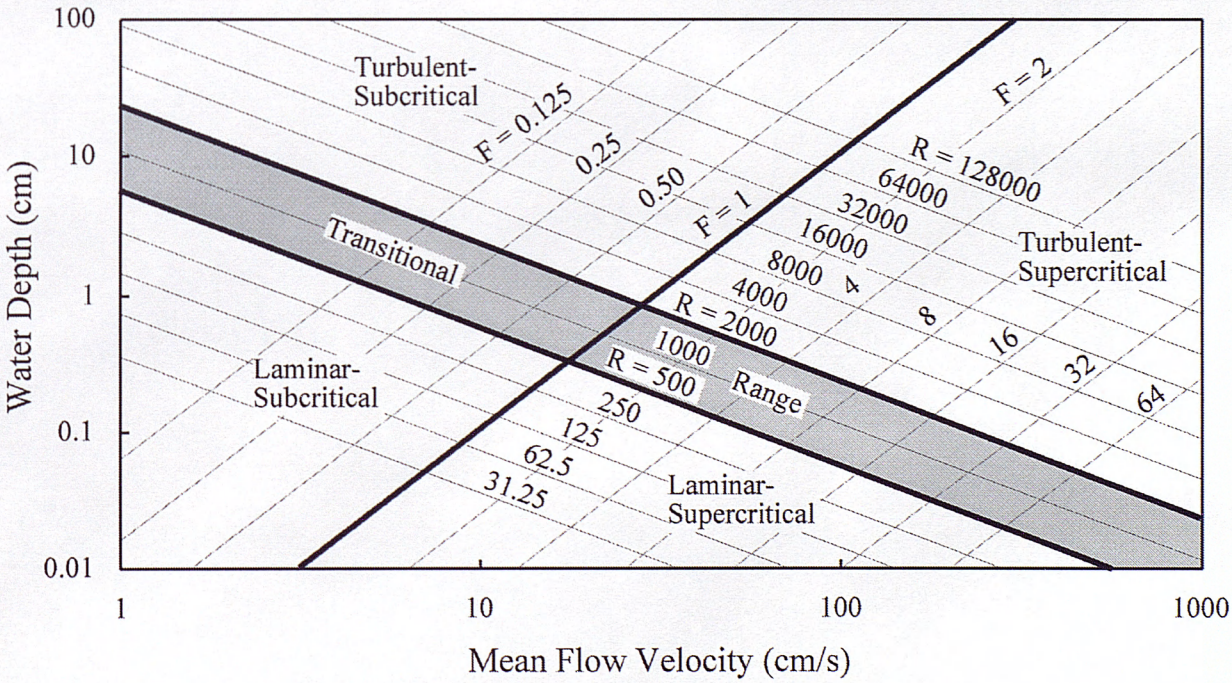

Figure 1: Depth-velocity relationships for four regimes of open-channel flow (adopted from Robertson and Rouse, 1941).

2.3 Statistical Description of Turbulent Motion

Most natural flows are characterised by irregular velocity fluctuations indicating turbulence. The structure of such turbulent flows has been studied by various authors (e.g. Schlichting, 1979; Townsend, 1976), who suggested that (in describing the flow mathematically) it is convenient to separate the velocity and pressure field, into mean and fluctuating parts. Using Cartesian co-ordinates, the mean flow velocity at any one instance and at any point in the flow may be represented by the sum of the instantaneous local velocity components, u, v and w in the three respective x (downstream), y (cross-stream) and z (vertically) orthogonal directions, such as:

$$U = u + v + w \tag{5}$$

Each of the instantaneous components of velocity can be represented by the sum of a temporal mean value and an instantaneous fluctuating component:

$$u = \bar{u} + u' \quad \text{(similarly } v = \bar{v} + v' \text{ and } w = \bar{w} + w'\text{)} \tag{6}$$

and pressure,

$$p = \bar{p} + p' \tag{7}$$

In a steady, one-dimensional turbulent flow the time-averaged velocities in the y and z directions will be zero. The turbulent fluctuations of velocity represent the deviations of the instantaneous components from the time-averaged value; because these are both positive and negative, they average out to zero; when the mean is taken. Such velocity fluctuations are, therefore, the random portions of the turbulent flow and are found, in general, to follow a Gaussian distribution (Hinze, 1975). Hence, the distribution of n measurements of the fluctuating components of velocity, over a sufficiently long period of time may be treated statistically (e.g. Monin and Yaglom, 1971 and 1975; Yalin, 1972; Hinze, 1975). The time-averaged values at a fixed point in space, over an extended period of time (long, in comparison to the time scale of the turbulent fluctuations) can be obtained:

$$\bar{u} = 1/n \sum_{1}^{n} u \tag{8}$$

The spread of the values about the mean is termed the standard deviation and is defined by:

$$\sigma^2 = 1/(n-1) \sum_{1}^{n} u'^2 \tag{9}$$

σ is sometimes termed the root mean square (RMS) of the turbulent fluctuation component and is considered as a good measure of their intensity. A measure of the reliability of the estimated mean is given by the standard error (SE):

$$SE = \sigma / \sqrt{n} \tag{10}$$

The relative longitudinal turbulent intensity (*LTI*), at a point, can be derived from:

$$LTI = \sigma/\bar{u} \quad \text{or} \quad \sigma/u_* \tag{11}$$

The total turbulent intensity (q) is given by:

$$\left(\bar{q}^2\right)^{1/2} = \left(\overline{u'^2} + \overline{v'^2} + \overline{w'^2}\right)^{1/2} \tag{12}$$

where $\overline{u'^2}$, $\overline{v'^2}$ and $\overline{w'^2}$ are the mean square fluctuation. The scales of the turbulent fluctuations may be estimated by defining an intermittency factor Y of a turbulent event (Anwar, 1981), given by:

$$\mathrm{Y} = \frac{\text{total duration of turbulent events}}{\text{total record duration}} \tag{13}$$

The difficulty in measuring Y from a time-series of a continuously fluctuating variable is caused by the ambiguity in defining an event. The kinetic energy per unit volume (E), produced by these fluctuations is given by:

$$E = 0.5\rho\, \bar{q}^2 \tag{14}$$

Other useful characteristics of a distribution are the skewness (Sk), which is a measure of the asymmetry of the distribution of a variable (zero is for normal or Gaussian distributions):

$$Sk = \frac{1}{n}\left(\sum_1^n u'^3 \Big/ \sigma^3\right) \tag{15}$$

and kurtosis (Kr), which is a measure of the flatness of the distribution;

$$Kr = \frac{1}{n}\left(\sum_1^n u'^4 \Big/ \sigma^4\right) \tag{16}$$

For normal distributions, Kr is equal to 3; a value less than 3 indicates a flat distribution, whilst a value greater than 3 indicates a peaked distribution. A peaked distribution of velocity fluctuations is an indication of intermittency of fluctuations (Heathershaw and Simpson, 1978; Anwar, 1981).

Information about velocity fluctuations at different points (or times) is given by correlation measurements. The correlation between two velocity fluctuations u_1' and u_2' is defined as $\overline{u_1' u_2'}$ and the correlation coefficient (Tritton, 1988) as:

$$\mathrm{R} = \overline{u_1' u_2'} \Big/ \left(\overline{u_1'^2\, u_2'^2}\right)^{1/2} \tag{17}$$

where u_1' and u_2' are simultaneous values of the same component of the velocity, at two different points separated by a distance r; the correlation coefficient depends upon the magnitude and direction of the separation r (Figure 2). If the correlation coefficient is zero, then there is no

correlation between the two points and the fluctuations will be independent of one another. However, complete independence, particularly for fluctuations at points relatively close to one another, is unlikely. In the case where velocity measurements are made at the same point, but at different times, then R is said to be an auto-correlated coefficient. Correlation of velocity measurements at two different points and times are also possible. Here, R is referred to as a space-time correlation, providing information on the trajectories of turbulent associated features.

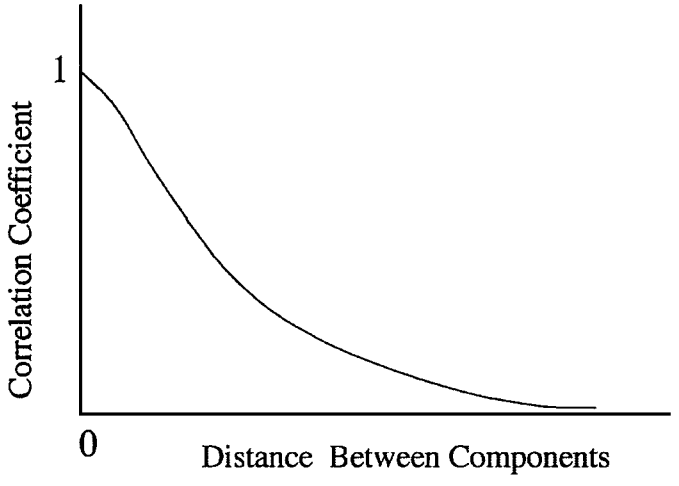

Figure 2: Typical (schematic) curve showing the correlation (R) between two velocity components at varying distance (r) in a turbulent flow; at large r, the velocity fluctuations become independent of one another and R asymptotes to 0 (R has a maximum value of 1, at r=0).

The fluctuations in velocity play an important role in sediment transport studies, especially upon the initiation of motion. Several definitions have been provided in the foregoing discussion, providing some idea of the magnitude of these fluctuations. However, in natural flows, velocity fluctuations constitute a complicated phenomenon, hence, an adequate approximation of them using some of the above coefficients, is a very considerable task. The velocity fluctuations are considered as a random phenomenon and, as such, it can be argued that processes (like the threshold of sediment motion and subsequent transport) are governed by such random effects. Such effects can be described in terms of probability theory, rather than by numerical and deterministic relationships.

2.4 Distribution of Shear Stress

2.4.1. Shear Stress in Laminar Flows

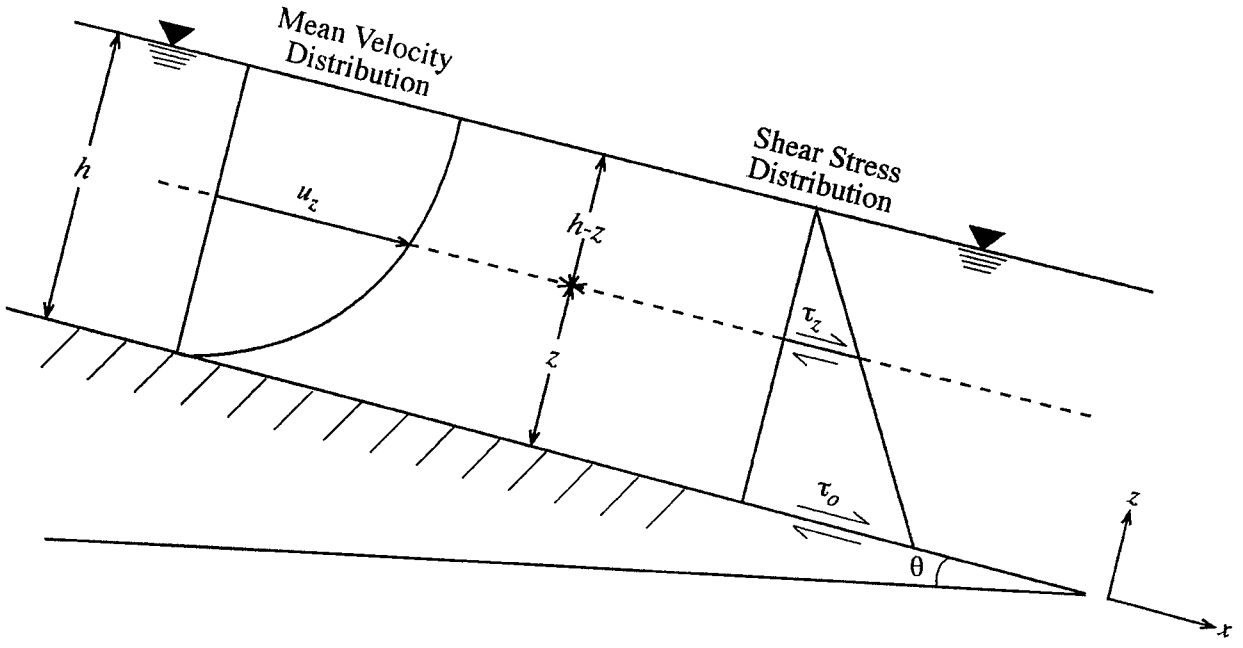

Figure 3: Definition diagram for the analysis of the mean stress distribution in turbulent one-dimensional open-channel flow (for details see text).

With reference to Figure 3, the shear stress (τ_o, dynes/cm^2) at the boundary exerted by the overlying fluid, is given by:

$$\tau_o = \rho g \sin(\theta) h \tag{18}$$

where θ is the slope of the boundary. Similarly, the shear stress of the fluid, overlying some imaginary plane parallel to the boundary and at a variable distance above it, can be expressed by:

$$\tau_z = \rho g \sin(\theta)(h - z) \tag{19}$$

and the stress at level z above the bed, in terms of τ_o, is given by:

$$\tau_z = \tau_o (1 - z / h) \tag{20}$$

The shear stress varies linearly, from zero at the surface to a maximum value at the boundary (Eq. 18). Consequently, the viscous shear at any point in a sheared fluid is related to the velocity gradient (du/dz), normal to the shear surface, by:

$$\tau_z = \rho \nu (du / dz) \tag{21}$$

Combining Eqs 20 and 21 give an expression for the velocity gradient, in terms of the bed shear stress, at any level:

$$du / dz = \tau_o (1 - z / h) / \rho \nu \tag{22}$$

The velocity at elevation z (u_z) is derived by integration of Eq. 22, with respect to z:

$$u_z = \frac{\tau_o z}{\rho \nu}(1 - z/2h) + C \tag{23}$$

Applying the 'no-slip' condition, which requires that the fluid in immediate contact with a solid boundary is stationary, the constant of integration (C) is found to be zero. Losing C and using the relationship of shear velocity $u_* = \sqrt{\tau_o/\rho}$ to substitute τ, Eq. 23 becomes:

$$\frac{u_z}{u_*} = \frac{u_* z}{\nu}(1 - z/2h) \tag{24}$$

Close to the boundary, where $z \ll h$, Eq. 24 reduces to:

$$\frac{u_z}{u_*} = \frac{u_* z}{\nu} \tag{25}$$

Both terms (u_z/u_* and $u_* z/\nu$) are dimensionless variables; the right hand side of Eq. 25 is the Reynolds number (Eq. 1, see Section 2.2.1). The above analysis applies to steady, one-dimensional open-channel flows above smooth beds, where the bottom stress is wholly a viscous shear stresses.

2.4.2 Shear Stress in Turbulent Flows

The transport of fluid, by turbulence, generates stresses on a much larger scale than the viscous stresses caused by molecular interaction. The mean distribution of shear stress caused by bed friction, within a turbulent boundary layer, is represented adequately by Eq. 20. The shape of the mean velocity profile differs from that given by Eq. 24, due to the presence of turbulent stresses.

The mean momentum flux across an arbitrary level z in one-dimensional flows, with positive mean velocity gradient ($du/dz > 0$) is $\rho\,\overline{u'w'}$ (where u' and w' are the velocity fluctuations in the x and z directions, respectively and the overbar denotes a mean). This turbulent shear stress is termed the Reynolds stress; it represents the transfer of mechanical energy from the flow to the turbulence, in the presence of a persistent mean velocity gradient. In reality, $\overline{u'w'}$ is negative, so that the mean momentum flux extracts momentum from the mean flow. Over a time period longer than the time-scale of the turbulent fluctuations, the average downstream momentum of the fluid (convected downward across the plane) will exceed that convected upwards. Figure 4 illustrates the generation of Reynolds stress, within a mean velocity gradient. If a particle of fluid travels vertically upwards, then the fluctuating vertical component of velocity (v') will be positive, whereas the fluctuating horizontal component (u') will be negative. This pattern exists

because the particle arrives at the new location, with a velocity less than the average of its new surroundings. Therefore, the total mean shear stress (τ_z) across a sharing plane (at an arbitrary level z) will be the result of both the Reynolds stress (actually, a mean momentum flux due to turbulent velocity fluctuations, which acts like a stress) and the viscous shear stress:

$$\tau_z = \rho g \sin(\theta)(h-z) = \rho \nu \frac{d\bar{u}}{dz} - \rho \overline{u'w'} \tag{26}$$

Using Eq. 18 (the bed shear stress) and rearranging, Eq. 26 may be written alternatively as:

$$\tau_o \left(1-\frac{z}{h}\right) = \rho \nu \frac{d\bar{u}}{dz} - \rho \overline{u'w'} \tag{27}$$

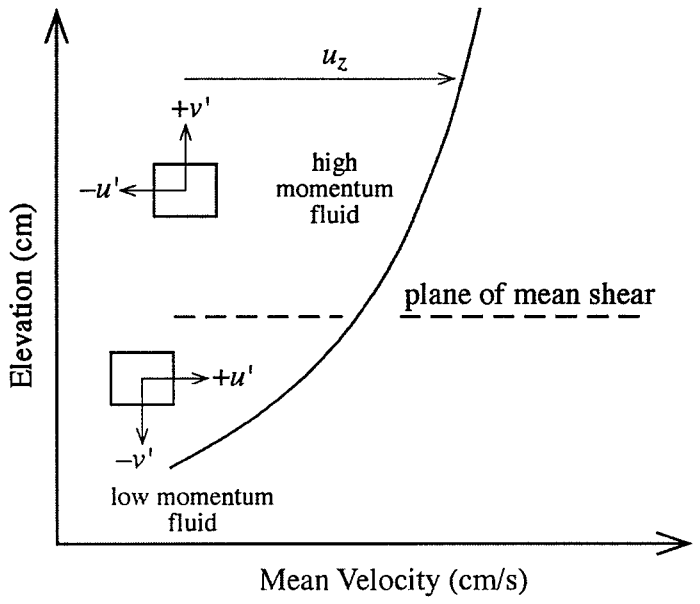

Figure 4: A schematic representation of the transport of momentum due to turbulent velocity fluctuation, in the generation of the Reynolds stress (turbulent shear stress).

The relative contributions of the viscous and turbulent shear stress, throughout the flow depth, are illustrated in Figure 5. The Reynolds stress accounts for the majority of the total stress, throughout most of the turbulent boundary layer. Damping of vertical velocity fluctuations close to the boundary (the no-slip condition) means that, here, the Reynolds stresses mush also approach zero; thus, the viscous stress term becomes the major component close to the bed, as in laminar flows (Eq. 22). However, well away from the boundary (z greater than about $50\nu/u_*$), the viscous stress term becomes increasingly smaller, so that Eq. 27 can be approximated to:

$$\tau_o \left(1-\frac{z}{h}\right) \cong -\rho \overline{u'w'} \tag{28}$$

This relationship indicates that, within this region, the Reynolds stress varies linearly with z.

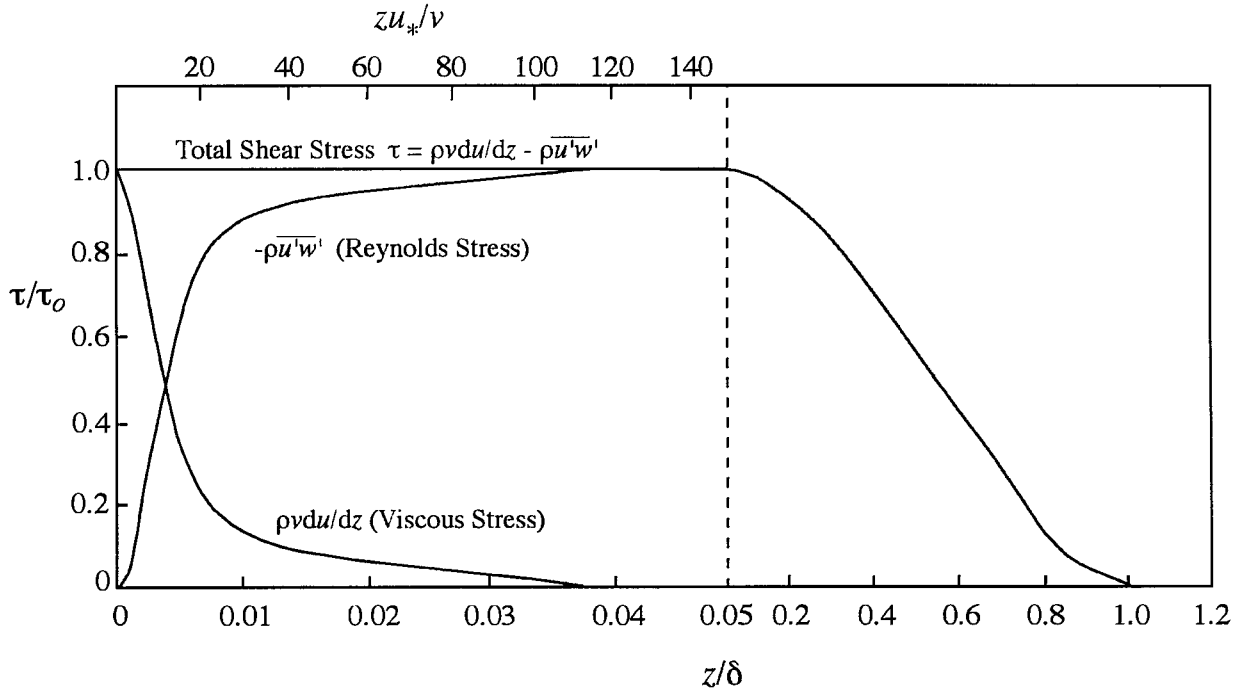

Figure 5: Relative contributions of the viscous and turbulent shear stress components to the total shear stress at different heights, throughout the boundary layer (adopted from Tritton, 1988).

2.5 Boundary Layer

2.5.1 Thickness and Development of the Boundary Layer

Assuming that the flow is laminar and of uniform velocity distribution, with no initial disturbances neither to the flow nor to the water surface, with an indefinitely large flow depth and constant roughness the velocity distribution will have a definite pattern. The velocity field will be diminished in a thin, downstream thickening zone, adjoining the boundary (Figure 6); this region is known as the boundary layer. The velocity within the boundary layer changes continuously normal to the boundary; at first, it increases rapidly and then more slowly. This change takes place as the velocity reaches 99% of the free-stream velocity at a distance away from the boundary, defined as δ (the boundary layer thickness). The effect of the boundary layer on to the flow is equivalent to the viscous (or frictional) forces, which become increasingly important toward the boundary because of the no-slip condition. Such a relationship means that the fluid velocity in immediate conduct with the solid boundary has the same tangential component of velocity as the boundary itself (i.e. stationary). The boundary layer thickness approximates to:

$$\delta \approx \left(\frac{X\nu}{U_s}\right)^{1/2} \quad \Rightarrow \quad \frac{\delta}{X} \approx \left(\frac{U_s X}{\nu}\right)^{-1/2} = \mathrm{Re}^{-1/2} \tag{29}$$

where X is the distance from the starting point of boundary layer development, ν is the kinematic viscosity, U_s is the free-stream velocity and Re is the Reynolds number (using X as the characteristic length). The value of Re is influenced strongly by the turbulent intensity, within the free-stream, and by the plate roughness. Over roughened (as opposed to smooth) beds, the boundary layer grows more rapidly and transition from laminar to highly turbulent conditions occurs much sooner, as a result of the enhanced vertical diffusion of momentum. At the beginning, the flow is entirely laminar and a laminar boundary layer is developed along the boundary surface; the velocity distribution in the layer is approximately parabolic. At a critical distance downstream from the initial point of boundary layer development, small-scale fluctuations appear in the laminar flow. The fluctuations occur at a Reynolds number of ~890 (Sleath, 1984), which mark the introduction of the transitional (neither laminar nor turbulent) stage of the boundary layer. These small-scale fluctuations evolve very quickly into larger turbulent eddies, known as vortices; at the same time, the boundary layer thickens rapidly. At this stage, the boundary layer is said to be fully turbulent, with a Reynolds number of ~5000 (Sleath, 1984). The boundary layer continues to grow until, eventually, it extends over the whole of the flow field; it is then said to be 'fully developed'. Thereafter, the velocity distribution will have a definite pattern, which can be shown analytically to be approximately logarithmic.

Within the upper part of the boundary layer, the Reynolds stress reduces the mean velocity gradient (i.e. the flow is effectively inviscid) to below that which would occur in a corresponding laminar flow. However, on approaching the boundary, the momentum is consumed increasingly by high shear resistance force, in order to maintain the 'no-slip' condition (when in contact with the boundary); this region is termed the viscous sublayer.

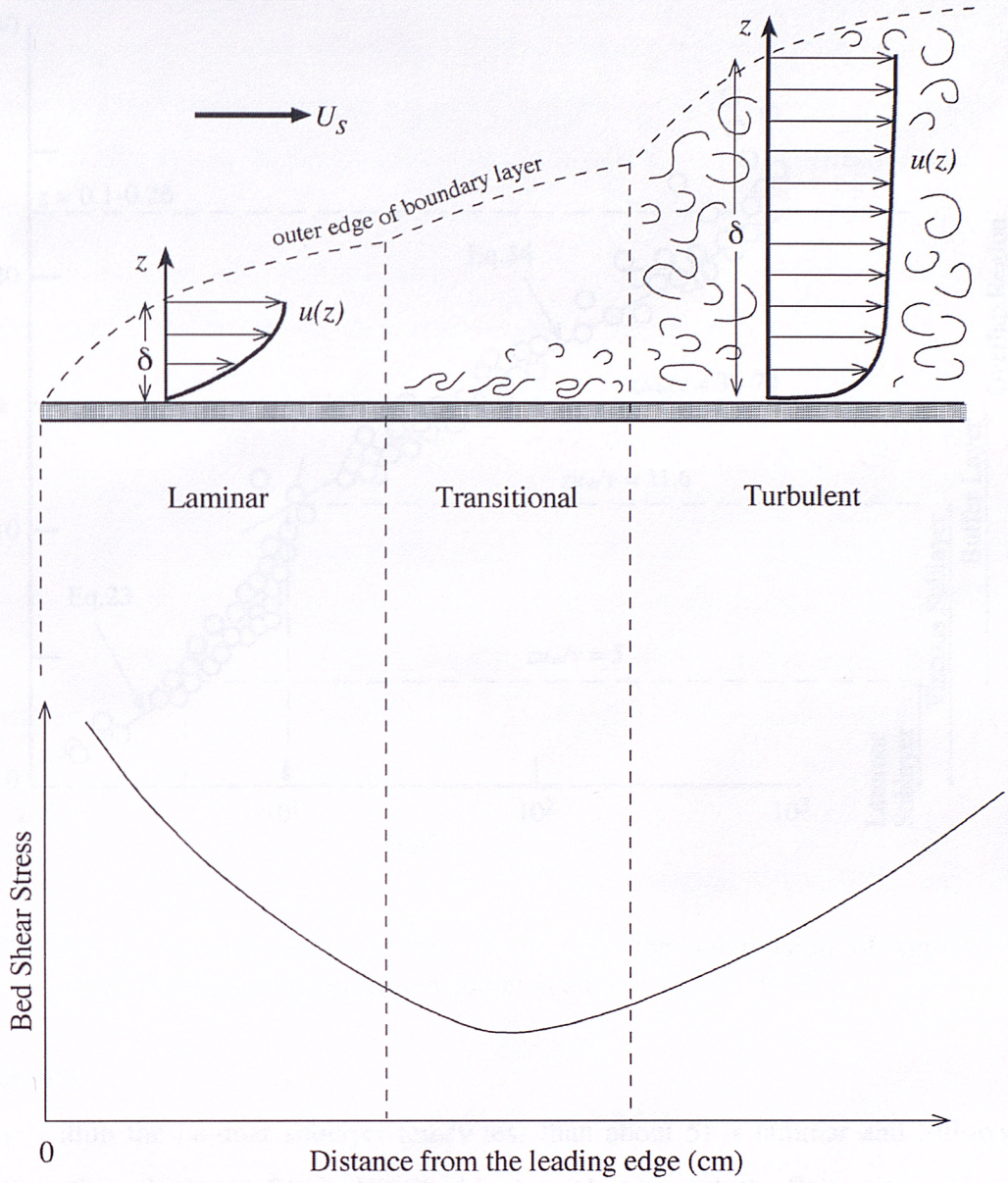

Figure 6: Growth of a boundary layer over a flat plate at zero incidence, suspended in a free-stream of velocity U_s; this illustrates the variation in bed shear stress with distance from the leading edge of the plate (adopted form Tritton, 1988).

2.5.2 Boundary Layer Regions

The boundary layer in turbulent flows is split usually into three regions, namely: (a) an inner region which is further subdivided into the laminar sublayer, viscous sublayer and buffer layer; (b) an overlap region, also known as the constant stress layer or the logarithmic layer; and (c) outer region, also known as the free stream layer. Figure 7 shows a series of velocity measurements made in turbulent flows in smooth pipes; this pattern is consistent with that for open-channel flows (Middleton and Southard, 1977).

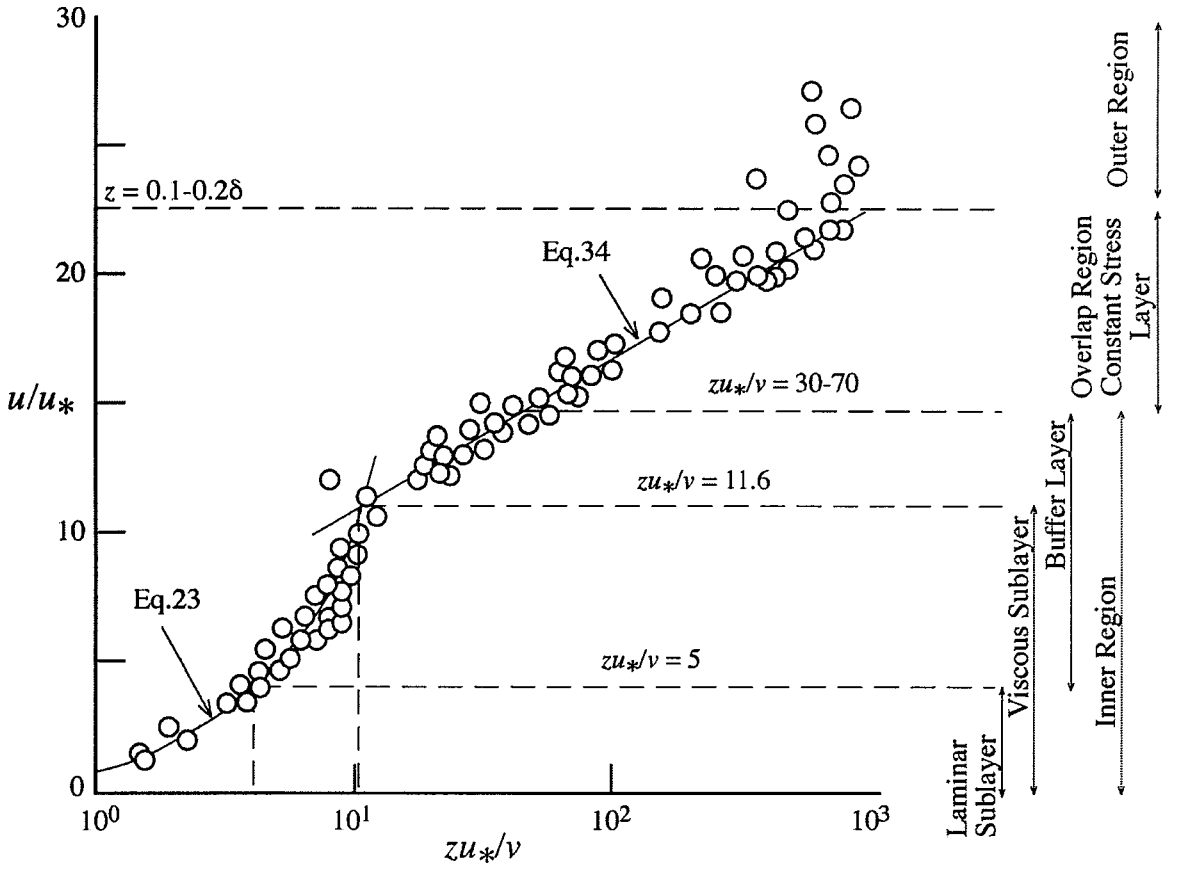

Figure 7: Use of velocity measurements to illustrate the subdivision of smooth turbulent boundary layer (adopted from Middleton and Southard, 1977).

Inner Region

The flow within the laminar sublayer (zu_*/ν less than about 5) is laminar and follows a linear distribution; the velocity profile is described by Eq. 24. Although the flow within the lower part of the inner region is predominantly laminar, it does experience some fluctuations which are generally parallel to the flow. Vertical motions are negligible in the vicinity of the boundary; they become zero at the boundary. These fluctuations are generated by a sequence of events, which is known as bursting process. The upper limit of the inner region is defined by values of zu_*/ν between 30 and 70 (50 is used frequently). In the upper part of the inner region (the buffer layer), the velocity profile ceases to be linear and the flow is predominantly turbulent (with a high velocity gradient); this is despite the fact that viscous forces are still dominating the flow. There is an outflow of turbulent eddies from within the buffer layer, which is replaced by an inflow of non-turbulent fluid. The level within the buffer layer, where the viscous and turbulent forces are equally dominant, defines the upper limit (zu_*/ν is about 11.6) of the viscous sublayer (δ_ν) (see Section 2.2.3).

Overlap Region

The overlap region (extending up to z=0.1-0.2δ) follows a logarithmic distribution; it is often termed the constant stress layer, or logarithmic layer, and the turbulent (Reynolds) stresses predominate in this region. Reynolds stresses work against the mean velocity gradient, to remove energy from the mean flow. This action provides energy for the generation of large-scale eddies which travel with a certain amount of momentum. As the eddies travel, they gradually give up their momentum in the diffusion process; this is due to the efficiency of these large-scale eddies in transporting momentum. The velocity gradient, within this region, is gentler. Progressive transfer of energy takes place from the large- to small-scale eddies, whose kinetic energy is dissipated, ultimately as heat by the action of viscous processes; this sequence of events is known as the 'energy cascade' (Tritton, 1988). The process of energy transfer involves the degeneration of individual large-scale eddies and is known as 'vortex amalgamation', which intensifies the vorticity of the small-scale eddies by the action of viscosity (Willmarth, 1975). Eventually, the eddies will have given up so much momentum that their relative contribution to the turbulent shear stress is negligible.

Prandtl (1904) derived an expression for the distribution of shear stress, with height above the bed, throughout the turbulent boundary layer (outside the inner region), by introducing the concept of a mixing length parameter (l):

$$\tau = \rho l^2 (du/dz)^2 \tag{30}$$

where l is the Prandtl's mixing length, corresponding with the distance traveled by an 'average' turbulent eddy, before it loses its integrity. The scale of the turbulent eddies increase with distance from the boundary and, hence, the value of l depends upon the distance above the bed,

$$l = \kappa z \tag{31}$$

where κ (dimensionless) is the von Karman's constant. The value for κ (equal to 0.4, for clear water) has been determined empirically and is used as universal value; however, there is some argument as to whether the value of κ is affected by sediment-induced effects (suspended sediment). Several authors have suggested that κ is reduced with increasing sediment concentration (e.g. Wang, 1981; Gust and Walger, 1976). However, Coleman (1981), having re-analysed the data, rejects the concept that suspended sediment alters the value of κ. The available evidence suggests that Coleman's view is more likely to be correct (Sleath, 1984).

Substituting l (using Eq. 31) and u_* (using the relationship of shear velocity $u_* = \sqrt{\tau/\rho}$), Eq. 30 becomes:

$$u_* = \kappa z (du / dz) \tag{32}$$

Integrating Eq. 32, yields a velocity distribution of the form:

$$\frac{u_z}{u_*} = \frac{1}{\kappa}\ln(z) + \text{constant} \tag{33}$$

This expression is known as the Prandtl-von Karman equation (Prandtl, 1935; von Karman, 1930), indicating that the velocity is a logarithmic function of z. Implicit in this derivation is that the shear stress is virtually constant, with height, in a 'constant stress layer' near the boundary. Eq. 30 has been verified experimentally (Yalin, 1972) for turbulent flows, between the lower and upper boundaries of the constant stress layer. Here, z_o is the lower limit, taken at an elevation above the bed equal to the larger of k_s (grain effective roughness height) and δ_v (the thickness of the viscous sublayer), and z is the upper limit of the constant stress layer (0.1 - 0.2δ). Integration of Eq. 33 between the limits [z_o : z], where u_z=u_o at z_o, yields:

$$\frac{u_z}{u_*} = \frac{1}{\kappa}\ln\left(\frac{z}{z_o}\right) + \left(\frac{u_o}{u_*}\right) \tag{34}$$

The constant z_o, known as the roughness length, can be determined through experimentation; it consists of two parts, the skin friction which depends on the dimensions of the bed's physical roughness, due to the presence of the sedimentary particles, and the form drag (which expresses the physical roughness of the seabed, in response to the bedforms). The magnitude of z_o depends upon the size of k_s (grain effective roughness), compared with the thickness δ_v of the viscous sublayer. The effective grain roughness has been expressed in many different ways in the literature; for example, as an absolute value calculated using different percentiles of the particle size distributions (e.g. Sleath, 1984) or as a function of the Chézy Coefficient $C_z = \bar{u}/(hI)^{1/2}$, where I is the water surface slope (for more details, see Van Rijn, 1982).

A general equation (analogous to the Prandtl-von Karman Eq. 33) can be derived (see Schlichting, 1979; Yalin, 1972):

$$\frac{u_z}{u_*} = \frac{1}{\kappa}\ln\left(\frac{z}{k_s}\right) + B \tag{35}$$

The quantity B is a dimensionless property of the flow in the vicinity of the bed; it depends upon the magnitudes of k_s/δ_v (their relationship is shown, schematically, in Figure 8). This ratio forms

a dimensionless quantitative property of the flow in the vicinity of the bed; it is a function of the grain Reynolds number (see Eq. 4, Section 2.2.3). Nikuradse (1933) investigated flows through pipes, covered uniformly with a single layer of mono-sized sand grains (involving several combinations of pipe and sand diameter), in an attempt to investigate the relationship between B and k_s. This investigator derived, empirically, the variation of B with Re_*; these experimental results are shown in Figure 9; two intersections can be identified on the B axis which are denoted usually by C_S and C_R.

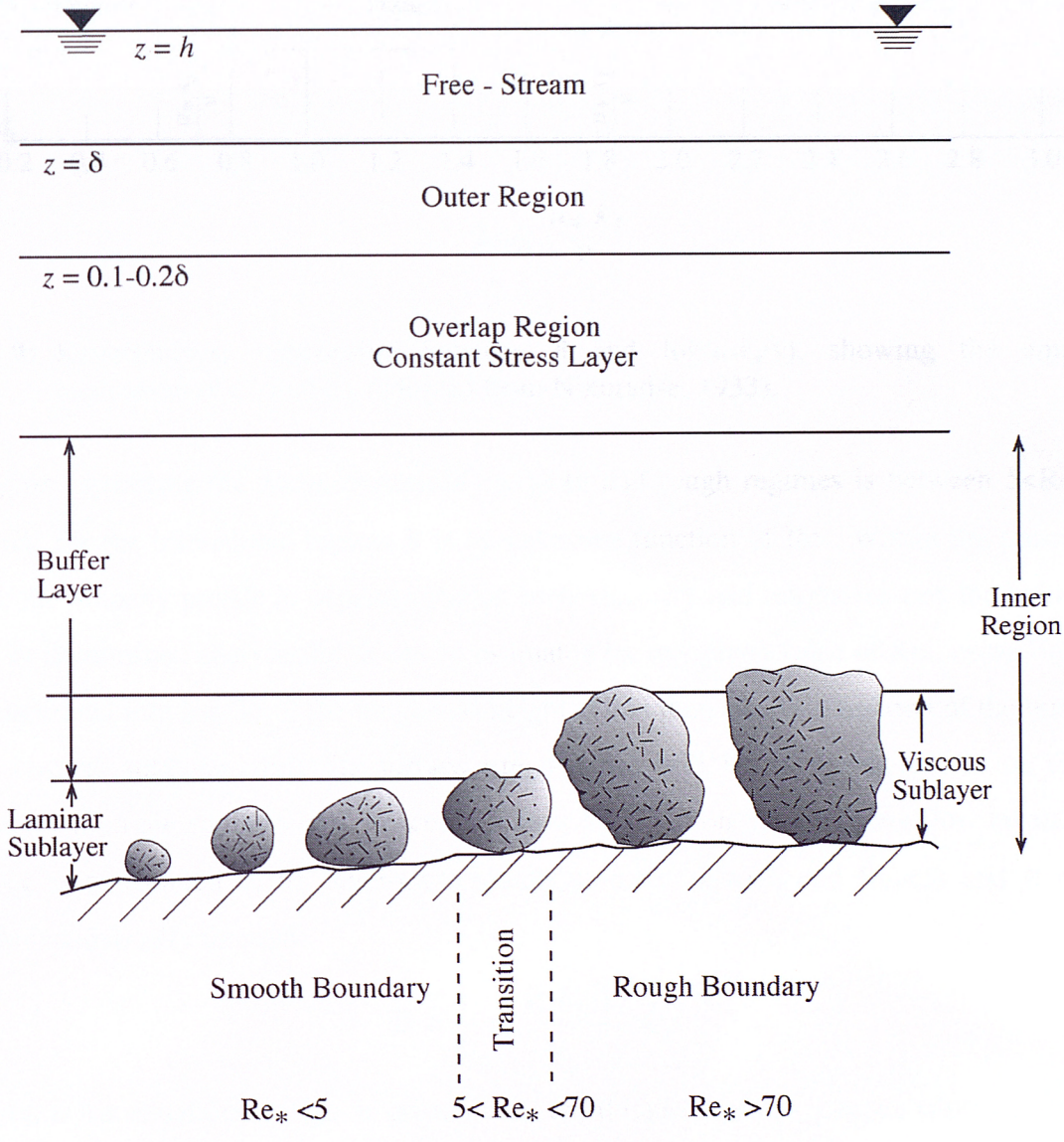

Figure 8: Schematic representation of the subdivision of smooth and rough turbulent boundary layers (not to scale).

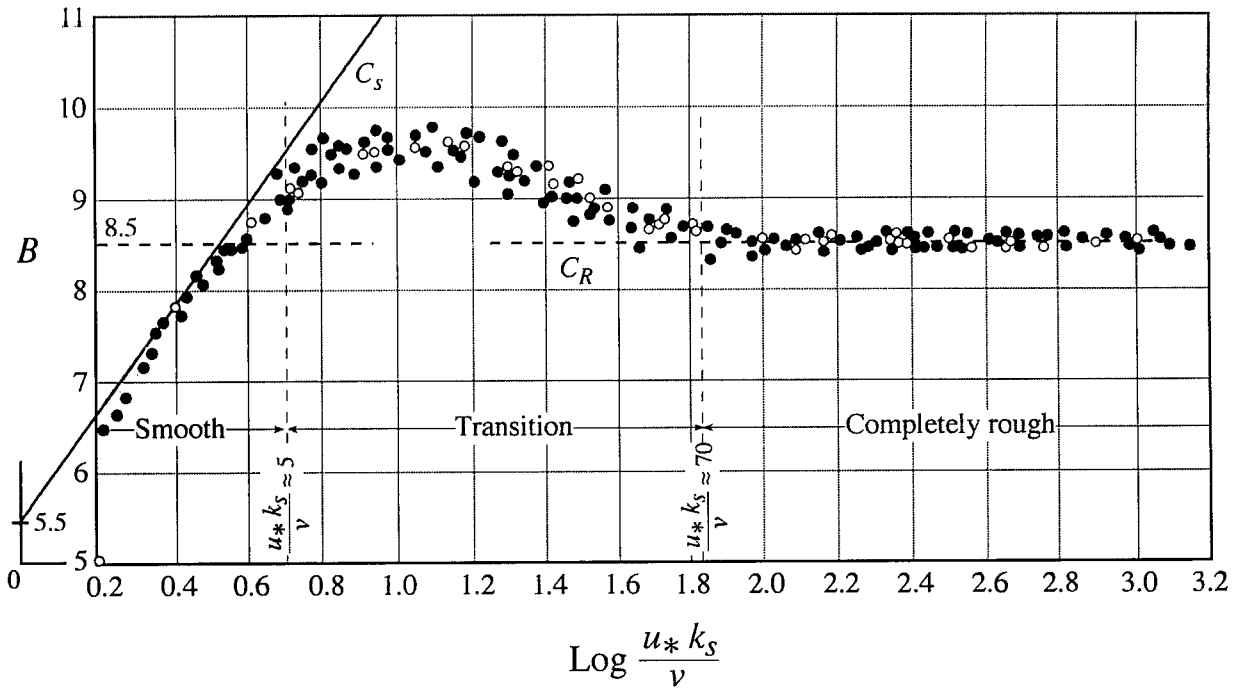

Figure 9: Experimental relationship between B and $\log(u_* k_s/\nu)$, showing the empirical evaluation of C_S and C_R (adopted from Nikuradse, 1933).

The region separating the hydrodynamically smooth and rough regimes is between $5<\text{Re}_*<70$, and $k_s \approx \delta_\nu$; for the transitional regime B is an unknown function of Re_*. Within the transitional regime, the velocity profile is dependent upon both viscosity and roughness and the value of B cannot be determined analytically; it can be estimated for any given value of Re_*, using Figure 9, then substituted into Eq. 35. If the roughness height is less than a certain fraction of the thickness of the viscous sublayer, then the surface irregularities will be small enough to be entirely contained within the sublayer and, hence, will have no effect on the overlying flow layers. Such a surface is considered to be 'hydrodynamically smooth' ($k_s \ll \delta_\nu$ and $\text{Re}_*<5$) and B can be estimated analytically through:

$$B = \frac{1}{\kappa}\ln\left(\frac{u_* k_s}{\nu}\right) + C_S \tag{36}$$

However, if the roughness height is greater than the thickness of the viscous sublayer, then the surface irregularities will be of sufficient magnitude to extend their effects into the overlaying layers; hence, to disturb the flow (producing a fully developed turbulent flow throughout the water column). Such a surface is considered to be 'hydrodynamically rough' ($k_s \gg \delta_\nu$ and $\text{Re}_*>70$) and B can be expressed as:

$$B = C_R \tag{37}$$

The commonly-accepted values for C_S and C_R are 5.5 and 8.5, respectively; these are indicated also in Figure 9. Combining Eq. 35 with Eqs 36 and 37, expressions for the mean velocity distribution can be defined for the hydrodynamically smooth and rough regimes, respectively:

$$\frac{u_z}{u_*} = \frac{1}{\kappa}\ln\left(\frac{z u_*}{\nu}\right) + C_S \tag{38}$$

$$\frac{u_z}{u_*} = \frac{1}{\kappa}\ln\left(\frac{z}{k_s}\right) + C_R \tag{39}$$

Outer Region

Within the outer region, referred to also as the 'wake region', the log-law does not apply. The mean velocity distribution can be represented through an empirical expression, as suggested by Coleman (1981):

$$\frac{U_s - U}{u_*} = \frac{1}{\kappa}\ln\left(\frac{z}{z_s}\right) + \frac{2P}{\kappa}\left(1 - \sin^2\frac{\pi z}{2 z_s}\right) \tag{40}$$

where U_s and z_s are the free-stream velocity and the elevation, which defines the lower limit of the outer region. In cases where the flow is fully developed, z_s should be replaced with the depth h and U_s should be taken as the maximum value of U. P is an empirical constant, which is related to the sediment concentration in suspension. For clear water, a value of 0.19 has been suggested; whereas for very heavy concentrations of sediment, P approaches 1.

2.6 Velocity Distribution in Turbulent Flows

2.6.1 Hydrodynamically Smooth Surfaces

The mean velocity in a steady, one-dimensional, open-channel flow above an hydrodynamically smooth surface can be expressed semi-empirically (Nezu and Rodi, 1986) as:

$$\frac{u_z}{u_*} = f\left(\frac{z u_*}{\nu}\right) + W\left(\frac{z}{h}\right) \tag{41}$$

where $f(zu_*/\nu)$ is an empirical wall function and $W(z/h)$ is a empirical expression for the wake correction.

The wake correction is much smaller than the wall function in the inner part of the flow (z/h less than about 0.2) and. Hence, the velocity distribution can be described adequately by the wall function; this is true for the wall region of any turbulent shear flow (e.g. open-channel flow, pipe flow, etc.) above an hydrodynamically smooth surface (Clauser, 1956). Within the viscous

sublayer (zu_*/ν less than about 5), the wall function can be approximated to zu_*/ν, whereas well outside the viscous sublayer (zu_*/ν greater than about 50) it is approximately logarithmic:

$$f\left(\frac{zu_*}{\nu}\right) \cong \frac{1}{\kappa}\ln\left(\frac{zu_*}{\nu}\right) + C_S \tag{42}$$

where C_S (~5.5) is the empirical constant defined previously (Section 2.5.2). Reichardt (cited in Landahl, 1967) proposed the following empirical expression valid for all zu_*/ν:

$$f\left(\frac{zu_*}{\nu}\right) = \frac{1}{\kappa}\ln\left(1+\kappa\frac{zu_*}{\nu}\right) + \alpha\left[1-\exp\left(\frac{zu_*}{\beta\nu}\right) - \left(\frac{zu_*}{\beta\nu}\right)\exp\left(-0.33\frac{zu_*}{\nu}\right)\right] \tag{43}$$

where α and β are empirical constants. If the values of 7.8 and 11 are used (for α and β, respectively) then the second part of the right hand side of Eq. 43 is equal to 5.5; this is the most commonly accepted value.

In the outer part of the flow (z/h greater than about 0.2) the wake correction (introduced by Coles, 1956), becomes significant. The strength of the wake correction depends upon the type of flow (e.g. larger in boundary layer, with zero pressure gradient, than it is in an open-channel flow); its shape is approximately similar for all wall-bounded turbulent shear flows. Coles (1956) proposed the following empirical expression:

$$W\left(\frac{z}{h}\right) = \frac{2\Pi}{\kappa}\sin^2\left(\frac{\pi z}{2h}\right) \tag{44}$$

where Π is an empirical parameter (the Coles parameter), which determines the strength of the wake correction. Nazu and Rodi (1986) found (for steady, one-dimensional, open-channel flows) that Π depends on the Reynolds number, increasing from a value of zero for Re<500 to a constant value of approximately 0.2 for Re>2000.

Neglecting the wake correction and using the approximation given by Eq. 36, the mean velocity profile above an hydrodynamically smooth surface, a logarithmic approximation may be obtained of the form:

$$\frac{u_z}{u_*} = \frac{1}{\kappa}\ln\left(\frac{zu_*}{\nu}\right) + C_S \tag{45}$$

Eq. 45 is the same as the expression derived earlier for the overlap region (Section 2.5.2), on a dimensional basis (Eq. 38); it is often referred to as the 'smooth-wall law' and is valid in the relatively thin layer, in which z is greater than about $50\nu/u_*$ but less than about $0.2h$.

The mean velocity profile in an open-channel flow above an hydrodynamically smooth bed is shown in Figure 10, based upon Eqs 41, 43 and 44, for conditions similar to those encountered in the 5m flume (a depth h of 8cm, a shear velocity u_* of 2cm/s and a kinematic viscosity ν of 0.01cm^2/s). Also shown in Figure 10 is the corresponding logarithmic approximation given by Eq. 45. For z less than about 0.2cm, the viscous correction to the logarithmic approximation is negative; for z greater than about 4cm, the wake correction to the logarithmic approximation is positive. The logarithmic approximation (Eq. 45) is accurate over less than 50% of the water column, in this particular example.

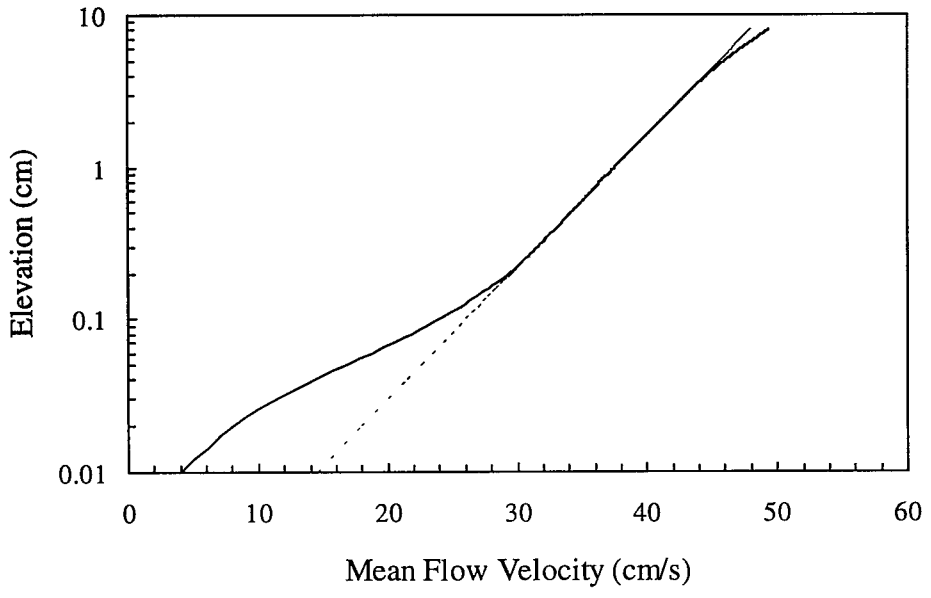

Figure 10: Example of a velocity profile in turbulent one-dimensional open-channel flow, derived theoretically, for conditions similar to those encountered in the 5m flume (h=8cm, u_*=2cm/s and ν=0.01cm^2/s). Solid line: complete profile based upon Eqs 41, 43 and 44. Dashed line: logarithmic approximation based upon Eq. 45.

The logarithmic approximation for the mean velocity profiles constitutes one of the most important results in the study of turbulent flows. Various velocity profiles, within a turbulent boundary layer, measured experimentally over smooth boundaries are plotted with log-linear coordinates in Figure 11; the corresponding equations which closely describe the various parts of the profile are also shown. Eq. 45 (see also Eq. 38) appears to be valid for the region $zu_*/\nu > 30$-70, whereas the profile departs from the logarithmic form when $zu_*/\nu < 30$, because of the importance of viscosity in this region. Within the laminar sublayer, defined by $zu_*/\nu < 5$, a linear mean velocity gradient occurs (with a logarithmic plot serving to expand this particular region) and is described by Eq. 25; it is evident that the experimental point corresponds closely with the

line, for $zu_*/\nu < \sim 8$. The buffer layer ($5 < zu_*/\nu < 30\text{-}70$) and the experimental data follows a smooth transition between the lines represented by Eqs. 25 and 45. The intersections of these two equations provide an estimate of the thickness of the viscous sublayer; this occurs when $u/u_* = zu_*/\nu = 11.6$. Hence,

$$\delta_\nu = 11.6\frac{\nu}{u_*} \tag{46}$$

which is the constant A used in Eq. 4 (see Section 2.2.3). Within the outer region of the boundary layer (zu_*/ν greater than about 500-1000, when $z/\delta > 0.15$), the observed data points diverge from the logarithmic profile and can be better represented by a power law distribution such as Eq. A-15 (see Appendix A).

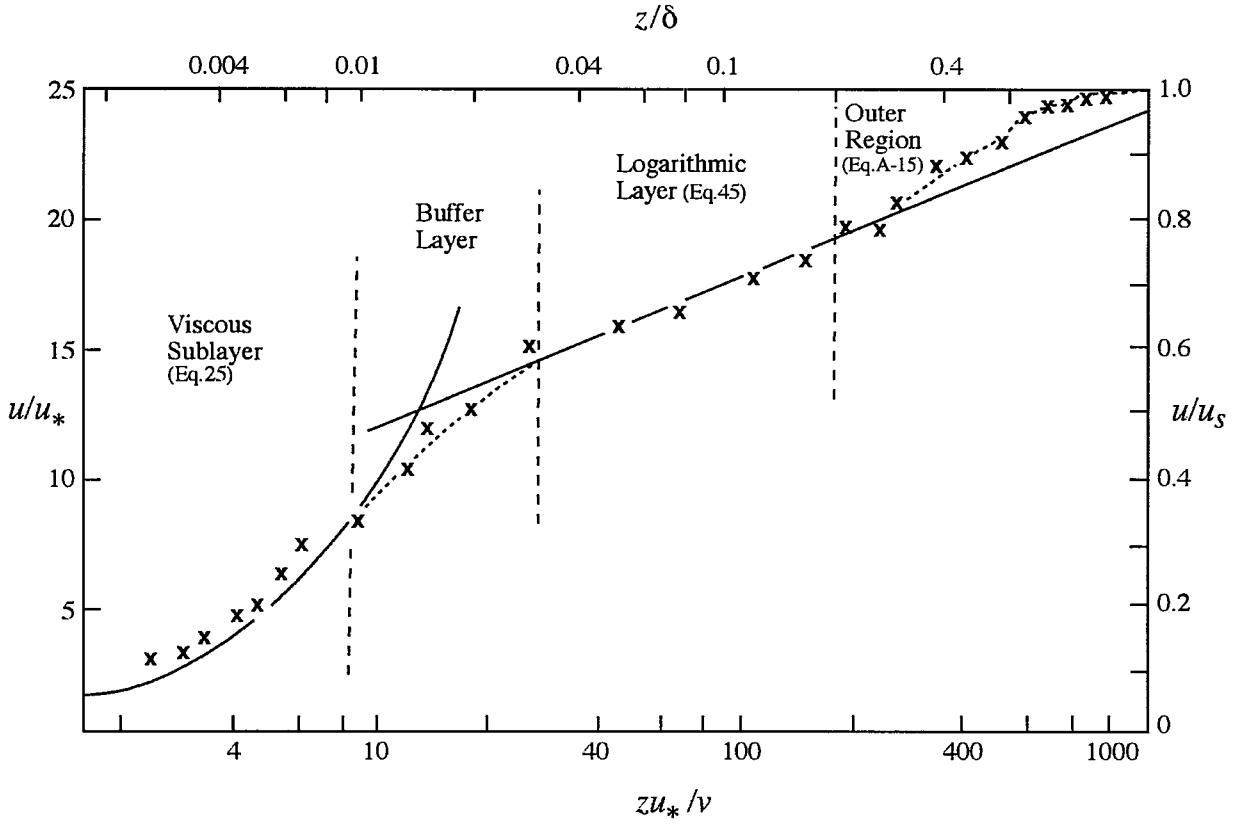

Figure 11: Example of a turbulent boundary layer mean velocity profile over a hydrodynamically smooth velocity profile, plotted on log-linear coordinates; the solid lines correspond to specific equations as indicated, whereas the dashed line shows the trend of data (adopted form Tritton, 1988).

2.6.2 Hydrodynamically Rough Surfaces

Within the hydrodynamically rough turbulent regime, the roughness height (k_s) is now much larger than the thickness of the viscous sublayer, which is no longer coherent. Eddies are shed and the resistance to flow is due predominantly to the form resistance of the sand grains, or other irregularities. If the surface is defined as being hydrodynamically rough, then the mean velocity distribution in a steady, one-dimensional, open-channel flow represented by Eq. 41 must be replaced:

$$\frac{u_z}{u_*} = f'\left(\frac{z}{k_s}, \frac{k_s u_*}{\nu}\right) + W\left(\frac{z}{h}\right) \tag{47}$$

In this expression, the wake correction remains unchanged, but the wall function is modified to incorporate the effect of bed roughness through the inclusion of k_s, as the size and form of the roughness elements become additionally important parameters. For zu_*/ν greater than about 50 and sufficiently large z/k_s (in practice, greater than approximately 1), $f'(z/k_s, k_s u_*/\nu)$ is logarithmic:

$$f'\left(\frac{z}{k_s}, \frac{k_s u_*}{\nu}\right) = \frac{1}{\kappa}\ln\left(\frac{z}{k_s}\right) + C_R \tag{48}$$

where C_R (~8.5) is the empirical constant defined previously (see Section 2.5.2). If $k_s u_*/\nu$ is less than about 5, Eq. 47 matches Eq. 42; this is since the surface is hydrodynamically smooth. If $k_s u_*/\nu$ is greater than about 70, then the surface is hydrodynamically rough and Eq. 48 must be used. Neglecting the wake correction and only considering the relatively thin region in which z/h is less than about 0.2, whilst z is greater than about $50\nu/u_*$ (or approximately k_s, whichever is the greater), the following commonly-used logarithmic approximation can be obtained (through the use of Eq. 48):

$$\frac{u_z}{u_*} = \frac{1}{\kappa}\ln\left(\frac{z}{k_s}\right) + C_R \tag{49}$$

This expression is, once again, the same as that derived earlier (see Section 2.5.2), on dimensional grounds (Eq. 39); it is often referred to as the 'rough-wall law'.

Within the boundary layer (where the wake correction can be neglected) a more general expression (logarithmic approximation) can be derived, which applies to both smooth and rough surfaces:

$$u_z = \frac{u_*}{\kappa} \ln\left(\frac{z}{z_o}\right) \tag{50}$$

where z_o is the bed roughness (Section 2.5.2) and can be obtained through:

$$z_o = \frac{k_s}{30}\left[1 - \exp\left(\frac{-u_* k_s}{27\nu}\right)\right] + \frac{\nu}{9\,u_*} \tag{51}$$

This relationship was suggested by Christoffersen and Jonsson (1985), who used the experimental results of Nikuradse (1933) to derive the expression; this is one of several expressions which can be found in the literature (for example, z_o being equal to $k_s/32.62$).

Plotting the height above the bed (elevation, z) against the corresponding velocities on a logarithmic scale, using Eq. 50, a linear relationship may be obtained. Assuming that κ=0.4, and changing the logarithmic expression from natural logarithm to a logarithm to the base 10 (log), Eq. 50 becomes:

$$u_z = \frac{u_*}{\kappa} \ln(10) \log\left(\frac{z}{z_o}\right) \tag{52}$$

Eq. 52 was derived on the assumption that the shear velocity within the boundary layer is constant; hence, the shear velocity ($u_*=(\tau_o/\rho)^{1/2}$) can be obtained from the slope of the velocity profile,

$$u_* = \frac{\kappa}{\ln(10)}\left(\frac{u_{z_2} - u_{z_1}}{(\log z_2 - \log z_1)}\right) \tag{53}$$

Ideally, in order to minimise the errors in the calculations, three simultaneous velocity measurements should be made for each estimation (Sternberg, 1972; Heathershaw and Langhorne, 1988). Using the value of the intercept on the elevation axis, an estimate for the roughness length can be obtained. There are several techniques available, recognised widely, by which the τ_o can be estimated (indirectly or directly) depending upon the flow conditions; some of these methods are described briefly in the Appendix.

2.7 Water Depth: A Note

The water depth is of considerable importance, when undertaking experiments in laboratory flumes, because of its relationship to the bottom friction velocity. An increase in water depth implies an increase in the bottom friction velocity. Laboratory flumes differ from natural conditions, in that the flume width is fixed. Considering the small depths used in laboratory studied, where the relative increase in depth is much greater than in environmental flows, it is

apparent that the bottom shear stress in natural flows is much less affected by changes in water depth than in the laboratory flumes. As the effect of any increase in the depth of the flow is more pronounced under laboratory conditions, the results of flume experiments deviate from the field data. The absence of field studies with the aim of understanding the direct influence of water depth on the magnitude of the secondary effects, in relation to incipient motion, such as the turbulent velocity fluctuations, reinforces the questionable reliability of laboratory measurements.

3. Experimental Procedure

3.1 Flow Characterisation Experiments

A number of experimental tests were undertaken, to establish both the cross-sectional nature of the flow (examining the side-wall effects) and the nature of the velocity profile, at a variety of flow rates (slow, moderate and fast). The experimental procedure and adopted methodology are outlined below. Both smooth (the bed of the flume) and rough (the artificial aluminium bed) surfaces were used as boundaries, examining the differences in the flow behaviour. A single grain thickness layer of sand (grain diameter of D=0.0651cm) was glued to the top aluminium plate of the bed (the recess section was excluded from these experiments, to allow for a uniform surface along the whole length of the flume).

The water depth used during the experiments depended upon the nature of each of the experimental tests, ranging from as shallow as 5cm up to 20cm. During the experiments, water depths and temperature were monitored. The bulk of the flow measurements were undertaken at the potential position of a sediment recess section, approximately 3.5m downstream of the flume channel entrance. The LDA and the Streamflo unit were used in combination, positioned in the appropriate locations within the flume, relating to the individual experiments. The Streamflo was used for the collection of data across the flume, because the mounting system of the LDA (designed on the basis of safety and accurate alignment) was only capable of obtaining measurements at the channel's centreline.

3.2 Observations and Data Acquisition

The data generated from each experimental run fall into four groups, namely: descriptive, visual, analogue and digital. Descriptive experimental data were in the form of: notes produced regarding the experimental arrangements; depth of flow velocity measurements; water depth and temperature; the operational frequency of the LDA and Streamflo; and any malfunctions of the equipment which may have occurred. The visual data took the form of descriptive notes. The analogue output data sets, from both the current meters, was in the form of a continuous DC voltage signal; these were recorded simultaneously onto two channels, on the computer, during an experimental run. The digital type represented the numerical data, derived from the analogue signals. The quality of the numerical data depends upon the relationship between the conversion resolution and the nature of the raw signal, in terms of amplitude and frequency. Estimates of the means and standard deviations of the turbulent fluctuations could be improved, by increasing the

sampling rate and/or the duration of the record; however, this would increase considerably the volume of the data set obtained. Sampling at 25Hz resulted in 1500 data points being collected, for every minute of recording duration; hence, the data records were confined to between 5 to 8 minutes, depending upon the experiment.

3.3 Experimental Errors

The accuracy and the inherent errors of each instrument have been discussed in a companion report (Paphitis and Collins, 2001). As the main instrument used in the experiments was the LDA, the errors were analysed statistically. In addition to the instrumental accuracy, a further error was introduced due to random electrical fluctuations; however, these may be assumed to be normally-distributed, about a mean value. The difference between the true and calculated standard deviations (σ) of one experimental run (U=28.63cm/s), was found to be 0.0268cm/s (~1.43%, with the true σ and calculated σ being equal to 1.8556cm/s and 1.8824cm/s, respectively). This difference was considered to be relatively insignificant, with respect to the variation experienced between the experimental runs. The accuracy of the digital output from the Streamflo current meter varied with the velocity, ranging between ±1 to 5% (generally, decreasing with increasing flow velocity). However, this error was decreased when the temporal mean values were calculated.

4. Results and Discussion

The measurement programme was designed with the intention of producing enough evidence to determine whether the 5m flume can, indeed, produce flows comparable to the idealised flow characteristics described in Section 2. During the whole of the measurement programme, the water was being maintained almost free of suspended sediment (a certain quantity of particles in suspension was desired for the effective operation of the LDA) and at a temperature of 15°C (±2°C). Under these fixed conditions the density was taken to be 0.999g/cm^3 and the kinematic viscosity 0.0114cm^2/s; these values are used in all the forthcoming calculations.

4.1 Accuracy of the Mean Velocity Measurements

The accuracy of the derived mean velocities, together with the subsequent statistical analyses, may be influenced by a variety of factors, the most important of which are: (a) sampling errors; (b) the flow measurements at different elevations not being synchronised; (c) positional error of the LDA and Streamflo current meters; and (d) the possible non-uniformity of flow, in the downstream direction. An appreciation of the factors discussed above is necessary for the subsequent interpretation of the results. In particular, these factors may be called to account for any discrepancies between the trends of the data from the present investigation, in comparison with the idealised trends proposed (Section 2).

4.1.1 Sampling Errors

Differences between the 'observed' and 'true' values of the flow velocity (u_z), at a given location, may occur due to the limited accuracy of the LDA and Streamflo current meters. These errors, in relation to the LDA system, have been discussed previously (Section 4.3) and have been shown to be 'self-cancelling', with respect to the mean velocity derivations. Similarly, standard deviations are overestimated by an insignificant amount (<5%).

4.1.2 Synchronicity of Flow Measurements at Different Levels

On the basis of obtaining measurements with a single LDA system and one Streamflo current meter, the velocity measurements for both the velocity profiles and the cross-sectional experiments were not undertaken simultaneously. Low-frequency fluctuations in the flow should be included in the mean velocity calculations, measured over a period of time. However, variation in the flow rate, during successive sampling periods, will result in an ambiguity when the calculated mean velocities are used to describe a single event (in time). Considering that the

water discharge in the flume remains (effectively) constant, then the duration of the longest period fluctuation (T) will be a function of the mean flow velocity (U) and a length scale (L); these characterise the largest dimension of the flow ($T=L/U$). Different length scale can be used in these calculations. Using the channel width (30cm), at velocities of 10, 20, 30 and 40cm/s, the fluctuations would have periods of 3, 1.5, 1 and 0.75s (i.e. frequencies of 0.33, 0.67, 1 and 1.33Hz), respectively. If the distance from the leading edge of the flume, to the experimental test section, is used (350cm) then the same velocities would relate to periods of 35, 17.5, 11.67 and 8.75s (i.e. frequencies of 0.029, 0.057, 0.086 and 0.114Hz), respectively. The latter would result in fluctuating periods of slightly over eleven times as long as those indicated using the first length scale. Hence, by using the original length scales, the period can be decreased, but the frequency fluctuation would be considerably increased; this, in turn, may not be detectable with the available instrumentation. Conversely, by increasing the length scale, the periods can be increased and the frequency fluctuations decreased. Using a length scale of 350cm, fluctuations of periods greater than 35s only arise if the flow is less than 10cm/s. However, all the experiments described here exceed this flow velocity. The influence of long-period fluctuations in the flow rate was estimated to be approximately of the order of ±0.5cm/s. Such fluctuations of the mean-velocity may be the result of long-term variations in the flume pump discharge rate. Variations of this order of magnitude may give rise to any irregularities observed in the mean velocity calculations.

4.1.3 Positional Error of the LDA and Streamflo

The LDA velocity measurements result from an integration over a vertical distance of 0.03cm (Paphitis and Collins, 2001). Using a vertical depth scale, the LDA measuring volume could be positioned to within ±0.005cm, with respect to the bed. However, the definition of z=0 (at the bed) for a rough boundary is somewhat ambiguous; this is due to the presence of the single grain layer (grains ranging from 0.0595 to 0.0707cm sieve diameter), which results in a positional uncertainty of ±0.0056cm. In terms of profile interpretation, such an error is only significant close to the bed, in areas of high mean-velocity gradients.

The positioning error of the Streamflo was slightly greater than that of the LDA, lying within the ±0.01cm error range. At high velocities, the Streamflo was observed to be displaced in the direction of the flow; these deviation in the horizontal (flow direction) were difficult to assess. Since consecutive measurements were made at vertical intervals of at least 2cm (for the cross-sectional experiments), this displacement error was considered to be insignificant.

4.1.4 Non-uniformity of Flow in the Downstream Direction

The flume channel was levelled to an accuracy of ±0.05° and maintained in an horizontal position throughout the experiments. Any (even slight) slope in the flume bed would have resulted in a small, but progressive, downstream variation in the shape of the boundary layer. Similarly, the roughened surface would lead to a progressive adjustment of the boundary layer, downstream of the leading edge. If the flow was allowed to encounter, at first, the smooth surface of the flume bed and then the roughened surface of the grains, then the temporal mean velocity profile (at a point downstream from the leading edge of the roughened surface) would have been observed to have two inflections; their relative position in the vertical would depend upon the flow characteristics. In order to achieve individuality in the velocity profile, when using the rough boundary, the leading edge of the roughened bed was made to coincide with the leading edge of the flume; in this way, the boundary encountered by the flow (upon its introduction into the working section of the flume) was either smooth or rough.

This investigation is concerned with one-dimensional, steady, uniform, open-channel flows which are considered as the fundamental type of flows in open channel hydraulics. In defining the flow within the flume as steady and uniform, the depth and discharge must remain constant, both in terms of time and distance. Flows generated in the flume were found to experience slight deviations from steady uniform flow conditions; these were related, most probably, to the pumping action which was found to give rise to a standing wave and introduce additional turbulence into the flow. Therefore, it was necessary to examine the nature and development of the flow, after its introduction into the open channel section of the flume. Spherical polystyrene particles of different diameters (permitting them to settle at different depths) were introduced into the flow; these were observed, visually, to establish the extent to which the different techniques were 'dumping' the excess turbulence and removing the standing wave from the system. A honeycomb-like structure was designed resembling those used in air tunnels, with the use of plastic tubes of 1cm internal diameter; this was introduced at the leading edge of the flow channel. It was found to remove the standing wave within the channel; at the same time, reducing the turbulence down to the tube diameter scale. Although this imposed certain limitations, it was concluded, on the basis of the visual investigation, that the introduction of the honeycomb-like structure was beneficial; overall, it appeared to improve the flow organisation and, hence, was maintained in its use throughout the study.

4.2 Preliminary Experiments

The preliminary experiments include a variety of tests designed to examine certain aspects of the 5m flume and the flows which it can produce. These tests form a necessary first step towards obtaining consistent results in the main experiments of the measurement programme.

4.2.1 Flow Development

Mean velocity profiles (shown on Figure 12) obtained at the centre of the channel, and at various distances (0.5, 1.5, 2.5 3.5 and 4.5m) from the entrance to the working section of the flume, indicate that the vertical structure of the flow is fully developed within about 3.5m or 45 water depths (~8cm) from the entrance, roughly as anticipated (Section 2.1). The scope of the logarithmic region of the velocity profile does not change appreciable between 3.5m and 4.5m. These results indicate that measurements, undertaken in subsequent experiments, should be carried out at least 3.5m downstream from the entrance to the working section.

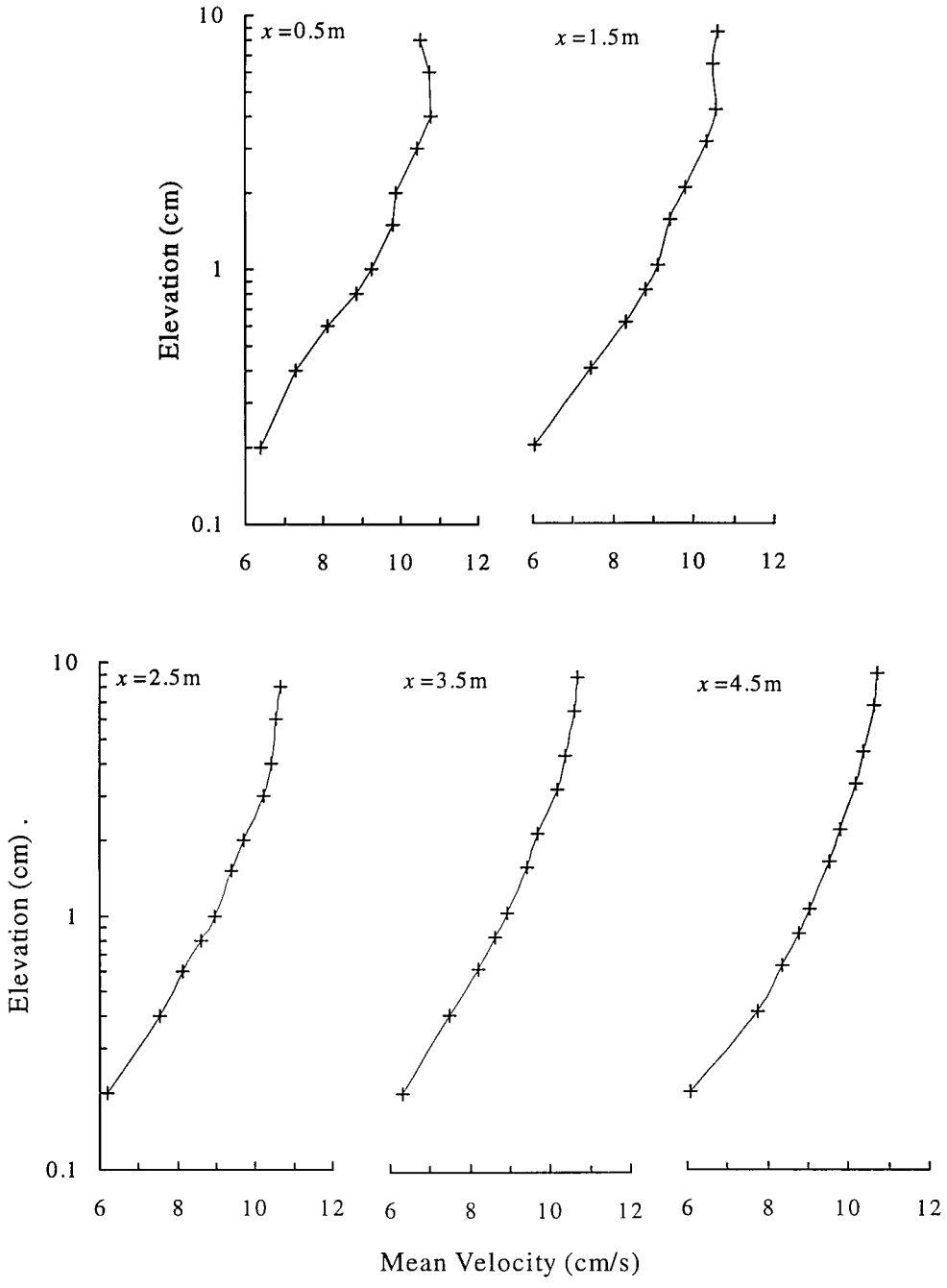

Figure 12: Profiles of mean velocity at various distances along the channel, obtained in the preliminary measurement programme. All measurements were taken along the centreline. The distance from the entrance to the working section is given by x.

4.2.2 Mean Velocity Estimations

In order to identify, in a simple way, the time required to produce estimates of mean velocities that are within a few percent of the 'true' mean (taken as the mean of the total record), a long record of the velocity at 2cm above the bottom was generated. From a 30min long data record, the running average $\hat{u}(t_+)$ was computed, as defined by

$$\hat{u}(t_+) = \frac{1}{t_+}\int_0^{t_+} u(t)\, dt \tag{54}$$

as a function of the averaging time t_+. Figure 13 shows the results of this calculation, in the form of a departure of the running average from the mean of the total record, normalised by the mean of the total record. Figure 13 indicates fluctuations of the order of 2% to 3%, for averaging times less than about 150s, and fluctuations that are an order of magnitude smaller for averaging times greater than about 150s. These results suggest that an averaging time of 5min is sufficient to produce stable mean velocities (that are within a few percent of the 'true' mean).

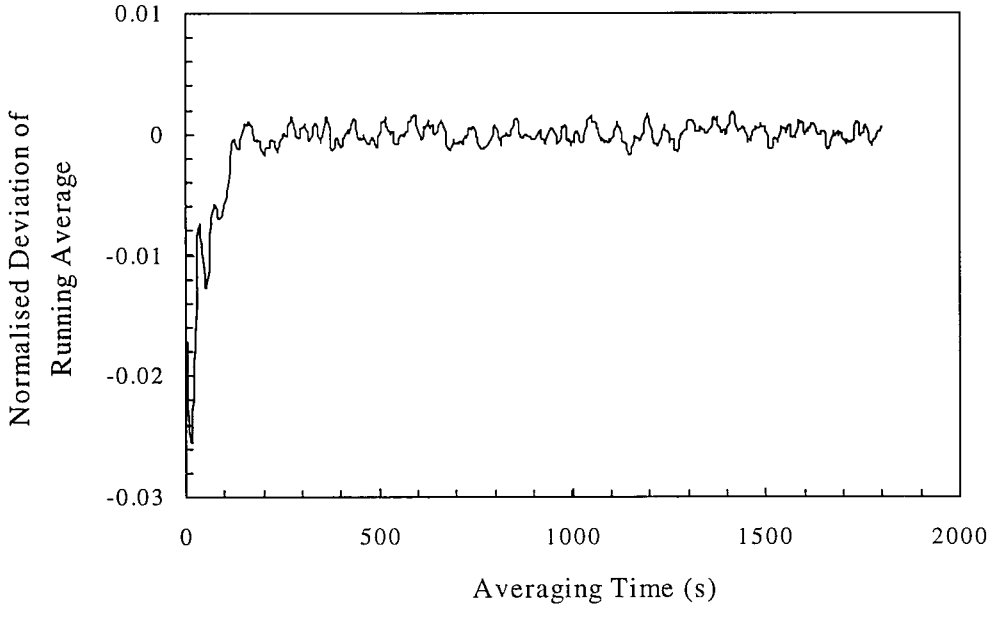

Figure 13: Running average $\hat{u}(t_+)$, as defined by Eq. 54, as a function of the averaging time t_+. The vertical axis is the departure of the running average from the mean of the total record, normalised by the mean of the total record.

4.2.3 Depth-Averaged Velocities

The depth-averaged flow velocity, using the profile measurements made for the study of the vertical structure of mean velocity, was determined by averaging all the velocities measured at the pre-specified elevations within the flow. The derived depth-averaged velocity of the flow was compared then with all the measured velocities of the vertical profiles; this was to identify at which elevation the velocity measurement best represented the estimated depth-averaged flow velocity. The identified elevation was converted into a percentage of the total flow depth. These experiments revealed that reliable estimates of depth-averaged flow velocity can be obtained at a level of 0.6 of the depth below the free surface (see also Chow1959). Maximum velocities were observed to be closer to the free surface, at levels between 0.2 and 0.3 of the depth below the surface.

4.2.4 Maximum Velocities

A series of experiments were undertaken to evaluate the maximum velocities capable of being generated in the flume, for different water depths. The control pump was completely opened (theoretically, pumping $0.03m^3/s$) and, by gradually varying the flow depth in steps of 1cm at a time, velocity measurements were obtained at an elevation from the bed equal to 60% of the total flow depth. Measurements at this level were found to provide good estimates of the depth average velocities for the generated flows (see above). The measured velocities are shown in Figure 14; these can be used as an indication of the levels of achievable velocities, with respect to depth, within the 5m flume. The velocity increases with decreasing flow depth; hence, velocities in excess of 2m/s are possible at flow depths below 5cm. For the safe operation of the flume, it should be noted that, by increasing the discharge whilst maintaining the tail gate at the same level, caution must be taken not to over-top the flume; water depth increases with velocity, as the amount of water flowing over the tail gate increases.

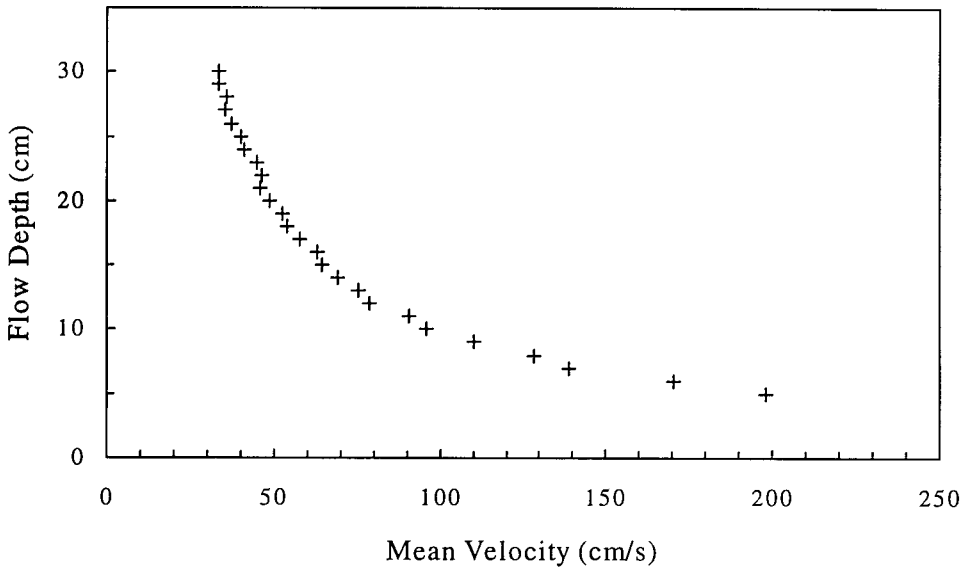

Figure 14: Possible flow velocities, that can be generated in the flume, at different water depths.

4.2.5 Streamflo Positioning

A series of tests were carried out to investigate the influence of the Streamflo sensor upon the LDA, when located above it, at a variety of positions. The LDA was placed at a height of 0.5cm above the bed and the Streamflo at a variety of elevations (z) (1, 2, 3, 4, 5, and 6cm). The velocity disturbances experienced by the LDA are shown in Figure 15, in the form of differences between the velocity measurement made prior to the introduction of the Streamflo, compared with those made after its introduction at the respective elevations. The positioning of the Streamflo within the flow produces turbulent eddies, which appear to increase the flow in the vicinity of the LDA (at least up to a height difference of 3.5cm). The mean velocity differences decrease, from 1.54cm/s to 0.04cm/s, between a height difference of 0.5cm and 3.5cm, respectively. At a height difference of 4.5cm (and 5.5cm), the mean velocity measurements (before and after) appear to be similar.

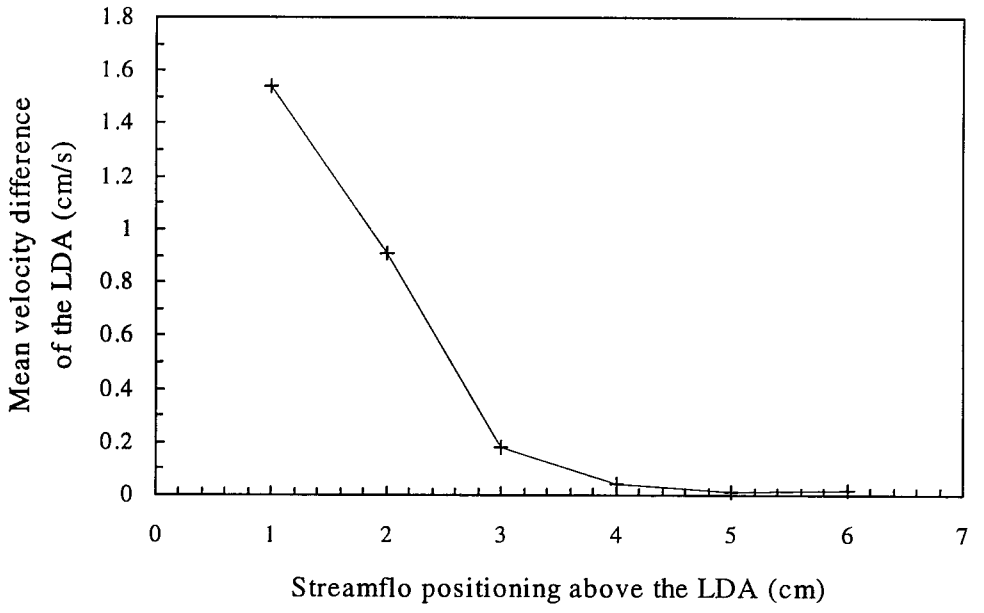

Figure 15: Diagram illustrating Streamflo positional effect on the recorded LDA velocity measurements.

4.3 Cross-sectional Character of the Flow

In response to the presence of a free (water) surface and to friction acting along the glass side-walls, the velocities in the flume are not distributed uniformly across the working section. A series of tests were undertaken to establish the cross-sectional character of the flow and, at the same time, the extent of the influence of the side-walls. Forming a grid sampling system (Figure 16), the pattern of the flow velocity distribution within the working section of the flume was obtained; the measurements were carried out at a position located 3.5m downstream from the leading edge of the flume. The LDA was used for obtaining the velocity measurements over the central part of the flume (axial line), in steps of 1cm, varying between 1cm and 19cm above the bed. All the other measurements were undertaken using the Streamflo current meter at the following distances (y, in cm) across the flume, with reference to the centreline:

-14, -13, -11.5, -10, -8.5, -6.5, -5, -2.5, (0), 2.5, 5, 6.5, 8.5, 10, 11.5, 13, 14

(where positive indicates the right hand-side (RHS) and negative the left hand-side (LHS) of the flume, looking in the downstream direction). The Streamflo measurements were made at a variety of elevations (z) within the flume, in 2cm steps, between 2cm and 18cm. The water depth was maintained at 20cm, with a mean (cross-sectional) flow velocity of ~20cm/s.

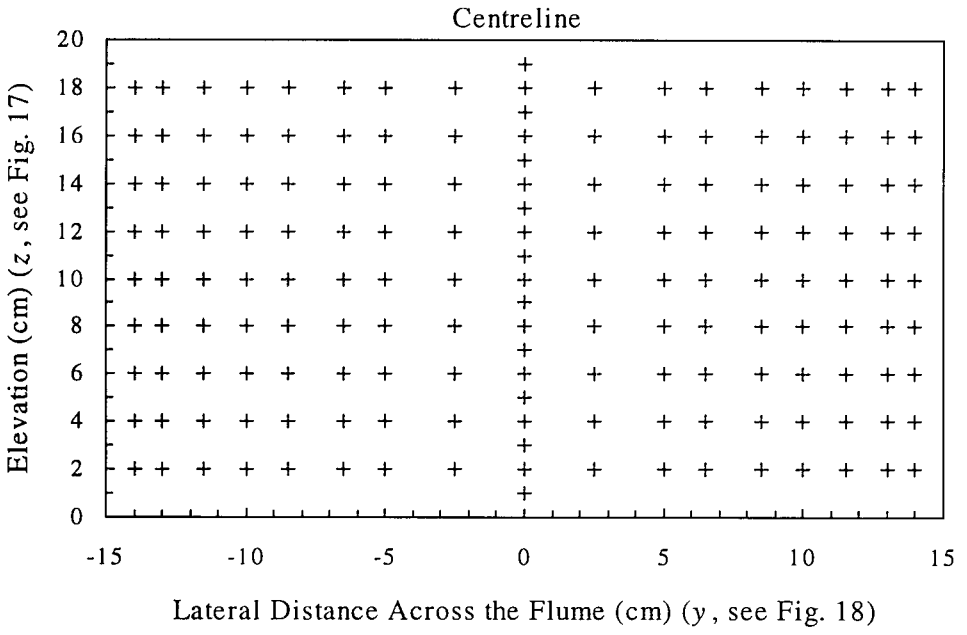

Figure 16: Cross-sectional diagram of the flume (looking downstream) showing the grid sampling system.

The lateral mean velocity (u_y) variations, across the flume, at various elevations (z) above the bed, are illustrated in Figure 17. Maximum velocities occur in the middle region (y=±7cm), with minimal variation. In approaching the side walls (from about ±8cm), u_y starts to decrease; this is due to the frictional effects, in order to satisfy the no-slip condition of zero velocities at the boundaries. In these regions, closer to the side boundaries, a general shift (of up to 1.54cm/s) can be observed, where the velocities on the LHS of the flume have been found to be higher. The gradient (du_y/dy) of these lateral profiles is observed to increase towards the bottom boundary. The larger changes in momentum experienced in this region (z<4cm) may be attributed to the combined influence of the bottom and side boundaries of the channel (flume).

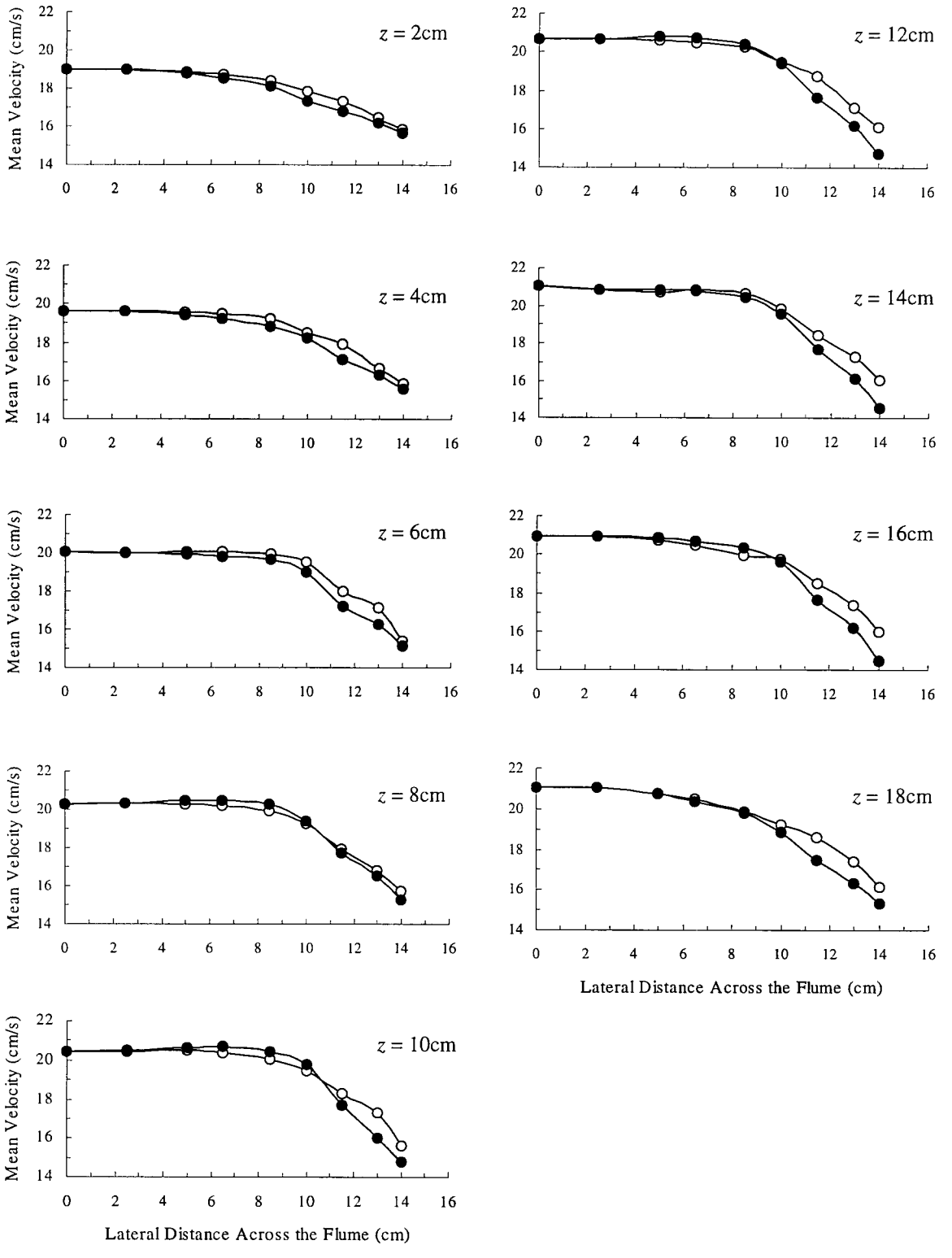

Figure 17: Lateral variations in the mean velocity (u, cm/s), with distance (y, cm) across the flume. z is the elevation above the bed, • RHS and o LHS (looking in a downstream direction).

Vertical mean velocity (u_z) variations at positions across the flume (y) are shown in Figure 18. Approaching the side boundaries, higher u_z values are observed on the LHS of the flume. Maximum velocities occur at some depth below the free surface. In smooth channels elsewhere (Schlichting, 1979), it has been observed that the flow at the free surface was not one-dimensional for narrow rectangular channels; likewise, that maximum velocities occurred below the free surface. Chow (1959) has indicated that maximum velocities occur at a level of 0.05 to 0.25 of the depth below the free surface; as the side walls are approached, the occurrence of the maximum velocity becomes deeper. In the present investigation, maximum velocities have been found to occur between 5.5cm to 6.5cm below the free surface (corresponding to an average 0.35 of the depth below the surface). However, a series of secondary maxima can also be identified, in certain cases, occurring between 15cm to 16cm below the surface; this suggests the presence of a high velocity cell of fluid close to the bed. It has been suggested elsewhere (Kennedy and Fulton, 1961) that, at least initially, two secondary currents on either side of the centreline may develop in flumes. The presence of these currents has the effect of delivering high velocity fluid particles to the bottom side-wall corners; similarly, to displace high velocity 'filaments' away from the bottom along the centreline and from the surface side-wall corners. With increasing flow and water depth in flumes, additional secondary currents may form, irrespective of the nature of the bed and side-walls (smooth, rough, or combinations of both surfaces) (Chow, 1959).

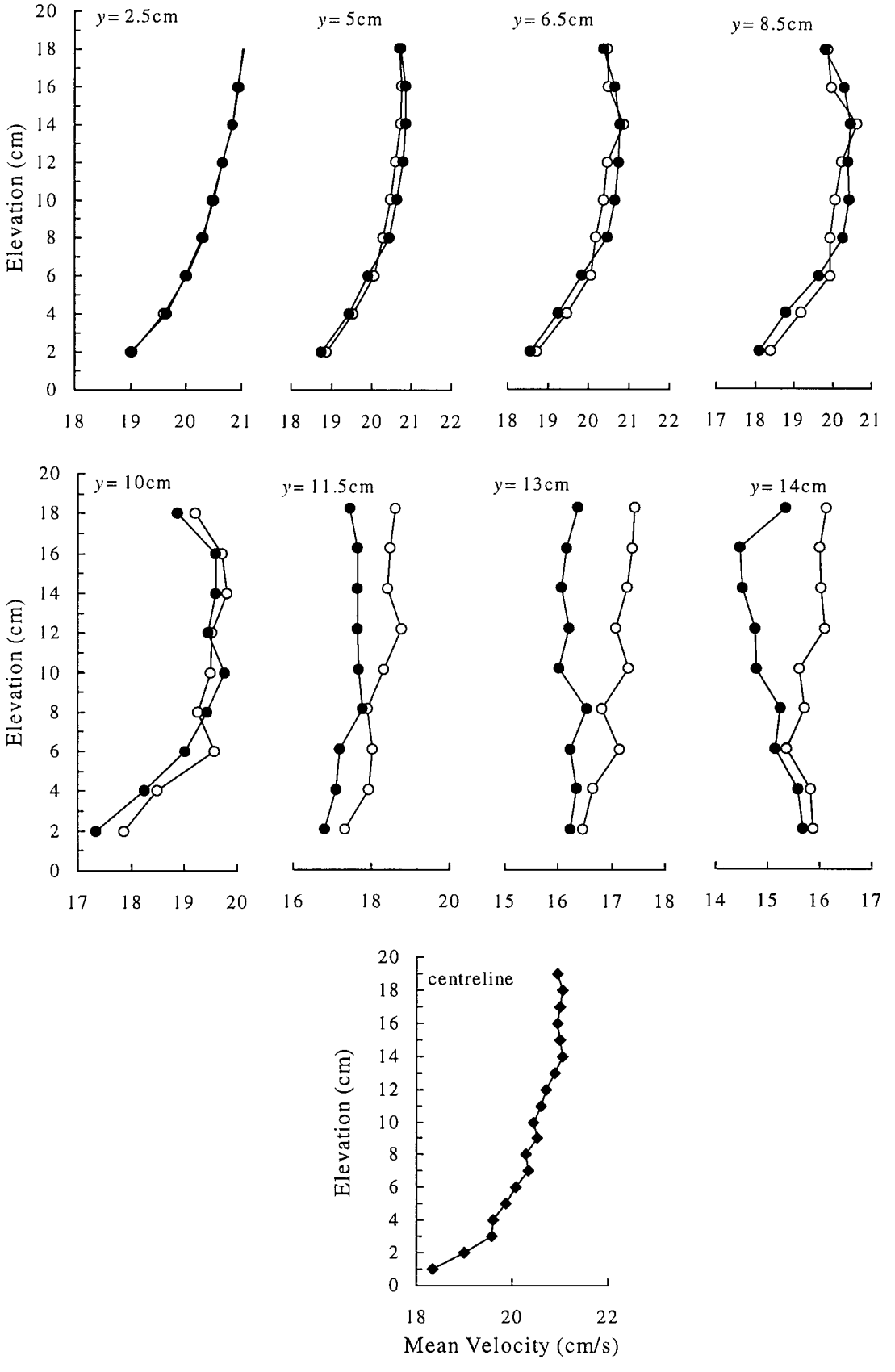

Figure 18: Vertical variations in the mean velocity (u, cm/s), with elevation (z, cm). y is the distance across the flume, • RHS and o LHS (looking in a downstream direction).

The flow pattern appears to be highly disturbed and complicated towards the side boundaries (±11.5cm outwards, from the centreline); this illustrates the increased disturbance of the velocity profile, as the side walls are approached. The extent of the complexity observed in these profiles, closest to the side boundaries, may be the result of the inability of the Streamflo current meter to measure accurately the velocity in these regions very close to the side panels.

The mean velocities have been found to increase continuously towards the central portion of the flume, as well as with elevation above the bed (Figures 17 and 18). The effects of the side and bottom boundaries are, therefore, at a minimum nearer to the water surface and towards the centre line of the flume. Figure 19 illustrates the general pattern of velocity distribution at the flume's cross-section; the contours represent equal velocities in the channel section. For the selected flow conditions (used elsewhere for threshold determinations, see Paphitis *et al.*, in press), with a mean velocity of 20cm/s, it can be concluded that the influences of the side walls extend to a distance of, at least, 6cm across the flume. Consequently, these results suggest that the central 15cm of the flow can be considered independent of cross-stream position; however, this will experience a gradual decrease, with increasing flow velocity.

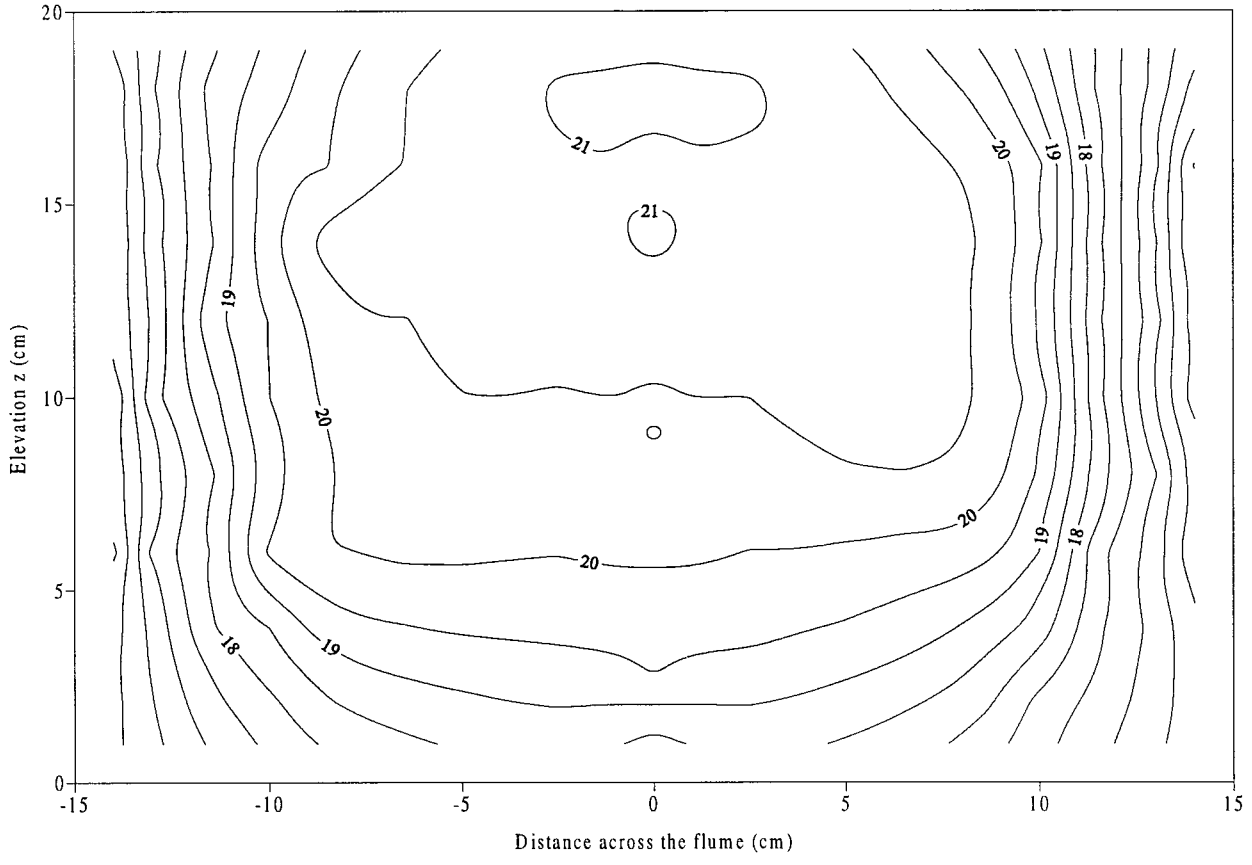

Figure 19: The general pattern of velocity distribution within the flume; the contours represent equal velocities in the channel section.

Using the cross-sectional mean velocity (~20cm/s) and the hydraulic radius (defined as $bh/(b+2h)$, where b is the channel width and h is the water depth), a Reynolds number of 1.7×10^4 was derived (see Eq. 2; in this the hydraulic radius was used instead of h as the characteristic length); this indicates that the flow was turbulent. In most open channels (and, indeed, in the natural environment), laminar flow occurs very rarely. The fact that the surface of the flow, in the above experiments, appeared smooth and glassy is by no means an indication that the flow was laminar; most probably, it indicates that the surface velocity was lower than that required for capillary waves to form. Laminar open-channel flows do occur, with the exceptions being flows of fluids of very high viscosity, or a thin sheet of water flow (Chow, 1959; Douglas *et al.*, 1979).

4.4 Vertical Flow Velocity Profiles

In order to investigate, in detail, the vertical structure of the mean velocity and turbulence intensity, three flow regimes (namely 'slow', 'moderate' and 'fast'), were selected for investigation at a fixed nominal depth of 12cm. In all cases, the measurement station was on the centreline of the flume, at a position 3.5m from the leading edge. Each vertical profile had 30 to 32 measurement stations and the record length at each station was 5min, as utilised in the preliminary experiments (see Section 4.2.2). The experiments were carried out over both rough (an artificially-prepared sandy bed) and smooth (flume's bed) surfaces. The derived velocity profiles are plotted on linear and semi-logarithmic scales in Figures 20 and 21, respectively. The identification given to the profiles is related to the flow regime (S-'slow'; M-'moderate'; and F-'fast') and the boundary condition (R-'rough' and S-'smooth').

The profiles (Figures 20 and 21) illustrate an increase in the velocity gradient (du/dz), with increasing flow; the velocity gradient decreases with increasing elevation above the bed. The maximum velocity gradient occurs within the lower 1cm of the flow. The mean velocity gradients (du/dz) of the individual profiles tend to decrease, progressively away from the bed; this is indicated by the general 'concave upwards' shape of all the (linear) profiles. A partially-developed boundary layer would be indicated if the velocity gradient was zero, at any part of the profile. With the exception of those profiles measured at the slow flow regime (z>5cm), all the other profiles indicate fully-developed boundary layers, as there are no regions of zero velocity gradient within these profiles.

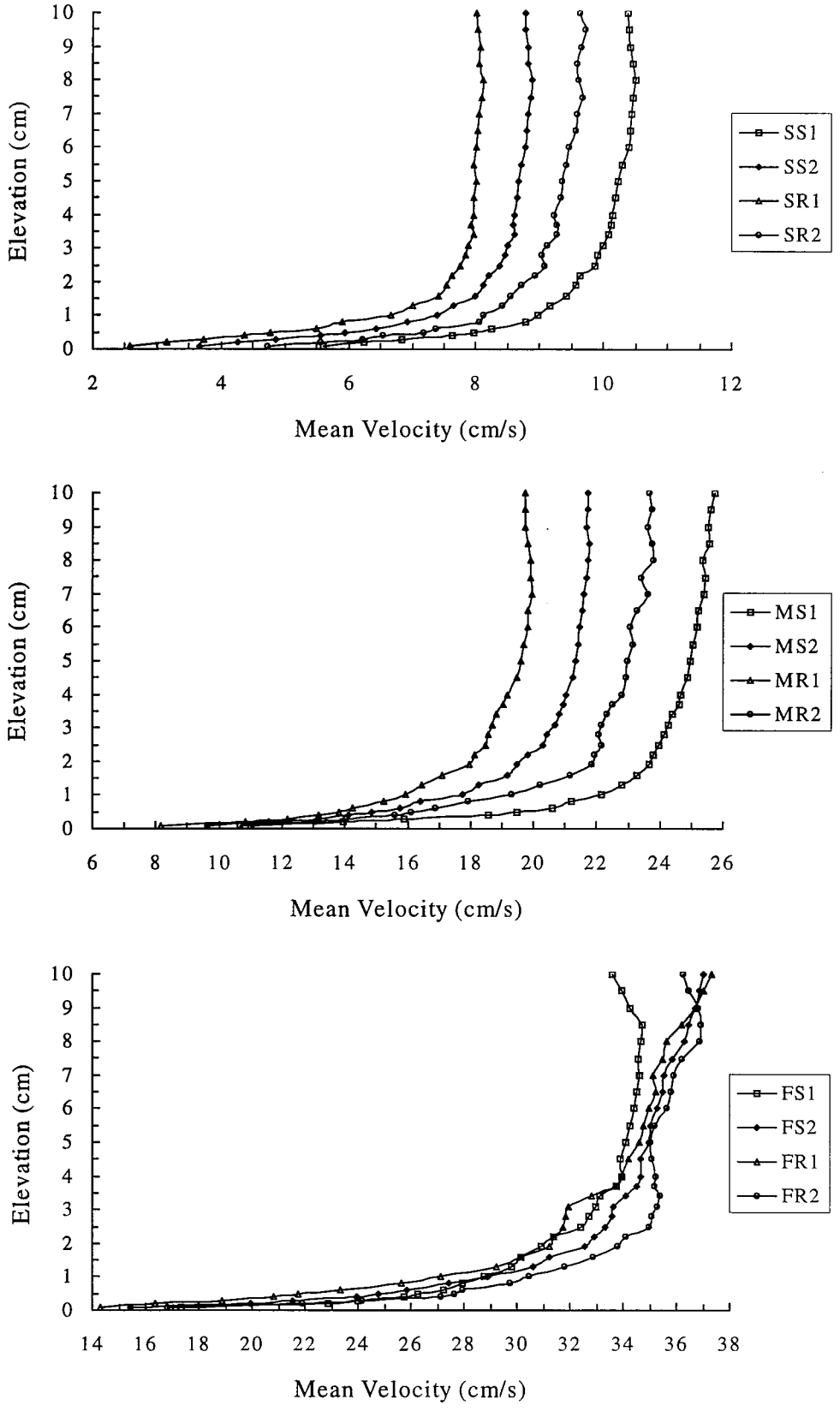

Figure 20: Mean velocity (u, cm/s) variations with elevation (z, cm) for the various flow rates. The identification given to the profiles is such that S (slow), M (moderate) and F (fast) relate to the flow rate, whereas R (rough) and S (smooth) relate to the boundary state (i.e. MR1 is the first profile under moderate flow rate over a rough boundary).

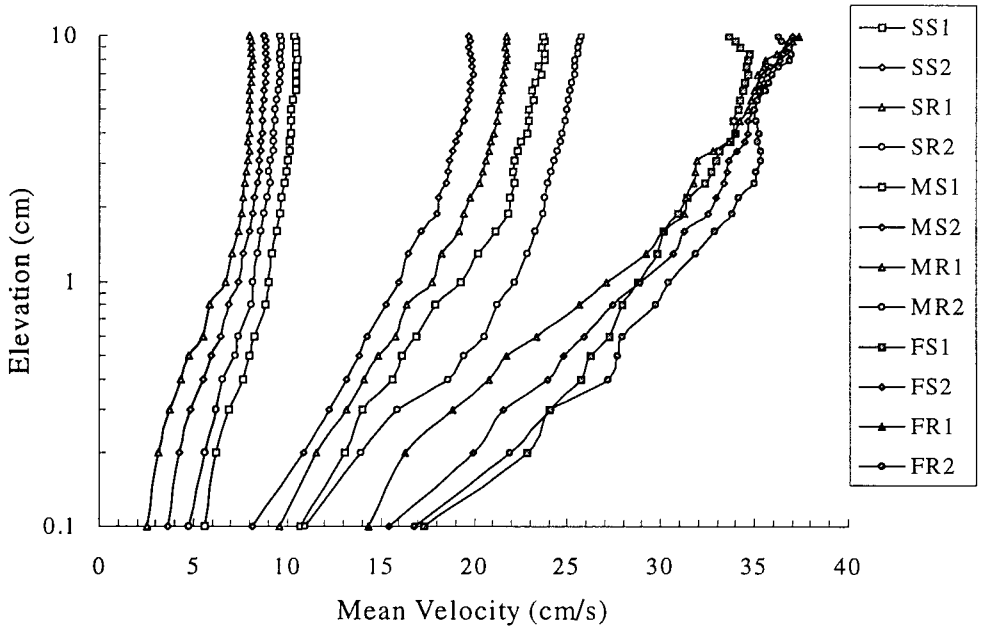

Figure 21: Mean velocity (u, cm/s) variations with elevation (z, cm) for the various flow rates, plotted on a semi-logarithmic scale.

The upper part of the profiles measured under fast flow regimes exhibit slight deviations from the expected theoretical logarithmic distribution (Figure 21). These deviations may be due to experimental uncertainty; the positional uncertainty of the LDA may account for some of the observed deviations particularly for data points lying close to the bed. Recirculating eddy motion, generated by secondary circulation effects, can cause major deviation in the mean velocity profiles; this cannot be inferred conclusively, because the magnitude of the error caused by such disturbances was not adequately quantified. Furthermore, the fact that individual velocity measurements at different elevations were not carried out simultaneously, may also account for some of the observed deviation. In most cases, such small deviations can be attributed to the averaging effect on the sharp mean velocity fluctuations near the boundary. However, the small measuring volume of the LDA reduces significantly such a possibility, suggesting that the deviations are likely to be a real phenomenon; this may be due to either certain flow conditions, or the presence of secondary roughness elements within the flume. The experimental runs were undertaken over a smooth boundary and a uniform surface of a single grain layer of sandy sediment; in both cases, the artificial bed was utilised, the presence of which might have created a certain roughness within the working section (and, hence, the small deviations from the theoretical distribution).

4.4.1 Standard Deviation

The velocity measurements carried out in these experiments were averaged over a sufficiently long period (5min); this provides a much more consistent result, for the mean flow, than the instantaneous measurements (this is so when turbulence is not being investigated). The random velocity fluctuations indicating turbulence are averaged out, with time, and the steady mean flow can be distinguished. Instantaneous local velocity measurements of the LDA, which only distinguishes the u component of velocity in the x direction (for one-dimensional flows produced in the flume, $\overline{v}$ and $\overline{w}$ are zero) can be expressed, therefore, as $u = \overline{u} + u'$ (see Eq. 6, Section 2.3). When the mean values of the fluctuations are taken over a sufficiently long time interval, they average out to zero.

The standard deviation (σ, see Eq. 9) in the velocity measurements can be used as an indication of the magnitude of the velocity fluctuations; the estimated values of the standard deviation are plotted, as vertical profiles, in Figure 22. The standard deviation is observed to decreases away from the bed (with the exception of the slow regime, smooth bed profiles); this illustrates the increasing importance of the presence of the boundary, on turbulence. The standard deviations in the velocity measurements experience an increase, as the flow rate increases from 'slow' to 'fast'. Under the examined flow rates, the smooth bed appears to have less influence on the flow, than the rough bed. At 'moderate' and 'fast' flow conditions, the smooth bed profiles appear to have a more pronounced reduction of the standard deviation, with elevation, when compared to the rough bed profiles. The influence of the roughened bed, upon turbulence, is affective to elevations of at least 8-10cm.

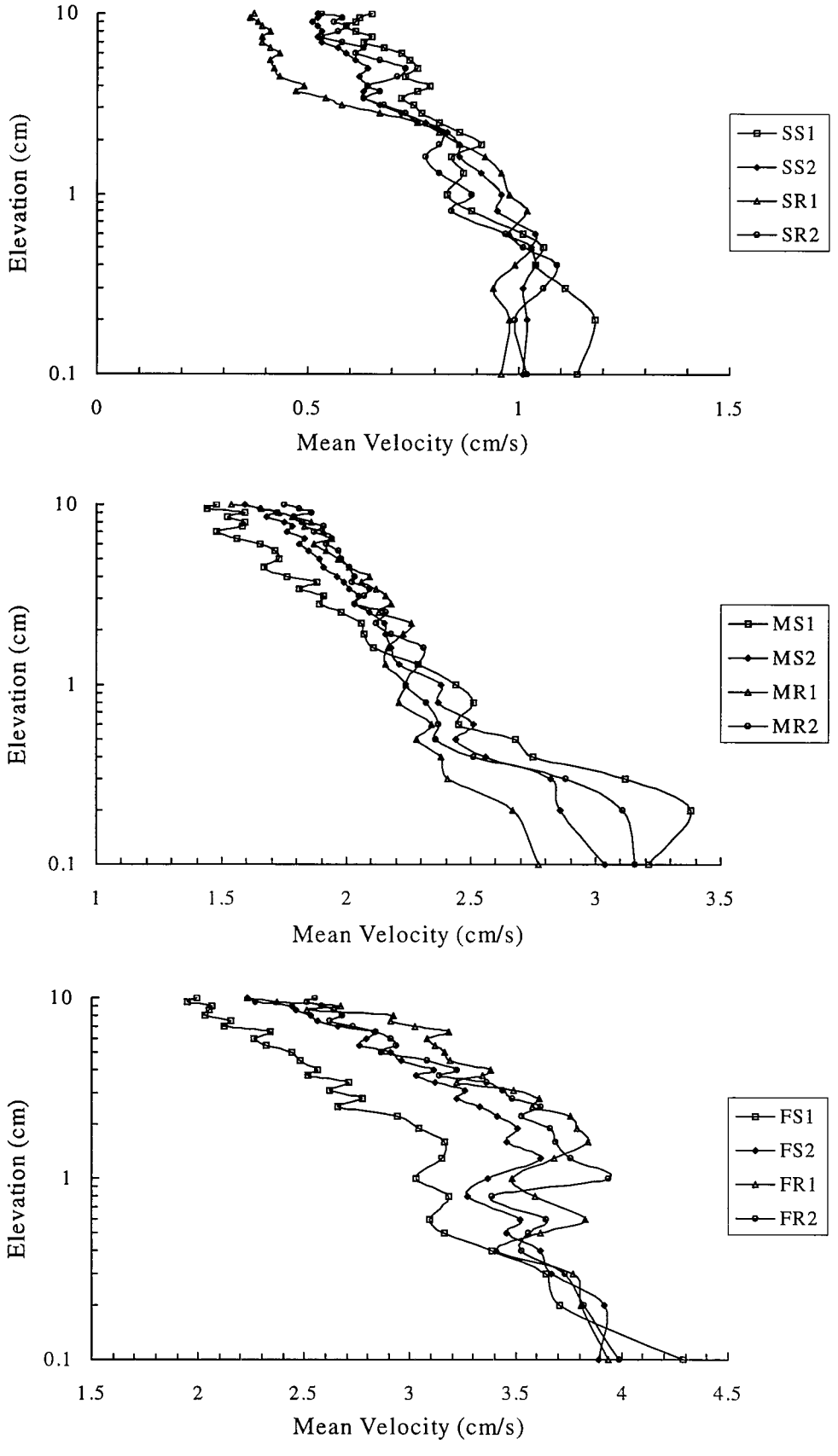

Figure 22: Standard deviation (σ, cm/s) variations, with elevation (z, cm), for the various flow rates (plotted on a semi-logarithmic scale).

4.4.2 Longitudinal Turbulence Intensity (LTI)

The effect of roughness elements upon the magnitude of the velocity fluctuations in the flow may be expressed in terms of the relative Longitudinal Turbulence Intensity (LTI=σ/u). Observations on the LTI near the bed have shown that, in the vicinity of a rough bed, the turbulent intensity increases towards the bed; it is influenced by the arrangement, size and shape of the roughness elements (Lyres and Woodruff, 1972). LTI values are plotted against elevation, on a semi-logarithmic scale, in Figure 23. The LTI values appear to be lower for smooth rather than rough boundary conditions, particularly close to the bed and up to an elevation of about 2cm.

LTI scales directly with mean velocity measurements, since they are related statistically; minimum turbulent intensity values coincide with maximum velocities (e.g. Mehta, 1979). LTI variation, with respect to elevation (z) and scaled to flow depth (h), are presented in Figure 24. With reference to the variety of flow regimes presented on Figure 24, the LTI can be seen to increase as the bed is approached (corresponding to the decrease of mean velocities).

The slow flow rate profiles emphasise the difference between the smooth and rough beds; an increase of the order 44% has been estimated at z/h=0.1 and a 18% increase at z/h=0.8. Similar results have been obtained elsewhere (McQuivey and Richardson, 1969), with 50% and 20% increases in LTI over a rough bed, at z/h=0.1 and 0.8, respectively. This pattern demonstrates that the divergence is not merely due to differing water depths. For the 'moderate' and 'fast' rough bed profiles, an increase in LTI of approximately 25% to 30% at z/h=0.1 and 11% to 14% at z/h=0.8 occurs, when compared to the smooth bed profiles. These differences are not as extensive as those observed between the corresponding slow flow rate profiles. Such variation is likely to be either due to the flow in the smooth 'moderate' and 'fast' profiles not being hydraulically smooth, or to an experimental error (Section 3.3).

The presence of roughness elements on the boundary creates additional turbulent intensity and, hence, in the near-bed region the LTI increases with increasing bed roughness. Bayazit (1976) attributes this reduction in LTI to: (a) the conversion of a part of the flow energy, into heat, in the separation zones between the roughness elements; and (b) the dampening of turbulence in the region away from the roughness elements, as a substantial part of the available energy of the mean flow is converted into turbulence in the separation zones. The available data are not sufficient, however, to make any firm conclusions about LTI reductions close to rough beds.

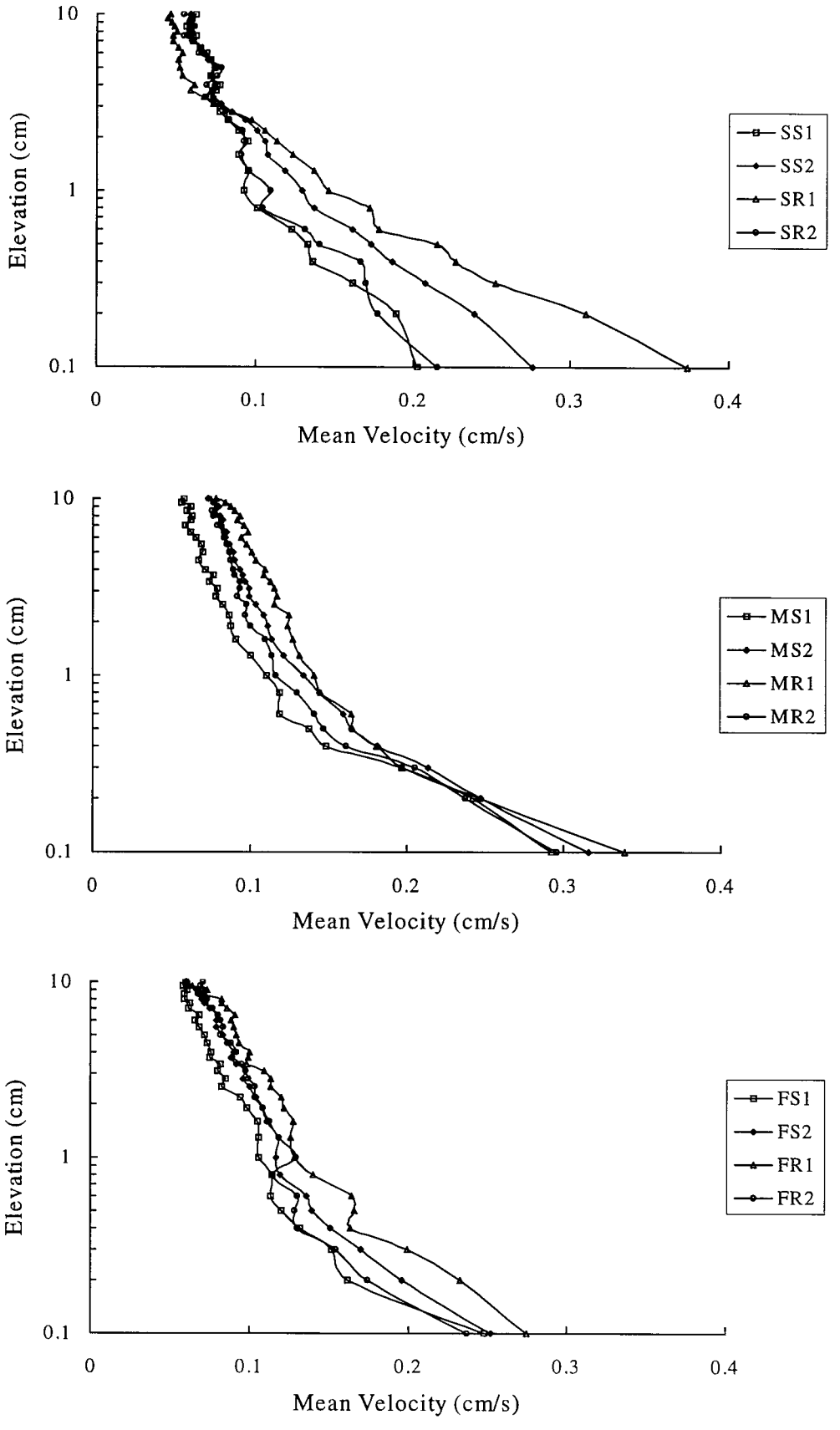

Figure 23: LTI variations, with elevation (z, cm), for the various flow rates (plotted on a semi-logarithmic scale).

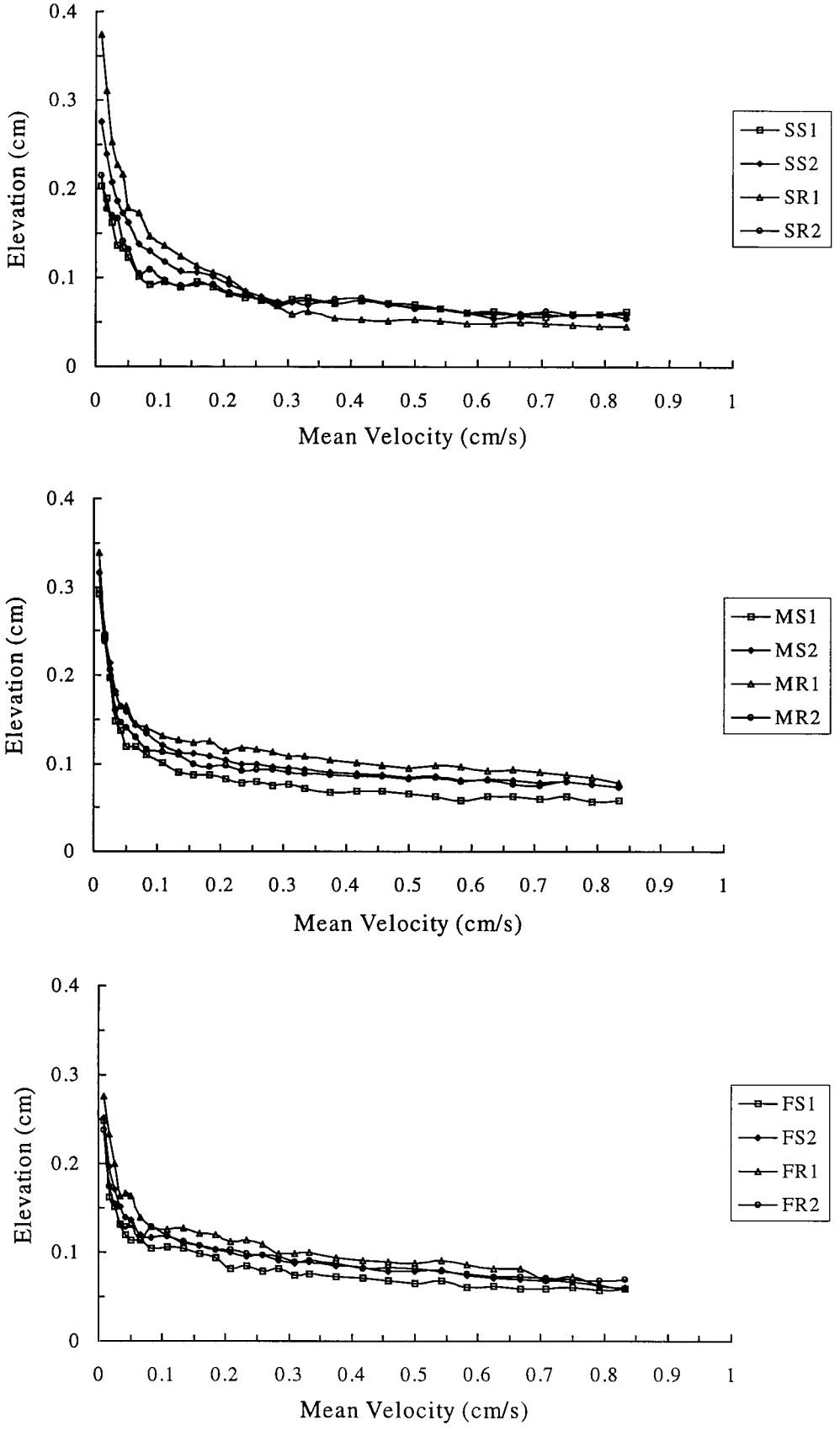

Figure 24: LTI variations, with elevation (z, cm), scaled to flow depth (h, cm) for the various flow rates (plotted on a linear scale).

4.5 Determination of Shear Velocity

In order to facilitate comparisons between the data of the various investigators, it is customary to summarise the experimental variability in terms of a limited number of independent variables (ρ_s, ρ, ν, h and τ_o, as defined in Section 2.2). Of these variables, the most difficult to measure is the bed shear stress, τ_o. Various methods of determining shear velocity (u_*) and, thereby τ_o, using mean velocity profiles are described in Section 2. The application of particular equations is dependent upon the prevailing flow regime (smooth, transitional or rough); this is a function of the grain Reynolds number, Re_* ($k_s u_* / \nu$, see Section 2.2.3).

Unless u_* is known (or estimated), Re_* and the corresponding type of flow regime will remain unknown. Therefore, it is not possible to predict which form of the logarithmic law should be used, in order to determine u_* from mean velocity measurements. Provided velocity measurements are made within the constant stress layer, where there is a logarithmic profile, this problem may be overcome by using the velocity gradient method (Eq. 51), which can be derived from both the smooth- and rough-wall logarithmic laws (Eqs. 44 and 48, respectively); this method is discussed below. Alternatively, u_* may be calculated from both equations, using individual pairs of velocity (u_z) and elevation (z) values. In such a procedure the problems arises as to which points (if not all), within the boundary layer profile, should be used; likewise, to that effect, the equation that best describes the prevailing flow conditions. In terms of the latter, the equation which produces the more realistic or consistent estimates of u_* may then be preferred. The corresponding values of Re_* (which can then be calculated using the estimates of u_*) may indicate the prevalent flow regime, at the time of the experimentation. Unfortunately, these methods of estimating shear velocity are not without problems; some of these are outlined below.

4.5.1 Problems with Shear Velocity Determinations

The determination of Re_* will indicate which flow regime prevails. Unfortunately, when the flow regime is transitional ($5 < Re_* < 70$), between smooth and rough, no simple empirical formula exists to predict the form of the boundary layer velocity profile. At such times, neither viscosity nor the bed roughness are insignificant, in terms of their influence on the near-bed flow. In this region flows can, at best, be approximated either by the smooth- or rough-wall laws, depending upon whether they are more nearly 'hydraulically smooth' or 'fully turbulent'.

The logarithmic laws are strictly only valid within the constant stress layer (Section 2.5.2). The lower limit of this region, for smooth turbulent flows, is given variously as $30 < zu_*/\nu < 70$. Consequently, it is only possible to determine whether a particular measurement of u_z was made below the constant stress layer, after u_* has first been estimated. If the zu_*/ν computation indicates that any of the velocity measurements, used in the u_* determination, were made below the constant stress layer, then these estimates should be considered unreliable (and, hence, ignored) and an estimate must be made using velocities measured farther away from the bed. The upper limit lies within the interval $0.1 < z/\delta < 0.2$. The estimation of δ (Eq. 28), the boundary layer thickness, involves a measurement of the free-stream velocity and relies upon fitting curves to experimental data; such a procedure is highly sensitive to experimental error. Alternatively, assuming that the boundary layer extends to the free water surface, then $\delta = h$ and values above $z/h = 0.2$ can be excluded (as deviation from the logarithmic equations occurs above this level). Determining the extent of the constant stress layer is important in deciding whether reliable estimates of u_* can be derived, using the logarithmic laws, from experimental measurements of u_z.

Experimental error is the third problem impairing the determination of u_*, from mean-velocity measurements. The true mean-velocity profile will be composed of a number of curves, corresponding to the inner, overlap and outer regions of the boundary layer (Figures 7 and 8) and, possibly, the free stream, if the boundary layer is only partially developed. Downstream variation in the profile or roughness of the bed may introduce further complexities. Furthermore, in smooth or transitional flows, the inner region will be further subdivided into the buffer layer and the viscous and laminar sublayers (Section 2.5.2). Within each of the layer, the mean-velocity data will follow a different curve. The general dimensionless form of the curves has been established here by a large number of individual measurements, which display some degree of scatter (see Figures 9 and 10). In order to establish the detailed form of a particular velocity profile, it is still necessary to make a number of observations for each component curve.

4.5.2 The Log-Profile Method

It is common practice, in both the marine environment (Sternberg, 1972) and in the laboratory (Sumer and Deigaard, 1981) to plot velocity profiles on semi-logarithmic axes; in such representations logarithmic relationships follow straight lines. Theoretically, it requires only two u_z measurements to show the form of the relationship, which is expected to be logarithmic.

However, in practice and in order to reduce experimental errors, the velocities at three or more points are measured. Curve-fitting is performed by regressing the mean velocity against log(z), in order to estimate the shear velocity (from the slope of the relationship). The acceptance, or rejection, of a relationship will then depend upon the magnitude of the scatter about the regression line, as given by a correlation coefficient.

The profiles plotted in Figure 21 do not reveal any well-defined linear trends. Similarly, it is extremely difficult to decide to what extent the complexities of the measured profiles are due to the actual velocity profile, as opposed to experimental uncertainty. Least-squares linear regressions were performed on these profiles to yield the best straight line fit. This approach is equivalent to fitting linear equations to log(z), u_* pairs, of the form:

$$u_z = a + b\log(z) \tag{55}$$

Eq. 55 may be combined with Eq. 53, to produce an estimate of u_*. Consider the form of Eq. 55, when z takes the values 1 and 10,

$$u_{10} = a + b$$

$$u_1 = a$$

and Eq. 53 reduces to,

$$u_* = \frac{\kappa}{\ln(10)}(u_{10} - u_1)$$

and by substitution:

$$u_* = \frac{\kappa}{\ln(10)} b \tag{56}$$

An observed logarithmic relationship, of the form represented by Eq. 55, does not necessarily imply that the data approximate to either form of the logarithmic profile law. The closeness of the approximation to the smooth-wall law may be determined as outlined below. Assume that Eqs. 45 and 55 define the same curve,

$$a + b\log(z) = \frac{u_*}{\kappa}\ln\left(\frac{z u_*}{\nu}\right) + u_* C_S$$

$$u_* C_S = a + b\log(z) - \frac{u_*}{\kappa}\ln(10)\log\left(\frac{z u_*}{\nu}\right)$$

using Eq. 56,

$$u_* C_S = a + b\log(z) - b\left(\log\frac{u_*}{\nu} + \log(z)\right)$$

$$C_S = \frac{1}{u_*}\left[a - b\log\left(\frac{u_*}{\nu}\right)\right]$$

substituting u_* from Eq.56,

$$C_S = \frac{\ln(10)}{\kappa b}\left[a - b\log\left(\frac{\kappa b}{\ln(10)\nu}\right)\right] \tag{57}$$

Hence, if κ and ν are known, C_S may be determined given Eq. 55. If the value of C_S is close to the empirical value of 5.5, then the data indicate a smooth turbulent velocity profile.

A similar procedure can be followed to show the approximation to the value of the constant C_R, from the rough turbulent profile law. Assume Eqs. 49 and 55 define the same curve:

$$a + b\log(z) = \frac{u_*}{\kappa}\ln\left(\frac{z}{k_s}\right) + u_* C_R$$

$$u_* C_R = a + b\log(z) - \frac{u_*}{\kappa}\left(\ln(z) - \ln(k_s)\right)$$

substituting b from Eq. 56,

$$u_* C_R = a + \frac{u_*}{\kappa}\left(\ln(10)\ln(z) - \ln(z) + \ln(k_s)\right)$$

$$C_R = \frac{a}{u_*} + \frac{1}{\kappa}\ln(k_s)$$

substituting u_* from Eq. 56,

$$C_R = \frac{a\ln(10)}{\kappa b} + \frac{\ln(k_s)}{\kappa} \tag{58}$$

Eq. 58 may be determined if k_s is known (or estimated). For the regression analysis, it is assumed (initially) that the measured regression line indicates a similar velocity profile to either the smooth or rough profiles; then the estimates of C_S and C_R enable a comparison with the respective empirical values of 5.5 and 8.5 (Nikuradse, 1932 and 1933), for the definition of the flow conditions. This procedure requires several arbitrary assumptions to be made, in relation to: (a) which values of y/δ and zu_*/ν should be used to define the limits of the constant-stress layer; and (b) what are the acceptable limits C_S and C_R. This method for determining shear velocity, herein referred to as the 'log-profile method', will be evaluated using the velocity profiles which where described previously in Section 4.4.

4.5.3 The Log-Profile Method: An Evaluation

Regressions were performed on the vertical velocity profiles presented in Section 4.4. One profile was selected from each flow regime (slow, moderate and fast); these were treated separately, with respect to smooth or rough boundary conditions. The resulting u_* estimates were subjected to several restrictions.

The boundary layer thickness (δ) could not be determined, with any certainty, from the shape of the profiles; therefore, it was assumed that δ was equal to h. The restriction of permissible u_z values, to below the upper limit of the constant stress layer ($z<0.2\delta$), required that u_z values measured above the level $z/h=0.2$, were not considered; this excluded data from elevations of 2.5cm and above. For the smooth-wall law, the lower limit of the constant stress layer may be defined by $zu_*/\nu<30$. Shear velocity estimates, which indicated that observations made below this level were used in their calculation, were rejected for being below the constant stress layer. Depending upon the nature of the boundary conditions being smooth or rough, regressions which implied C_S and C_R values outside the arbitrary ranges $4<C_S<7$ and $7< C_R<10$, respectively, were rejected. The nearest empirical values to 5.5 and 8.5 were accepted, as being the closest to the smooth- and rough-wall law, respectively.

The purpose of the procedure adopted for the regression analysis was to determine which points (if not all) within the boundary layer profile can be used, with confidence, for shear velocity estimations. Consequently, regressions were performed on 3 or more adjacent points along the profile. Commencing at the lowest point, a line of best fit was calculated incorporating the point itself and the points located immediately above it. From the 13 pairs of u_z and $\log(z)$ measurements (all those below 2.5cm, see above), it is possible to calculate 11 regressions of u_z on $\log(z)$, involving 3 adjacent points of z; 10 regressions involving 4 adjacent points of z; 9 regressions involving 5 adjacent points of z; and so on, until the line of 'best fit' was calculated involving all 13 points. In total, there are 66 different possible groupings of 3 or more adjacent points. The resultant regression of each group were used to calculate u_* values, using Eq. 56 and C_S and C_R values from Eq. 57 and 58, respectively.

Smooth Boundary

A plot of u_* 'isovels' calculated from Eq. 45 with κ=0.4, C_S=5.5 and ν=0.0114cm^2/s, is shown as Figure 25. Also plotted are the curves representing equal zu_*/ν values, of 11.6, 30 and 70. Using the u_* estimates from the regressions, zu_*/ν values were calculated; these was to reject the estimates that included u_z measurements which were obtained below zu_*/ν<30 (where z is the minimum elevation used in each regression). The calculated C_S values (Eq. 57) formed a further criterion for accepting or rejecting a u_* estimate, from the regressions. Finally, u_* estimates were rejected if the correlation coefficient and the associated p-value of the regression was below the minimum acceptable level.

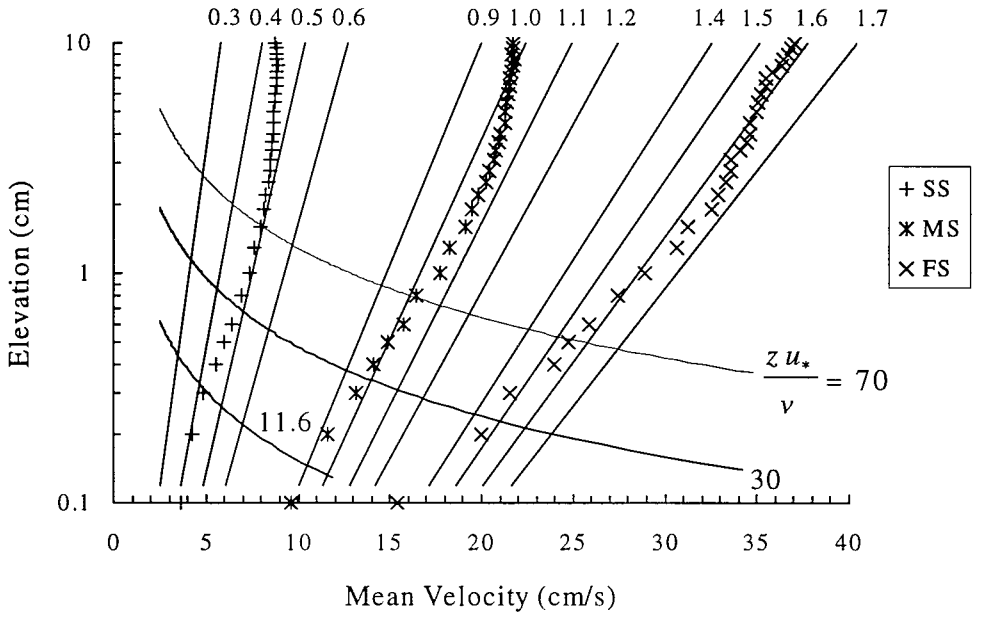

Figure 25: Mean velocity (u, cm/s) variations with elevation (z, cm) for the various flow rates over the smooth boundary. The Figure shows the u_* isovels for the smooth-wall law and zu_*/ν contours (plotted on a semi-logarithmic scale); u_* isovels calculated from Eq. 45, with κ=0.4, C_S=5.5 and ν=0.0114cm^2/s.

Calculations of the zu_*/ν values have indicated that u_z measurements made below 0.8cm, 0.3cm and 0.2cm for the slow, moderate and fast flow regime, respectively, were below the lower limit of the constant stress layer. Observations of the zu_*/ν=30 isovel, as shown in Figure 25, confirms the identified levels on the basis of the multiple regression analysis.

Within the interval 0.8 to 2.5cm, which provided the optimum regression for the slow flow regime, the data points show a close approximation to the local trend of the isovels. The optimum u_* value of 0.49cm/s agrees also with the value of the isovels and the derived C_S value

was found to be 5.52. This particular regression was associated with a correlation coefficient of 0.975, with an insignificantly small p-value; this suggests a very strong relationship. In the majority of regressions, the derived C_S values were outside the acceptable (arbitrary) range of the C_S values. For the moderate flow regime, the optimal regression was provided within the interval 1 to 2.2cm, resulting in a u_* value of 1.11cm/s and a C_S value of 4.59 (with a correlation coefficient of 0.981 and a p-value<<0.001). In the case of the fast flow regime, the interval 1.3 to 2.5cm was found to offer the optimum regression (0.955 correlation coefficient and a p-value<0.004), which provided a u_* value of 1.76cm/s and a C_S value of 4.17.

The process outlined above, by which an optimum regression was obtained using the three profiles, entailed a highly subjective method of selecting criteria for acceptance or rejection of the results obtained. Application of the criteria resulted in the rejection of all but three regressions for the slow and moderate flow regime and only a single regression for the fast flow regime; this was due to violation of acceptable zu_*/ν and C_S limits and low correlation coefficients. Nonetheless, the regressions which were accepted offered good estimates of u_* and C_S values; these correspond closely to the isovels and the empirical values, respectively.

Rough Boundary

The plots of shear velocity isovels, calculated according to Eq. 49, are shown in Figure 26. The value of k_s was taken as 0.065cm; this corresponds to the (mean) diameter of the sand grains, constituting the roughened surface. The u_* estimates, derived using the rough-wall law, were accepted or rejecting on the basis of the calculated C_R values being within the acceptable (arbitrary) range and the resulting correlation coefficients. However, the presence of a rough boundary does not necessarily suggest hydrodynamically rough boundary conditions and, hence, the results of the multiple regression analysis were treated in the same manner as for the smooth boundary; shear velocity isovels, calculated according to Eq. 45, are also included. This procedure was adopted because initial indications suggested that the grain Reynolds number defines the hydrodynamically smooth and transitional flow regimes.

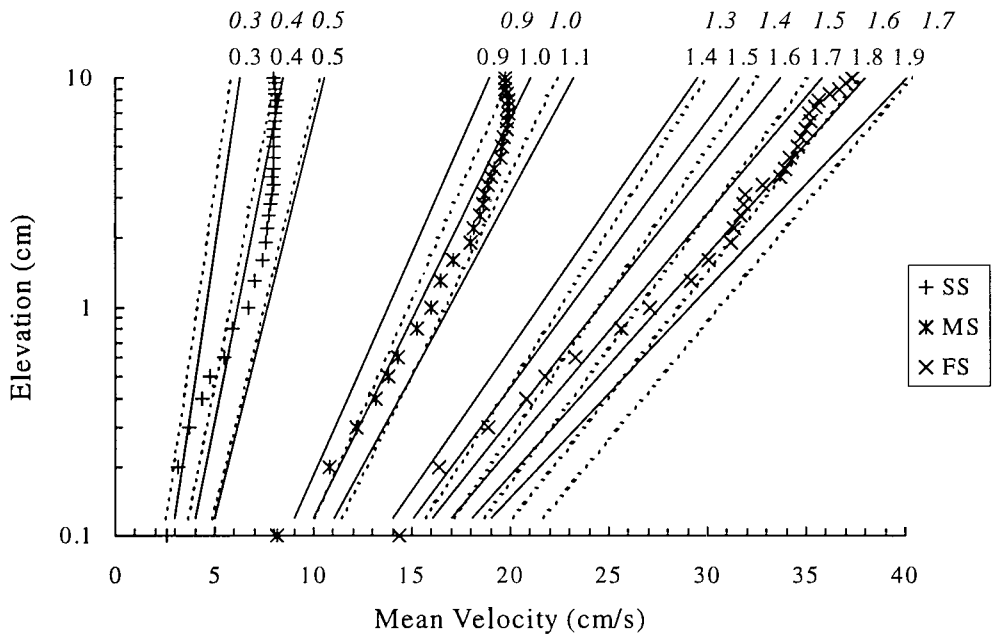

Figure 26: Mean velocity (u, cm/s) variations with elevation (z, cm) for the various flow rates over the rough boundary, illustrating the u_* isovels for both the smooth-wall law (dashed lines, with italic labels) and the rough-wall law (solid lines, with normal labels), plotted on a semi-logarithmic scale. u_* isovels calculated from Eqs 45 and 49, respectively, with κ=0.4, C_S=5.5, k_s=0.0651cm, C_S=8.5 and ν=0.0114cm^2/s.

The profile data obtained from the slow (flow) regime correspond closely to the trend of the u_* isovels between 0.4 and 0.5cm/s. This observation is in agreement with the u_* estimates provided by the accepted regressions, which were between 0.43 and 0.51cm/s. The optimal regression (within the interval 1 to 2.5cm, with a correlation coefficient 0.956 and a p-value<0.008) of the slow flow regime resulted in a u_* value of 0.43 and a C_R value of 9.04. The optimal regression (0.993 correlation coefficient and p-value<0.008) of the moderate flow regime, within the interval 0.8 to 1.6cm, provided a u_* value of 1.05 and a C_R value of 8.37. With the fast flow regime, the optimal regression (correlation coefficient 0.962 and p-value<0.03) was within the interval 1.3 to 2.2cm, providing an estimate for u_* of 1.75 and for C_R of 9.19.

Applying the smooth-wall law on these rough boundary profiles yields slightly different estimates. The optimum regression for the slow flow regime was provided within the interval 1.3 to 2.5cm; the data points also approximate closely to the local trend of the corresponding isovels. The optimum u_* value was estimated at 0.47cm/s (accepted regressions ranging between 0.43 and 0.48cm/s), with a corresponding C_S value of 5.27 (this regression offered a correlation coefficient of 0.979 and a p-value<0.001). Within the interval 0.6 to 1.9cm/s, which provided the

optimal regression for the moderate flow regime, a u_* value of 0.98cm/s and a C_S value of 5.13 were calculated (with a correlation coefficient of 0.971 and a p-value<0.004). The interval 1 to 2.2cm was found to offer the optimum regression for the fast flow regime (with a 0.966 correlation coefficient and a p-value<0.005), resulting in a u_* value of 1.57cm/s and a C_S value of 5.71.

The estimated values of u_*, from the optimal regressions in conjunction with k_s (0.0651cm), together with the 5 and 70 Re_* isovels are shown in Figure 27. Using all the u_* estimates from the multiple regression analysis (resulting from both the smooth- and rough-wall laws), Re_* values were calculated and found to range between $1.5<Re_*<6.5$, $4<Re_*<9.5$, $4<Re_*<19$ for the slow, moderate and fast flow regimes, respectively. In the present investigation, Re_* never exceeded 20; thus, fully-turbulent flows were not encountered. It can be seen from these calculations, together with the observation on Figure 27, that the generated flows were in the hydrodynamically smooth turbulent regime and the lower Re_* region of the transitional flow regime. Therefore, it might be reasonable to accept the u_* estimates provided by the smooth-wall law, as they may represent a better prediction of the mean velocity profile.

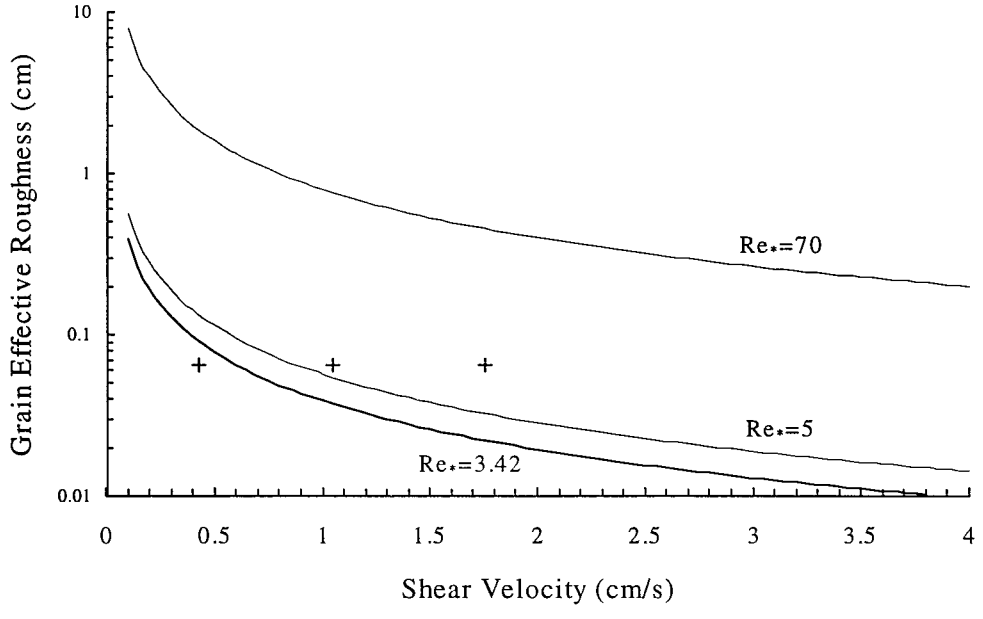

Figure 27: Shear velocity (u_*, cm/s), as a function of the grain effective roughness (k_s, cm). Re_* (u_*k_s/ν) isovels (at 15°C) are also included, indicating the surface classification limits (Re_*=3.42 isovel, at 15°C is also included).

It may be shown easily that the smooth- and rough-wall laws (Eqs 45 and 49) describe the same curve, when the following equality is satisfied:

$$k_s = e^{\kappa(C_R - C_S)} \nu / u_* \tag{59}$$

With the values of C_S, C_R and κ assumed for this investigation (5.5, 8.5 and 0.4 respectively), this equation reduces to:

$$\mathrm{Re}_* = \frac{u_* k_s}{\nu} = 3.42 \tag{60}$$

This line is included in Figure 27 showing the combinations of u_* and k_s for which Eqs. 45 and 49 will both define the same mean velocity profile.

4.5.4 Shear Velocity Estimates using the Single Point Method

From a single measurement of u_z, u_* may be derived from Eq. 49, by simply inserting values of u_z, z and k_s. The derivation of u_* from Eq. 45, for the same values of u_z and z, may be undertaken graphically, or by successive approximation. The latter method was employed in a reiterative computer program, in this study. Graphical estimation may be carried out using plots of u_* isovels for a fixed value of ν, as in Figure 26. When Re_* exceeds 3.42, the deviation between the values of u_* predicted by the different equations increases with the values of u_z and u_*. Figure 28 shows the range of u_*, given by Eq. 49 (for k_s=0.0651cm) and by Eq. 45, for a single value of u_z, at levels of 0.5 and 2.5cm. Also shown are the u_* estimates of all the profiles at these levels and the common Re_* value of 3.42, where the two equations intersect. The deviations between u_* estimates given by the same equation, using the experimental measurements of $u_{0.5}$ and $u_{2.5}$, appears to be less than the differences resulting from the use of the different equations, for a given observation of $u_{0.5}$ and $u_{2.5}$. However, in general the variation between the estimates of u_* given by the different equations, at the same elevation, decreases with u_z (as long as Re_* exceeds 3.42).

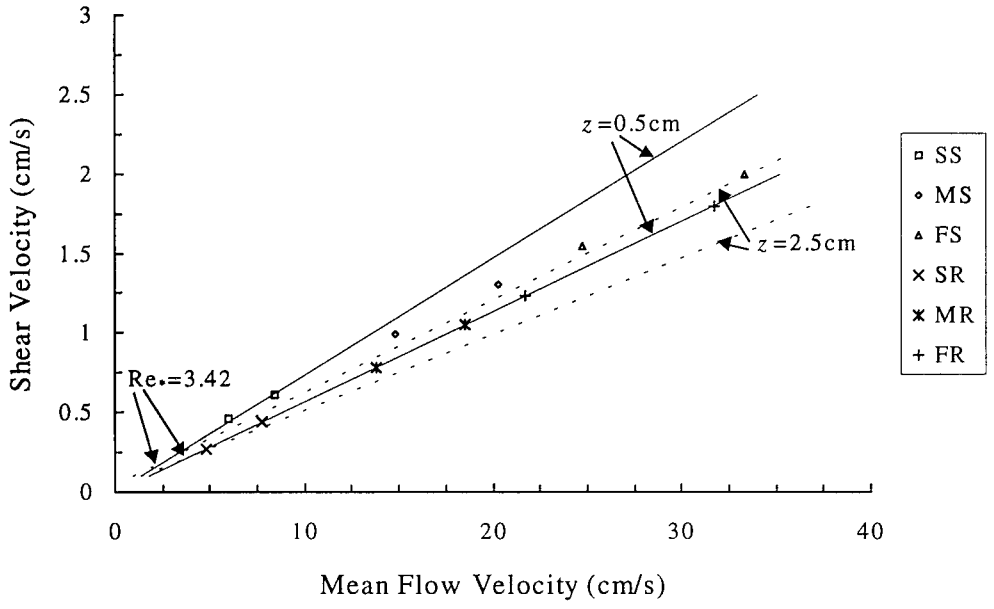

Figure 28: A comparison of u_* estimates derived from the smooth- (dashed line) and rough- (solid line) wall laws (Eqs 45 and 49, respectively), based upon $u_{0.5}$ and $u_{2.5}$ (κ=0.4, C_S=5.5, k_s=0.0651cm, C_S=8.5 and ν=0.0114cm^2/s).

Estimates of u_*, based upon the single observation method and using Eqs. 45 and 49, were calculated for each measurement of u_z; they are plotted for each profile in Figures 29(a) and 29(b), for the smooth and rough boundaries, respectively. These Figures show, in a different manner, the relationships between the individual data points and the u_* isovels, which are exhibited in Figures 26 and 27. Also plotted in Figure 29, are the one-point estimates of u_*, calculated reiteratively from the seventh power law (Eq. A-15). There is a very good agreement between these values and those determined using Eq. 45 (Figures 29(a) and 29(b)). Such agreement is not surprising, as both equations are based on the same variables and are represented by coinciding curves over the constant stress layer (Figure 11). A good agreement appears also to exist between Eqs 45, A-15 and 49, for the slow flow regime. Having the moderate and fast flows being described by the transitional flow regime probably explains, at least partially, the difference in the u_* derivations. On the basis of the evidence presented, the single point method appears to produce more consistent and less subjective estimates of u_*, than the multiple regression method.

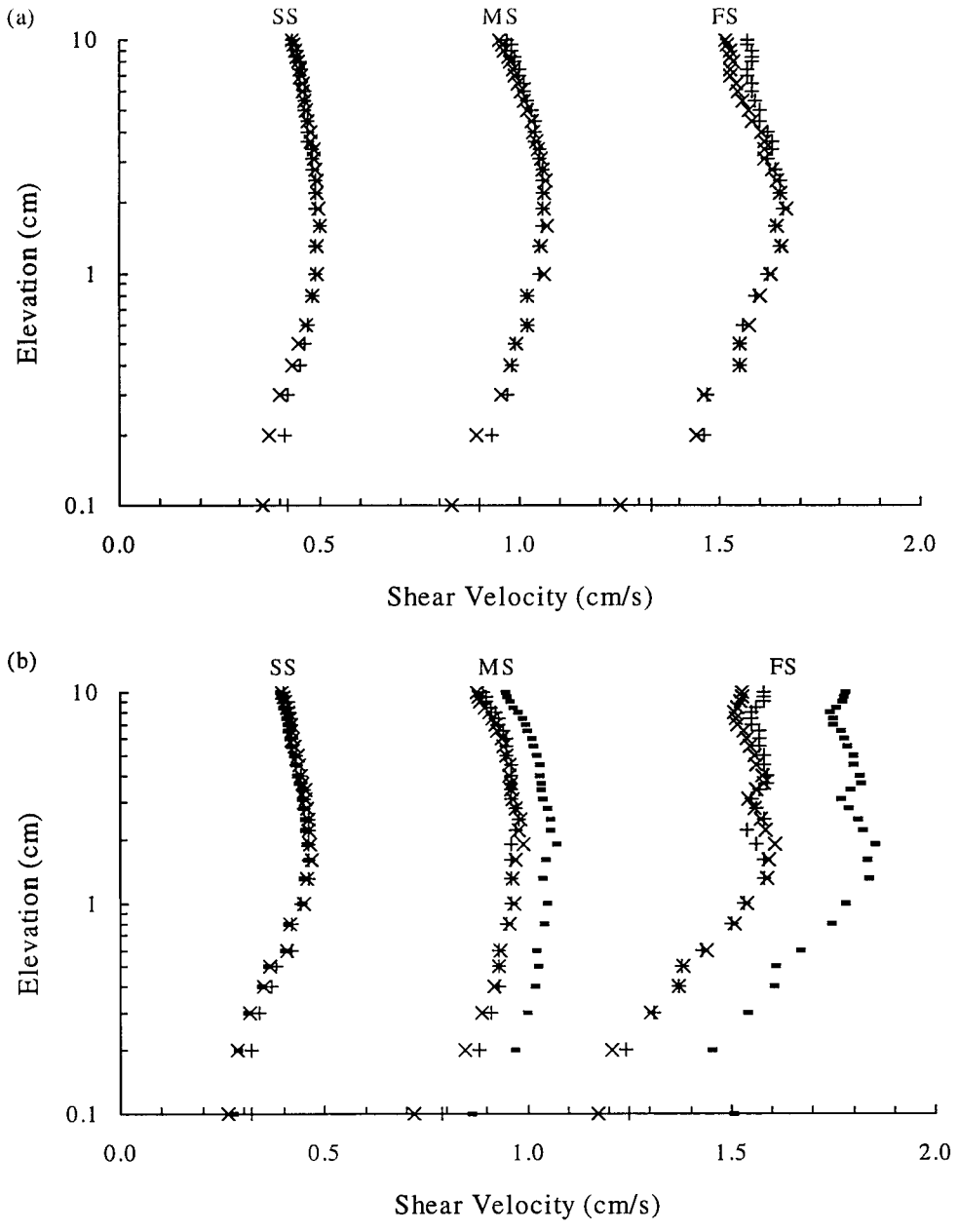

Figure 29: u_* profiles derived from the single observation method according to various relationships ((+) Eq. 45; (×) Eq. A-15; and (-) Eq.49): (a) over the smooth boundary; and (b) over the rough boundary.

Table 1: Comparative results between the different methods for estimating shear velocity.

u_* Estimation Method	u_* (Range) (cm/s)		u_* (Range) (cm/s)		u_* (Range) (cm/s)	
	SS		MS		FS	
Eq. 45	0.46	(0.41-0.50)	1.01	(0.90-1.06)	1.58	(1.33-1.58)
Eq. A-15	0.46	(0.36-0.50)	1.01	(0.83-1.07)	1.56	(1.25-1.67)
Log-Profile Method (Smooth-Wall Law)	0.49	(0.28-0.89)	1.10	(0.83-1.60)	1.75	(1.13-2.61)
	SR		MR		FR	
Eq. 45	0.42	(0.32-0.46)	0.94	(0.79-0.98)	1.52	(1.24-1.59)
Eq. 49	0.40	(0.27-0.45)	1.00	(0.85-1.06)	1.73	(1.45-1.84)
Eq. A-15	0.41	(0.26-0.47)	0.93	(0.72-0.99)	1.50	(1.17-1.61)
Log-Profile Method (Smooth-Wall Law)	0.47	(0.26-1.06)	0.98	(0.73-1.32)	1.57	(0.72-2.61)
Log-Profile Method (Rough-Wall Law)	0.43	(0.26-1.11)	1.05	(0.73-1.59)	1.75	(0.72-3.30)

4.5.5 Detailed Analysis of Mean Velocity Profiles

In order to resolve the differences between the estimates of the shear velocity, based upon the log-profile method and the one point estimates (and the seventh power law), a somewhat more sophisticated analysis of the mean velocity profile was employed. The procedure involved fitting mean velocity measurements within the entire water column to Eqs 41 and 47 (Section 2.6) for the hydrodynamically smooth and rough boundary conditions, respectively, with the wall function $f(zu_*/\nu)$ (given by Eqs 43 and 48 for smooth and rough, respectively) and the wake correction $W(z/h)$ (Eq. 44). Having established that the velocity profiles over the rough boundary were, most probably, in the hydrodynamically smooth turbulent and transitional flow regimes, the fitting procedure was performed for Eq. 41, as well as for Eq. 47.

Eqs 41 and 47 were fitted to the measured mean velocity profiles, through the use of least-squares regression, using the shear velocity (u_*) and the Coles parameter (Π). The Coles parameter was used as a fitting parameter, because its value is not well established for open-channel flows, and, likewise, because Nezu and Rodi (1986) found that it may depend upon the Reynolds number. The non-linear regression problem was solved by using an iterative procedure, in which the problem was linearised in relation to estimates of the fitting parameters; it was then solved, repeatedly, updating the fitting parameter estimates at each iteration. This method of shear velocity determination was termed the 'profile-fitting method'. Table 2 shows the shear velocity estimates, based upon the profile fitting method; these appear to be consistent with the estimates based upon the log-profile method (using the smooth-wall law) and Eqs 45 and A-15 (Table 1).

Table 2: Shear velocity estimations, using the 'profile-fitting method'.

Estimation Method	u_* (Range) (cm/s)		u_* (Range) (cm/s)		u_* (Range) (cm/s)	
	SS		MS		FS	
Eq. 41	0.49	(0.47-0.50)	1.04	(1.01-1.07)	1.59	(1.54-1.61)
	SR		MR		FR	
Eq. 41	0.44	(0.43-0.46)	0.97	(0.95-0.99)	1.53	(1.48-1.57)
Eq. 47	0.40	(0.34-0.43)	1.03	(0.97-1.05)	1.75	(1.69-1.81)

The measured mean velocity profiles over a smooth boundary and the fitted curves, based upon Eq. (41), are shown in Figure 30. Figures 31(a) and (b) show the measured mean velocity profiles over a rough boundary and the fitted curves, based upon Eqs (41) and (47), respectively. It is evident from the results shown in Figure 31, that Eq. 41 describes better the rough boundary velocity profiles. Thus, suggesting that the flows (MR and FR) which were characterised, initially, as transitional, may be better defined from equations (such as Eq. 41) used for hydrodynamically smooth surfaces. Curves constructed in this manner compare reasonably well with the measurements of mean flow velocity, especially at lower flow speeds (Figures 30 and 31). At higher flow velocities (especially for the FR velocity profile) the measurements appear to diverge from the calculated semi-empirical values; this is more pronounced close to the boundary (Figure 31(a)). A possible explanation as to why the measured mean velocities depart from the calculated semi-empirical values very near the bottom and at higher flow speeds, may be the potential presence of weak secondary mean flows in the y and z directions; this may transfer momentum vertically and, thus, change the turbulent transfer of momentum. A second possible explanation may be the interference of the bed with the light beams from the laser. In the absence of measurements of the z component of the mean velocity, the presence of weak secondary mean (flow) motions cannot be confirmed conclusively. Elsewhere, the measurements obtained by Nezu and Rodi (1986) are insufficient to address this particular question, in detail. These particular investigators did not measure the z component of the velocity at points lower than 14mm above the bottom; here, the differences between the measured and calculated values appear to exist.

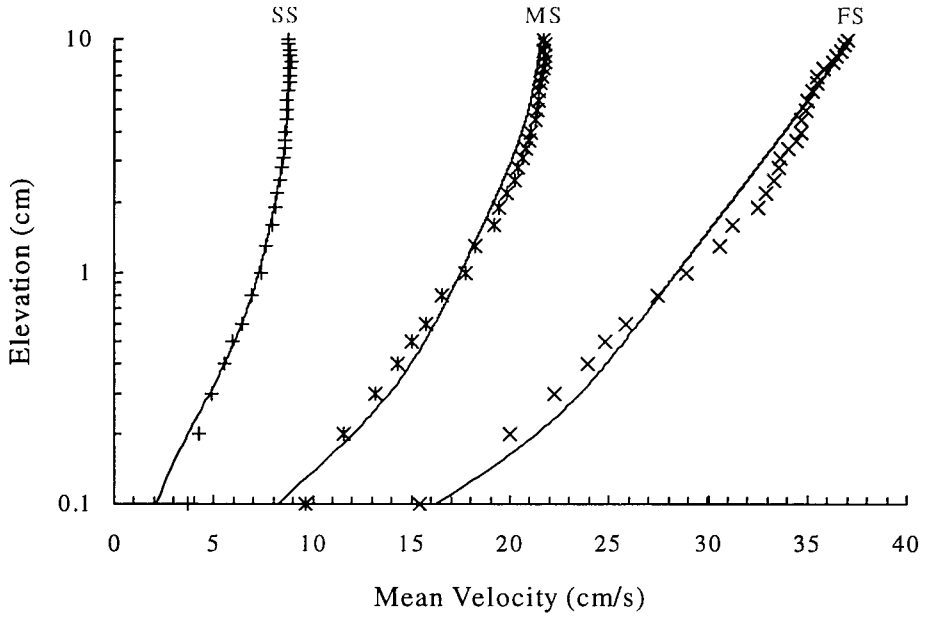

Figure 30: Mean velocity profiles for the various flow rates over the smooth boundary. Solid line: semi-empirical expression based upon Eqs 41, 43 and 44.

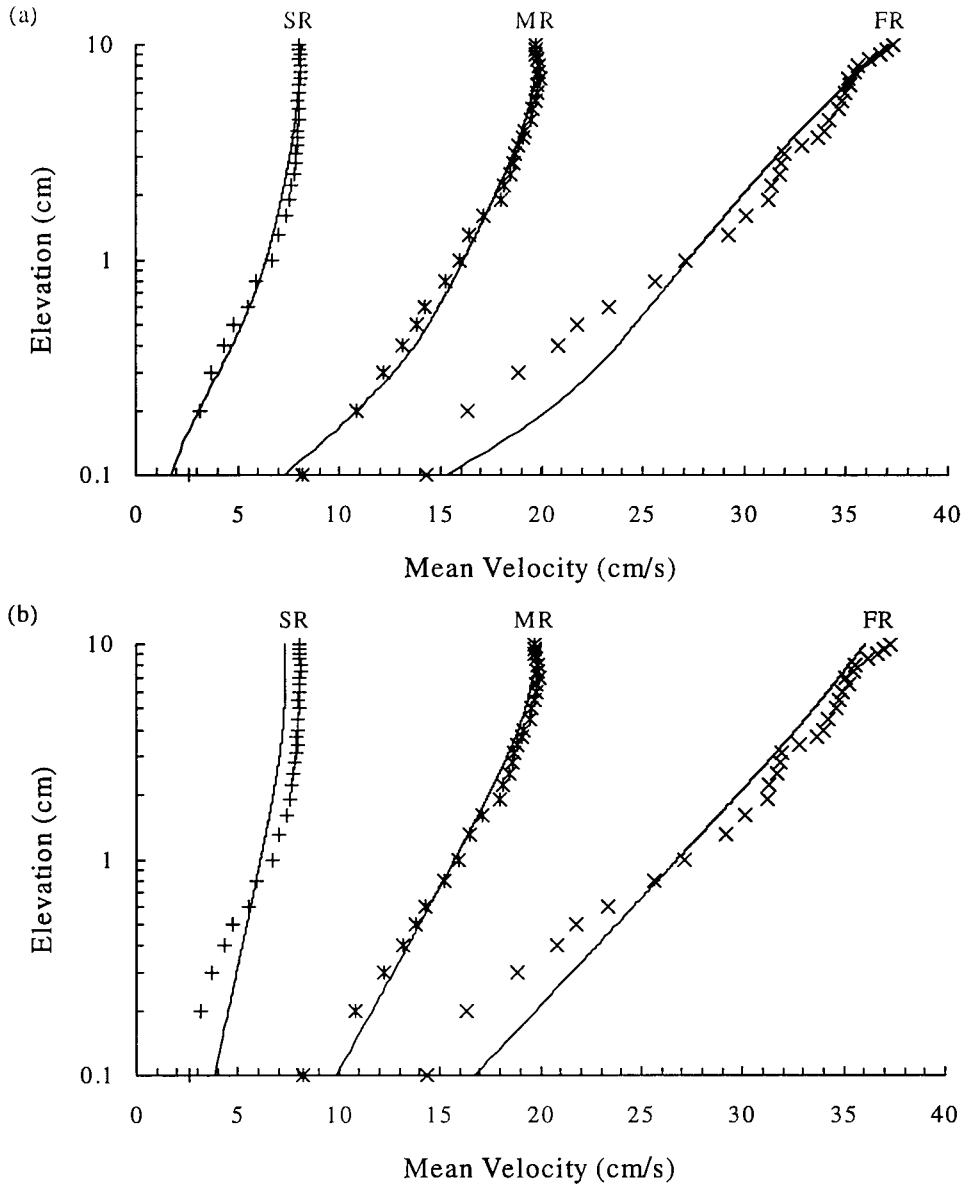

Figure 31: Mean velocity profiles for the various flow rates over the rough boundary. Solid line: semi-empirical expression based upon: (a) the hydrodynamically smooth boundary equations (Eqs 41, 43 and 44); and (b) the hydrodynamically rough boundary equations (Eqs. 47, 48 and 44).

5. Summary and Conclusions

In this Report, some of the important properties of one-dimensional turbulent open-channel flow have been summarised, based upon existing theoretical analyses and previous laboratory measurements undertaken (Section 2). A measurement programme carried out in the 5m flume was designed to determine the extent to which the flow characteristics are consistent, with expectations based upon the theoretical analysis of one-dimensional open-channel flows and the extent to which vertical mean velocity profiles are independent of along-channel and cross-channel positions. Using the generated vertical mean velocity profiles, different shear velocity determination methods have been evaluated, in order to identify which method was providing 'consistent' estimates of shear velocity. In addition, several simple experiments were set up and performed, in an attempt to test the performance and capabilities of the 5m flume, together with the use of associated equipment and instrumentation.

Unexpected oscillations were observed to be present in the velocity records; these may have been caused by small-amplitude standing surface waves. Although they do not seem to have an important effect on the derived mean quantities, they may be important if the low-frequency part of the spectrum is of particular interest, in some applications. The effect of these oscillations was reduced to an almost insignificant level by the introduction of the 'honeycomb-like' structure at the entrance of the working section. Some unexpected low-frequency fluctuations were observed also to be present in the flume. With the measurements which were performed, the results described in this report could not identify conclusively the cause of such fluctuations. However, it is reasonable to assume that they may have been caused by small fluctuations in the performance of the pump, due possibly to fluctuations in the power supplied to the pump (or fluctuations due to the mechanical behaviour of the pump itself). These low-frequency fluctuations were not found to have an important effect on the mean flow quantities and low-order statistics, except for the fact that somewhat longer record lengths (than expected) may be required, in order to obtain accurate estimates of the mean values. The installation of the 'honeycomb-like' structure and the head tank, at the entrance of the flume, have almost eliminated these low frequency fluctuations; these effectively insulated the flow from the fluctuations in the pump performance.

From the cross-sectional investigation of flow (Section 4.3) undertaken it was identified that the corner and wall regions influence the flow across the flume; these extends to distances of ±6cm

and up, to an elevation, of (at least) 4cm. The velocity distributions within the central portion of the flume (+6cm<z<-6cm) appear to be undisturbed by the presence of the boundaries. Such a result suggests that, in sediment investigations, the recess section should be located within the central part of the flume (if it is to be undisturbed by the side walls and corner regions of the flume).

The 5m flume appears to be able to produce a flow that is relatively one-dimensional, in which the mean velocity and turbulent intensity have (approximately) the expected structure. The LDA, as presently configured, appears to be able to produce accurate measurements of the mean (flow) velocity and the turbulent intensity. From the experiments undertaken on vertical flow velocity profiles, it has been established that the mean velocities are partly logarithmic, over the three flow rates and above both smooth and rough boundaries. The derived Re_* values have indicated that the tests were conducted under either the hydraulically smooth or transitional flow regimes. Increasing bed roughness was found to have an increasing effect on the turbulent character of the flow (as illustrated by the mean velocity and the LTI profiles).

The evaluation of the several methods available for the shear velocity determinations have indicated that the single-point method of estimating u_*, have proved to be more consistent than the log-profile method (i.e. utilisation velocity gradient). This observation is important in sediment investigations where only a single or two velocity measurements are usually carried out above the bed, at pre-specified elevations.

On the basis of the identified influence of the Streamflo on the LDA, the former must be positioned at least 4.5cm away from the LDA; this relates to applications where simultaneous velocity measurements are required at (two) different elevations.

Reference

Anwar, H.O., 1981. A study of the turbulent structure in the tidal flow. *Estuarine, Coastal and Shelf Science*, 13: 373-387.

Bayazit, M., 1976. Free surface flow in a channel of large relative roughness. *Journal of Hydraulic Research*, 14: 115-125.

Bohlen, W.F., 1977. Shear stress and sediment transport in unsteady turbulent flows. In: *Estuarine Processes (Volume II): Circulation, Sediments, and Transfer of Material in the Estuary.* M. Wiley (editor), Academic Press Inc., London, England, 428pp.

Chow, V.T., 1959. *Open Channel Hydraulics.* McGraw-Hill Book Co., New York, 680pp.

Christoffersen, J.B. and Jonsson, I.G., 1985. Bed friction and dissipation in a combined current and wave motion. *Ocean Engineering*, 12(5): 387-423.

Clauser, F.H., 1956. The turbulent boundary layer. *Advanced Applied Mechanics*, 4: 1-51.

Colebrook, C.F. and White, C.M., 1937. Experiments with fluid friction in roughened pipes. *Proceedings of the Royal Society*, 161: 367-381.

Coleman, N.L., 1981. Velocity profiles with suspended sediment. *Journal of Hydraulic Research*, 19: 211-229.

Coles, D., 1956. The law of the wake in the turbulent boundary layer. *Journal of Fluid Mechanics*, 1: 191-226.

Douglas, J.F., Gasiorek, J.M. and Swaffield, J.A., 1979. *Fluid Mechanics.* Pitman Press, Bath, 721pp.

Dyer, K.R., 1986. *Coastal and Estuarine Sediment Dynamics.* John Wiley, Chichester. 342pp.

Gust, G. and Walger, E., 1976. The influence of suspended cohesive sediments on boundary layer flow structure and erosive activity of turbulent sea water flow. *Marine Geology*, 22: 189-206.

Halliwell, A.R. and O'Connor, B.A., 1968. Shear velocity in a tidal estuary. American Society of Civil Engineers, Proceedings of 11th Conference on Coastal Engineering, Chap. 88, 1377-1396.

Heathershaw, A.D. and Langhorne, D.N., 1988. Observation of near-bed velocity profiles and seabed roughness in tidal currents flowing over sandy gravels. *Estuarine, Coastal and Shelf Science*, 26(5): 459-482.

Heathershaw, A.D. and Simpson, J.H., 1978. The sampling variability of the Reynolds stress and its relation to boundary shear stress and drag coefficient measurements. *Journal of Estuarine, Coastal and Marine Sciences*, 6: 263-274.

Heathershaw, A.D., 1979. The turbulent structure of the bottom boundary layer in a tidal current. *Geophysical Journal of the Royal Astronomical Society*, 58: 394-430.

Hinze, J.O., 1975. *Turbulence.* (2nd edition) McGraw-Hill Book Co., New York, 790pp.

Huntkey, D.A., 1988. A modified inertial dissipation method for estimating seabed stresses at low Reynolds numbers, with application to wave/current boundary layer measurments. *Journal of Physical Oceanography,* 18: 339-346.

Kennedy, R.J. and Fulton, J.F., 1961. The effect of secondary currents upon the capacity of a straight open channel. *Transactions of the Engineering Institute of Canada*, 5: 12-18.

Komar, P.D., 1976. *Beach Processes and Sedimentation.* Prentice-Hall, Eaglewood Cliffs, New Jersey, 429pp.

Landahl, M.T., 1967. A wave-guide model for turbulent shear flow. *Journal of Fluid Mechanics*, 29: 441-459.

Lyles, L. and Woodruff, N.P., 1972. Boundary layer flow structure: Effects on detachment of non-cohesive particles. *In: Sedimentation.* H.W. Shen (Editor), Fort Collins, Colorado, Chap. 2.

McQuivey, R.S. and Richardson, E.V., 1969. Some turbulence measurements in open-channel flow. *Journal of Hydraulic Division*, ASCE, 95: 2179-2184.

Mehta, P.R., 1979. Flow characteristics in two-dimensional expansion. *Journal of Hydraulic Division*, ASCE, 105: 501-516.

Middleton, G.V. and Southard, J.B., 1984. *Mechanics of Sediment Movement.* S.E.P.M Short Course No.3 (2nd edition), Tulsa, Oklahoma, 401pp.

Monin, A.S. and Yaglom, A.M., 1971. *Statistical Fluid Mechanics: Mechanics of turbulence. Volume 1.* MIT Press, Cambridge, Massachuetts, 769pp.

Monin, A.S. and Yaglom, A.M., 1975. *Statistical Fluid Mechanics: Mechanics of turbulence. Volume 2.* MIT Press, Cambridge, Massachuetts, 874pp.

Nakagawa, H., Nezu, I. and Tominaga, A., 1983. Secondary currents in straight channel flow and the relation to its aspect ratio. *Fourth Symposium on Turbulent Shear Flows*, Karlsruhe, Fed. Rep. Germany, 3.8-3.18.

Nezu, I. And Rodi, W., 1986. Open channel flow measurements with a Laser Doppler Anemometer. *Journal of Hydraulic Engineering*, 112: 335-355.

Nikuradse, J., 1932. Gesetzmässigkeiten der turbulenten Strömung in glatten Rohren. *Verein deutscher Ingenieure, Forschungshelf No. 356, Berlin.* English Translation as: Laws of turbulent flow in smooth pipes.

Nikuradse, J., 1933. Strömungsgesetze in rauhen Rohren. *Verein deutscher Ingenieure, Forschungshelf No. 361, Berlin.* English Translation as: Laws of flow in rough pipes.

Paphitis, D. and Collins, M.B., 2001. The 5m Long Recirculating Flume at the School of Ocean and Earth Science (SOES), University of Southampton. Part I: Descriptive Manual. Southampton Oceanography Centre, Internal Document, No. 67, 22pp.

Paphitis, D., Velegrakis, A.F., Collins M.B. and Muirhead, A.. Laboratory investigations into the threshold of movement of natural sand-sized sediments, under unidirectional, oscillatory and combined flows. *Sedimentology* (in press).

Prandtl, L., 1904. Uber Flussigkeitsbewegung dei sehr kleiner Reibung. In: *Verhandungeng*. Vol. III, *International Mathematical Congress*, Heidelberg, 484-491.

Prandtl, L., 1935. The mechanics of viscous fluids. In: *Aerodynamic Theory*. W.F. Durand (Ed), Vol. III, Springer-Verlag, Berlin, 142pp.

Raudkivi, A.J., 1990. *Loose Boundary Hydraulics (3rd Edition)*. Pergamon Press. 538pp.

Robertson, J.M. and Rouse, H., 1941. On the four regimes of open-channel flow. *Civil Engineering*, 11(3):169-171

Schlichting, H., 1979. *Boundary Layer Theory*. (7th edition) McGraw-Hill Book Co., New York, 817pp.

Sleath, J.F.A., 1984. *Sea Bed Mechanics*. John Wiley & Sons, Chichester, 335pp.

Soulsby, R.L., 1983. The bottom boundary layer of shelf seas. In: *Physical oceanography of coastal and shelf seas*. B. Johns (Editor), Elsevier, Amsterdam, 189-266.

Sternberg, R.W., 1972. Predicting initial motion and bedload transport of sediment particles in the shallow marine environment. *In: Shelf Sediment Transport, Process and Pattern*. D.J.P. Swift, D.B. Duane and O.H. Pilkey (Editors), Dowden, Hutchison and Ross., Strasburg, pp. 61-82.

Sumer, B.M. and Deigaard, R., 1981. Particle motion near the bottom in turbulent flow in an open channel. *Journal of Fluid Mechanics*, 86: 109-127.

Townsend, A.A., 1976. *The structure of the turbulent shear flow*. (2nd edition) Cambridge University Press, Cambridge, 429pp.

Tritton, D.J., 1988. *Physical Fluid Mechanics*. (2nd edition, 1995 reprint), Oxford University Press, Oxford, 519pp.

Van Rijn, L.C., 1982. Equivalent Roughness of Alluvial Bed. *Journal of Hydraulic Division, ASCE*, 108(HY10).

Von Karman, T., 1930. Mechanische Ahnlichkeit und Turbulenz (Mechanical similitude and turbulence). *Proceedings of the 3rd International Congress for Applied Mechanics*, Vol. I, Stockholm, 85-93.

Wang, S.Y., 1981. Variation of Karman constant in sediment-laden flow. *Journal of Hydraulic Research*, 104: 407-417.

Willmarth, W.W., 1975. Structure of turbulence in boundary layers. *Advanced Applied Mechanics*, 15: 159-254.

Xu, J.P., Wright, L.D. and Boon, J.D., 1994. Estimation of bottom stress and roughness in lower Chesapeake Bay by the inertial dissipation method. *Journal of Coastal Research,* 10(2): 329-338.

Yalin, M.S., 1972. *Mechanics of sediment transport*. Pergamon Press, New York, 290pp.

Appendix: Other Methods of Estimating Shear Stress

Quadratic Stress Law

Experimental evidence, provided originally by Sternberg (1972), has shown that the boundary shear stress in a turbulent flow is proportional to the fluid density and the square of the mean velocity; thus, by introducing a proportionality coefficient,

$$\tau_o = C_D \, \rho \, u_z^2 \tag{A-1}$$

where C_D is the drag coefficient. For practical purposes and, in most cases, the equation allows the bed shear stress to be evaluated from a single velocity measurement at a particular level above the bed. The drag coefficient is a function of the bed roughness (z_o) and can be calculated from (Soulsby, 1983):

$$C_D = (\kappa / \ln(z/z_o))^2 \tag{A-2}$$

Reynolds Stress or Eddy Correlation

The Reynolds stress method makes use of instantaneous velocity fluctuations (used as averages, over a suitable time increment), in a three-dimensional flow; hence, the bed shear stress is given by

$$\left| \tau'/\rho \right| = (u'w')^2 + (v'w')^2 \tag{A-3}$$

The direction of mean stress with respect to the u component of the horizontal current is,

$$\theta_\tau = \tan^{-1}\left(\frac{\overline{v'w'}}{\overline{u'w'}} \right) \tag{A-4}$$

This method is not used very extensively, because it requires more sophisticated measurements and analytical procedures. Laboratory experiments have confirmed, extensively and elsewhere, that the theory that the Reynolds stresses are constant within the boundary layer (Nece and Smith, 1970; see Dyer 1986); however, measurements in the sea do not always show that (Bowden and Fairbairn, 1956; see Bohlen, 1977).

Inertial-Dissipation Method

The inertial-dissipation method makes use of the spectra of turbulent fluctuations, which are measured within the constant stress layer. Assuming that advection and diffusion of turbulent kinetic energy are negligible, then, at the boundary of turbulent flow, the dissipation of the kinetic energy by viscosity is equal to the energy production by velocity shear (Heathershaw, 1979),

$$\varepsilon = -u'w'(du/dz) \tag{A-5}$$

where ε is the rate of energy dissipation, by viscosity, and the product of u' and w' is the kinematic Reynolds Stress. At the boundary, the mean shear velocity is given by Eq. 31 and, hence, by substituting into Eq. 56,

$$u_* u'w' = \varepsilon \kappa z \tag{A-6}$$

An expression relating the bed shear stress to the energy dissipation can be obtained, by assuming a constant-stress layer (i.e. $u'w' = u_*^2$), such as:

$$u_* = (\varepsilon \kappa z)^{1/3} \tag{A-7}$$

Huntley (1988) suggested a modification that extends the inertial-dissipation method so that it could be applied under combined waves and currents. Xu *et al.* (1994) tested the applicability of this method in the field, for estimating the temporal and spatial variability of bed shear stress in large estuaries; these investigators concluded that a reasonable agreement is obtained between the estimated values using the inertia-dissipation method.

Water Surface and Energy Slope

The tilting of a particular channel section (i.e. bathymetric variations), as well as shear induced on the bed surface, will cause a slope in the free water surface. In order to model the effect of the water slope on the bed shear stress the study will consider a simple case. A layer of water of constant thickness is flowing down an inclined channel of known dimensions; steady state is assumed and that the system operates under uniform atmospheric pressure. At one instant along the channel a water unit is considered (Figure A-1).

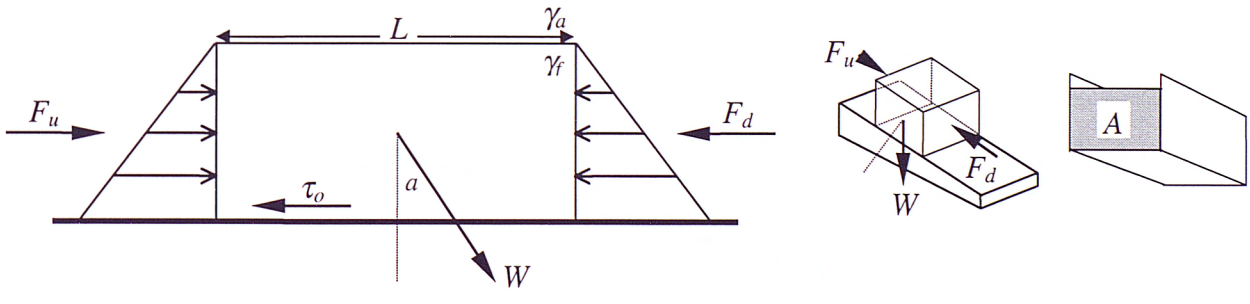

Figure A-1: Definition sketch for the surface water slope associated with bed shear stress. Key to symbols: F_u is the upstream hydrostatic force, F_d is the downstream hydrostatic force, W is the resultant gravitational force, L is the selected unit length, γ_f is the specific gravity of water, γ_a is the specific gravity of air, A is the cross-sectional area, a is the angle of slope and τ_o is the bed shear stress.

According to Newton's first law there must be a balance of forces and therefore:

$$F_u + W \sin a = F_d + \tau_o \, P \, L \tag{A-9}$$

where P is the wetted perimeter. Having considered conditions of steady state and a water of constant thickness, the hydrostatic forces will balance ($F_u = F_d$). The resultant gravitational force (W) is given by:

$$W = \Delta\gamma \; A \; L \tag{A-10}$$

where $\Delta\gamma$ is the difference in specific gravity between air and water. Substituting into (18):

$$\tau_o = \frac{\Delta\gamma \; A \sin a}{P} \tag{A-11}$$

where A/P can be replaced by R the hydraulic radius and sin(a) can be replaced by I the slope of the surface, and so Eq.21 becomes:

$$\tau_o = \Delta\gamma \; R \; I \tag{A-12}$$

The case that was considered here was for a uniform flow under conditions of steady state, but non-uniform, environmental flows will almost certainly result in different water slopes.

For the energy head concept reference is made to Halliwell and O'Connor (1968). These investigators have identified the difficulties arising in the measurements of surface slope and they used the energy slope to calculate the bed shear stresses. Figure A-2 illustrates the basic concept of this method.

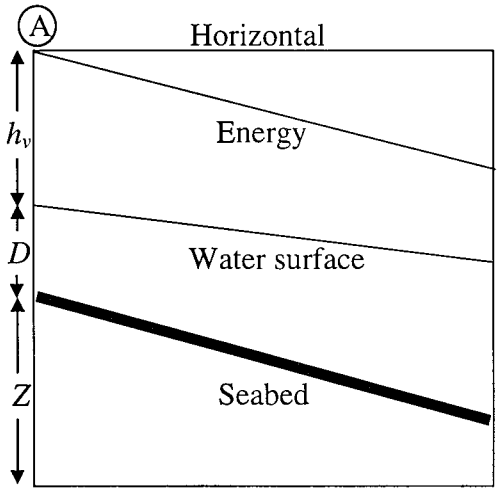

Figure A-2: Definition sketch for the energy head associated with bed shear stress.
Key to symbols: h_v kinetic head (=[$v_A^2/2g$] where v_A is the kinematic viscosity and g is the acceleration due to gravity), $D + Z$ add to give the potential head (where D is the density slope and Z the seabed slope).

The absolute head at A it is estimated using:

$$H_A = D + Z + h_v \tag{A-13}$$

But in the specific study by Halliwell and O'Connor (1968) the bed shear stress (τ_o) was calculated using the energy head (S) given by:

$$S = I - D + \Delta_I + F_I \tag{A-14}$$

where I is the water surface slope, Δ_I is the inertial slope (determined from cross-sectional mean velocities at surface and near bed) and F_I is the kinetic energy slope.

Seventh Power-Law

Another method of predicting the turbulent boundary layer and free surface flows is to use a simple power-law relationship, of the form:

$$\frac{\overline{u}}{u_*} = 8.74\left(\frac{z u_*}{\nu}\right)^{1/7} \tag{A-15}$$

This formula can be regarded only as an approximation, since the exponent has been found to vary with the total flow Reynolds number (from 1/5 to 1/10), the smaller value being for the larger Reynolds numbers. The expression provides a reasonable description of the mean velocity distribution to the part of the inner region, where overlap takes place between the log-laws and the laminar distributions and the outer region (zu_*/ν is greater than about 100 -1000).

Southampton Oceanography Centre
European Way
Southampton SO14 3ZH
United Kingdom
Tel: +44 (0)1703 596666
Fax: +44 (0)1703 596667